Constraining Cenozoic exhumation in the Faroe-Shetland region using sonic transit time data

David R. Tassone*[1], Simon P. Holford[1], Martyn S. Stoker[2], Paul Green[3], Howard Johnson[2], John R. Underhill[4], Richard R. Hillis[5]

(1) Australian School of Petroleum, Centre for Tectonics, Resources and Exploration (TRaX), University of Adelaide, North Terrace, Adelaide, SA 5005, Australia.

(2) British Geological Survey, Murchison House, West Mains Road, Edinburgh EH9 3LA, United Kingdom.

(3) Geotrack International Pty Ltd, 37 Melville Road, Brunswick West, Victoria 3055, Australia.

(4) Institute of Petroleum Engineering, Heriot-Watt University, Edinburgh EH14 4AS, United Kingdom.

(5) Deep Exploration Technologies CRC, 26 Butler Boulevard, Burbridge Business Park, Adelaide Airport, SA 5950, Australia

**Corresponding author (email: david.tassone@woodside.com.au)*

Running Header: Cenozoic exhumation of the Faroe-Shetland basins

Abstract

The Mesozoic-Cenozoic basins located between the Faroe, Orkney and Shetland Islands along the NE Atlantic Margin are actively explored oil and gas provinces whose subsidence histories are complicated by multiple tectonic factors, including magmatism, inversion and regional-scale uplift and tilting, that have resulted in spatially variable exhumation. These basins also exhibit non-burial related, transient Cenozoic heating anomalies that make thermal history interpretation and burial history reconstructions problematic. In this study we have applied a compaction-based approach, which is less susceptible to distortions from transient heating, to provide new constraints on Cenozoic burial and exhumation magnitudes in the UK sector of the Faroe-Shetland region using sonic transit time data from Upper Cretaceous marine shales of the Shetland Group in 37 wells. Since estimates of exhumation magnitude depend critically on the form of the normal sonic transit time-depth trend, a new marine shale baseline trend was firstly constructed from shales presently at maximum burial, consistent with other marine shale baseline trends of different ages from nearby basins. Our results indicate that Upper Cretaceous marine shales are presently at or near (i.e. within ≤100 m net exhumation) maximum burial depths in the Møre and Magnus basins in the northeast of the study area as well as in the deeper-water Faroe-Shetland Basin (i.e. Flett and Foula sub-basins). However, Upper Cretaceous strata penetrated by wells in the southwest have been more deeply buried, with the difference between maximum burial depth and present-day values (net exhumation) increasing from ~200-350 m along the central and northeastern parts of the Rona High to ~400-1000 m for wells located in the West Shetland Basin, North Rona Basin and southwestern parts of the Rona High. Although the precise timing of exhumation is difficult to constrain due to the complex syn- to post-rift tectonostratigraphic history of vertical movements within the Faroe-Shetland region, our estimates of missing section, together with available thermal history constraints and seismic-stratigraphic evidence, implies that maximum burial and subsequent exhumation most likely occurred during an Oligocene to Mid-

Miocene tectonic phase. This was probably in response to major post-breakup tectonic reshaping of this segment of the NE Atlantic Margin linked to a coeval and significant reorganisation of the northern North Atlantic spreading system, suggesting that fluctuations in intraplate stress magnitude and orientation governed by the dynamics of plate-boundaries forces exerts a major control on the spatial and temporal variations in differential movements along complexly structured continental margin.

Key words: Exhumation, uplift, NE Atlantic margin, sonic transit times, Faroe-Shetland region

1 Introduction

The NW European rifted continental margin is anything but 'passive', with the basins along the margin having experienced a complex Mesozoic–Cenozoic history with multiple phases of extension, subsidence, magmatism, compression, broad uplifts, erosion and exhumation (Lundin & Doré 2002). It is increasingly recognised that exhumation, which is defined as the removal of overburden material such that previously buried rocks are brought towards the surface (Doré *et al.* 2002), has affected many of the world's important hydrocarbon provinces and that it can have both negative and positive impacts on petroleum systems (Doré & Jensen 1996; Doré *et al.* 2002). Accurate knowledge of exhumation and burial is necessary for predictions of source rock generation, reservoir quality and seal integrity (Corcoran & Doré, 2005). A number of methods are commonly used to investigate the exhumation of onshore and offshore sedimentary basins and Corcoran & Doré (2005) generalise these to four different frames of reference: compactional, thermal, tectonic or stratigraphical. A thorough exhumation study ideally integrates two or more of these methods to reduce uncertainties and to better constrain exhumation magnitudes (e.g.

Japsen & Chalmers 2000; Corcoran & Mecklenburgh 2005; Japsen *et al.* 2007a; Holford *et al.* 2008; Tassone *et al*. 2013).

Our study area is located offshore between the Faroe and Shetland islands, and includes the Faroe-Shetland Basin, West Shetland Basin, East Solan Basin, West Solan Basin, South Solan Basin, North Rona Basin, and the southern end of the Møre Basin, which we collectively refer to as the Faroe-Shetland Region (FSR; Fig. 1). This region is relatively underexplored given its large aerial extent of >50,000 km^2, with approximately 200 exploration and appraisal wells drilled during the past 30 years in water depths that vary between <200 to 1500 m (Quinn *et al.* 2011). Three producing fields have resulted from this exploration (Clair, Foinaven and Schiehallion/Loyal) and a number of additional oil and gas discoveries including Rosebank, Solan, Strathmore, Victory, Tormore, Laggan, Cambro; Quinn *et al.* 2011).

Substantial Cenozoic exhumation in this region is inferred from stratigraphic observations and evidence for breached traps and biodegraded oil columns in the West Shetland Basin and the East Solan Basin (Doré *et al.* 2002), but the distribution, magnitude and chronology of exhumation, both within these basins and across the wider FSR region, is poorly constrained. Previous thermal history studies in the FSR, using apatite fission track analysis (AFTA) and vitrinite reflectance (VR) data (e.g. Duddy *et al.* 1998; Green *et al*. 1999; Parnell *et al*. 1999, 2005) have confidently identified Cenozoic heating related to deeper burial in only one well, 204/19-1; Parnell *et al.* (2005). In other wells, Duddy *et al.* (1998); Green *et al*. (1999); and Parnell *et al*. (1999, 2005) have reported Cenozoic heating characterized by low palaeogeothermal gradients or non-linear to arcuate palaeotemperature profiles (e.g. wells 205/23-1, 206/09-2 and 206/12-2; Fig. 2) suggesting that heating was caused by hot fluid movements rather than enhanced heat flow or deeper burial. AFTA and VR data from deeper Palaeozoic stratigraphy in wells around the Clair Field also indicates a palaeo-heating event prior to the Cenozoic whereby cooling is attributed to ~2 km of Late Palaeozoic exhumation (Mark *et al.* 2008). Where palaeothermal measurements are dominated by transient heating due to hot fluid flow (Fig. 2), it can be difficult to resolve the palaeothermal effects of deeper burial from non-burial effects, making burial history reconstructions in Cenozoic sequences within the FSR problematic.

Some constraints on the distribution and timing of Cenozoic exhumation in the FSR have been achieved through regional mapping of unconformable surfaces using seismic reflection data (e.g. Stoker *et al.* 2002, 2005a,b,c; Cermicola *et al.* 2005; Praeg *et al.* 2005). Significant, regional unconformities identified and mapped in these studies are shown in Fig. 3 and include the Mid Paleocene (MPU), Lower Eocene (LEU), Upper Eocene (UEU), base Neogene (BNU), intra-Miocene (IMU) and intra-Pliocene (IPU). These regional boundaries have been mapped throughout the NE Atlantic margin, between Mid Norway and Ireland (Stoker *et al*. 2005a). Booth *et al*. (1993) reported a major mid-Cenozoic erosional unconformity extending across the West Shetland Platform and the Solan and West Shetland Basins, with Pliocene strata overlying Eocene to Early Eocene units. Exhumation thus occurred in the interval late Oligocene to Mid-Miocene, with up to 1250 m of section removed at the crest of the Rona Ridge. Other studies have employed tectonic backstripping to estimate permanent uplift in the FSR (e.g. Clift & Turner 1998), but these do not give quantitative estimates of thicknesses of section removed during exhumation (cf. Jones *et al.* 2001).

The above discussion highlights the need for additional independent, but complementary, constraints on palaeoburial depths and exhumation magnitudes in the FSR. Such results can be obtained from sedimentary rock compaction data, which are less susceptible to distortions from transient heating (Corcoran & Doré 2005). In this study, we present estimates of Cenozoic 'net' exhumation magnitudes, that is, the difference between present-day and maximum burial depths (Corcoran & Doré 2005), from 37 petroleum wells in the FSR. We employ a compactional approach (i.e. sonic transit time analysis) to assess the degree to which Campanian to Danian marine shales from the Shetland Group record overcompaction (i.e. anomalously low porosities) with respect to empirically derived baseline trends (e.g. Hillis *et al*. 1994; Hillis 1995a,b; Hansen 1996; Japsen 1998, 1999, 2000; Ware & Turner 2002; Storvoll *et al*. 2005; Japsen *et al*. 2007b; Holford *et al*. 2009; Tassone *et al*. 2013). To date, there has been no systematic application of this technique to quantify exhumation magnitudes in the FSR, despite its widespread and successful application in other basins around the British Isles (Hillis, 1995a; Mackay & White 2006) such as the North Sea Basin (Hillis 1995b; Japsen 1998, 1999, 2000), Inner Moray Firth (Hillis *et al*. 1994), West Orkney Basin (Evans 1997), East Irish Sea Basin (Ware & Turner 2002; Holford *et al.* 2009) and Slyne Basin (Corcoran & Mecklenburgh 2005). One exception is the study by Iliffe *et al.* (1999), who report conducting a shale velocity analysis for Well 204/19-1 on the Westray High. They estimated ~500 m of removed sediment at both base and mid Cenozoic unconformities, but did not present any supporting data or results.

2 GEOLOGICAL SETTING OF THE FAROE–SHETLAND REGION

The FSR forms part of the Atlantic passive continental margin of NW Europe, and so its geological history has been inextricably linked to the evolution of the NE Atlantic rift system. The structural framework of the study area is dominated by the Faroe-Shetland Basin, which is approximately 400 km long and up to 200 km wide and consists of a generally NE-trending complex of sub-basins and intra-basinal highs (Fig. 1). This basin is contiguous to the northeast with the Møre Basin, and is flanked on its southeast margin by a series of smaller 'marginal' basins, including the West Shetland, North Rona, East Solan, West Solan and South Solan basins.

This chain of basins developed as a precursor to continental break-up between NW Europe and Greenland (Doré *et al*. 1999; Roberts *et al*. 1999). Extension in the FSR occurred episodically during the Cretaceous with phases of rifting in the Valanginian-Hauterivian, Aptian-Albian and Turonian-Maastrichtian (Dean *et al*. 1999; Lamers & Carmichael 1999; Larsen *et al*. 2010; Ritchie *et al*. 2011), though continental break-up in this region was not achieved until the Early Eocene (Fig. 3; Passey & Jolley 2009). Break-up was accompanied by extensive volcanism, which exploited weak spots in the increasingly thinned and rifted lithosphere of the NW European plate, including the FSR (Passey & Hitchen 2011).

The Paleocene–lowest Eocene succession is punctuated by a number of unconformities, including the MPU, which separates the Shetland Group from the overlying Vaila Formation, as well as unconformities that separate the Vaila, Lamba and Flett/Balder formations (Ebdon *et al*. 1995; Dean *et al*. 1999) (Fig. 3). All of these unconformities relate to episodes of deformation within the FSR prior to continental breakup. The development of the MPU reflects a phase of uplift and localised Mid-Paleocene rifting in the Faroe-Shetland Basin (Dean *et al*. 1999; Doré *et al.* 1999; Lamers & Carmichael 1999), and has been attributed by some authors (e.g. White & Mackenzie 1989; Ritchie *et al*. 1999; Saunders *et al*. 2007) to the 'arrival', beneath Greenland, of the Icelandic mantle plume. This, in turn, led others (e.g. Shaw Champion *et al*. 2008; Lovell, 2010; Hartley *et al*. 2011) to interpret a sub-aerial drainage network associated with an unconformity that forms a sequence boundary between the Late Paleocene Lamba and Flett formations, in the southern part of the FSR, in terms of dynamic uplift driven by this thermal anomaly over an interval of 2–3 Myr. Whether this uplift – reportedly up to ca. 1 km (Hartley *et al*. 2011) – occurred as a result of a mantle plume or by some other process continues to be a matter of debate (e.g. Foulger 2002; Lundin & Doré 2005; Ellis & Stoker in press).

Following breakup, it has been previously assumed that the dominant process affecting vertical movement of the Faroe-Shetland Basin was post-rift thermal subsidence accompanied by a decrease in sediment flux (Turner & Scrutton, 1993; Jones *et al*. 2002). However, in common with passive margin basins throughout the NE Atlantic region (e.g. Rockall, Norway and Vøring basins), the post-rift structural development of the FSR has been considerably influenced by tectonic activity at various stages throughout the Cenozoic (Fig. 3), including:

- In the Eocene, several phases of post-rift uplift and erosion of the Munkagrunnur Ridge (Ölavsdöttir *et al*. 2010, 2013), the Flett High (Robinson *et al*. 2004), and the West Shetland–Orkney-Shetland High (Stoker & Varming 2011; Stoker *et al*. in press) led to the progradation of sedimentary wedges into the Faroe-Shetland Basin immediately following breakup (associated with the development of the LEU, which separates the post-rift Stronsay Group from the syn-breakup units) as well as during the Mid- and Late Eocene, which were locally deformed by early growth on compressional domes, including the Judd and Westray anticlines (Fig. 3: Ritchie *et al*. 2003, 2008; Davies *et al*. 2004; Smallwood 2004; Johnson *et al*. 2005; Stoker *et al*. 2005c). This clastic input – including the Middle Eocene basin-floor fan deposits (Fig. 4a) – is primarily a response to episodic uplift and erosion of the eastern and southern flank (i.e. West Shetland Platform) of the Faroe-Shetland Basin, and expressed by the development of unconformities, including the ILU (Stoker *et al*. 2010, in press; Stoker & Varming 2011).
- Towards the end of the Eocene, and spanning the Oligocene to Mid-Miocene interval, the area was subjected to compression, which resulted in inversion and/or uplift of the Wyville Thomson, Munkagrunnur and Fugloy ridges (Boldreel & Andersen 1993; Johnson *et al*. 2005; Stoker *et al*. 2005a,b; Ritchie *et al*. 2011) as well as the Judd and Westray anticlines (Ritchie *et al*. 2008), together with the general uplift of the Faroe and West Shetland platforms and/or subsidence of the Faroe-Shetland Basin (Andersen *et al*.

2000; Ritchie *et al*. 2011; Stoker & Varming 2011), which were, at least in part, coeval (Fig. 3). The formation of the UEU, BNE and INU are all expressions of this phase of instability.

- In the Early Pliocene, the West Shetland Shelf was tilted to the northwest (basinwards) by <1°, which generated uplift of the shelf and hinterland, created accommodation space along the West Shetland margin, and initiated the deposition of large-scale Pliocene-Pleistocene prograding sediment wedges (Stoker 2002; Praeg *et al*. 2005; Stoker *et al*. 2005a,b) (Fig. 3). The IPU is a widespread subaerial to submarine unconformity formed at this time. Subsequent major erosion and sedimentation was sustained throughout the Pliocene-Pleistocene by climate-driven processes, including glaciation of the West Shetland and Faroe shelves, as well as the ensuing effects of glacio-isostatic readjustment.

The Oligocene–Mid-Miocene phase of tectonic activity had the strongest influence on the post-rift shaping of the FSR, with the Fugloy, Munkagrunnur and Wyville Thomson ridges all forming major present-day bathymetric highs (Fig. 1b; Stoker *et al*. 2005c). The disposition of the Eocene succession, which is folded about the axes of these uplifted areas (Stoker *et al*. 2010, in press; Ritchie *et al*. 2011), indicates that concomitant differential subsidence resulted in a deepening of about 1 km in the FSR that gave rise to the Neogene instigation and configuration of the underfilled deep-water basins of the Faroe-Shetland and Faroe bank channels (Stoker *et al*. 2005a,b).

3 ESTIMATING THE MAGNITUDE OF EXHUMATION USING A COMPACTION-BASED APPROACH

This study employs a compactional frame of reference to estimate Cenozoic exhumation magnitudes in the FSR. Compaction refers to the reduction in sediment volume during burial as the result of mechanical and thermo-chemical processes (Giles *et al.* 1998). Here we consider the simplest case of compaction when the maximum principal effective stress is vertical at the time of maximum burial, and porosity loss with increasing depth is largely irreversible and caused predominately by burial (Giles *et al.* 1998). If some mechanical porosity reduction has been achieved by horizontal compaction when the maximum principal stress direction was horizontal, exhumation amounts may be overestimated, especially in the hangingwalls of inverted fault blocks where tectonic compression has increased mean effective stresses (Holford *et al*. 2009).

We use compressional sonic transit times, Δt_P (i.e. the reciprocal of sonic velocity, V_P), as a proxy for compaction because it is strongly dependent on porosity (Hillis *et al.* 1994) (while also being sensitive to processes such as pressure solution and progressive rock stiffening, Japsen *et al*., 2007b). Unlike density wireline logs that record the total porosity of a sedimentary rock, compressional sonic transit time data records the primary porosity because sonic waves avoid open fractures and void spaces (Rider & Kennedy 2011).

Quantifying the exhumation magnitude of a selected stratigraphic unit for any given well location using a compaction-based approach first requires the identification of a lithology-specific reference or normal sonic transit time-depth trend (referred herein as ‘baseline’; Japsen *et al.* 2002). Such trends describe how sonic transit times decrease with depth in relatively homogeneous, hydrostatically pore-fluid pressured and brine-saturated sedimentary units, as porosity is reduced during normal mechanical and thermo-chemical compaction (Japsen *et al.* 2007b). The baseline is usually defined when a sedimentary succession is presently at its maximum burial depth (i.e. the thickness of the overburden has not been reduced by exhumation (Japsen *et al.* 2007b). Therefore exhumed basins tend to exhibit anomalously low porosities (or low sonic transit time, Δt_P) at a given depth compared to continuously subsiding, 'normally-compacted' basins (Corcoran & Doré 2005). Shales and mudstones from thick and laterally extensive stratigraphic successions are preferred in sonic transit time analysis because they often exhibit relatively simple baselines with porosity decreasing rapidly with depth (Magara 1978). They are often more homogeneous in terms of grain size and mineralogy than coarser-grained sediments such as sandstones, and they do not act as aquifers with the consequent porosity variations (Japsen *et al.* 2002).

The displacement of the observed, present-day, sonic transit time values, on the depth (vertical) axis, from the baseline for a particular formation or lithology yields an estimate of *net exhumation* (E_N) (Corcoran & Doré 2005). The simple relationship between net exhumation (E_N), maximum burial depth (B_{max}) and the present-day burial depth ($B_{present\text{-}day}$) is expressed by:

$$B_{\max} = E_N + B_{present-day} \qquad (1)$$

Where post-exhumation re-burial (B_E) has occurred, *gross exhumation* (E_G) can be calculated using (Hillis 1995a; Japsen 1998; Corcoran & Doré 2005):

$$E_G = E_N + B_E \qquad (2)$$

This concept is graphically illustrated in Fig. 5a-c. Net exhumation is synonymous with other terms commonly used in the literature such as net uplift (Doré & Jensen 1996), apparent exhumation (Hillis 1995a,b) and negative burial anomaly (Japsen 1998, Japsen et al. 2002), and will equal gross exhumation only in the case where the erosional unconformity is at the seabed or present-day ground level (Corcoran & Doré 2005). Equation 2 shows that estimates of net exhumation can easily be converted to estimates of gross exhumation if the timing of the exhumation event prior to maximum burial is known and correlates to a tectonic unconformity. We note that rapid burial of rocks with low permeability (e.g. mudstones) can lead to anomalously high sonic transit times (i.e. undercompaction). In this case vertical displacements from the baseline result in negative net exhumation magnitudes (or positive burial anomalies; cf. Japsen 1998, 1999), possibly indicating overpressures generated by disequilibrium compaction (Fig. 5d; Osborne & Swarbrick 1997).

Corcoran & Doré (2005) provide a comprehensive overview of the advantages and limitations of estimating exhumation magnitudes using a compactional approach. Given that wireline well logs represent *in situ* measurements, they are not subject to errors associated with rock sample collection and processing (Corcoran & Doré 2005). A practical advantage of using sonic transit times as a proxy for porosity is their wide availability and coverage due to their routinely acquisition during formation evaluation in petroleum wells. Furthermore, sonic transit times prescribe simple constraints on both physical and geological parameters since acoustic waves are affected by bulk properties as they propagate through the sediment (Japsen *et al*. 2007b). For this reason, sonic transit times have reduced susceptibility to distortions by transient heating (Corcoran & Doré 2005), which is a critical factor in the FSR (Duddy *et al.* 1998; Mark *et al.* 2008). Nevertheless uncertainty related to the identification of a uniform lithology for which the baseline is defined and to the selection of data for similar formations for which exhumation is to be determined may cause erroneous results (Japsen *et al*. 2007b).

A key disadvantage of a compaction-based approach is that the absolute timing of exhumation cannot be constrained independently (Corcoran & Doré 2005), and thus, requires integration with thermal history and/or stratigraphic data (e.g. Corcoran & Mecklenburgh 2005; Japsen *et al*. 2007a, 2012; Tassone *et al*. 2013). Discrepancies between net exhumation magnitudes for two temporally different stratigraphic and relatively homogeneous units penetrated and logged in the same well, nevertheless, can shed light on the burial history of a particular location (see Japsen's (2000) Fig. 1 and Fig. 7: e.g. Japsen 2000; Japsen *et al.* 2007a).

4 DATASET

All wells examined in this study are located within the UK sector of the FSR and the digital wireline well log data and additional well information were provided by the British Geological Survey. The well log data acquired for this study consists of 43 wells from the FSR and Orkney Basin along the NE Atlantic margin (Fig. 1) drilled between January 1974 and June 1987. Only 37 wells contained digital sonic transit time and gamma ray wire-line well-log data, and for one of those 37 wells, no chronostratigraphic data was available (Fig. 1).

Most well-log data used in this study was of reasonably good quality with minimal evidence for significant noise or spiking. The quality of the well log data at the start and ends of each run were often of poor quality and were consequently removed along with any invalid data (e.g. casing response) prior to data processing. The gamma ray response in wells 214/27-1 and 209/12-1 were considered to be of poor quality with extremely low and unusually high responses recorded, respectively. In addition, the sonic transit time response below ~1400 m measured depth below seabed (MDbSB) in 219/27-1 was deemed unreliable due to a significant increase in sonic transit time that was at odds with the earlier recordings of the sonic tool. The complete log data were not always available for all the drilled formations and/or wells. Many wells contained multiple runs over the same interval or runs over different intervals in which the most complete sonic transit time and gamma ray logs were carefully selected and/or spliced together when necessary.

5 SONIC TRANSIT TIME ANALYSIS

5.1 Stratigraphic Units Analysed

Information regarding the stratigraphic tops (as well as water depths, total drilling depths and Kelly bushing elevations relative to mean sea level) of individual wells were compiled from the United Kingdom's Department of Energy and Climate Change (DECC) online database. This database, which is based largely on composite well logs, differentiates stratigraphic tops with respect to their chronostratigraphy. Thus, chronostratigraphic tops are often quoted in this study rather than lithostratigraphic formation stratigraphic tops. No chronostratigraphic top data was available for well 205/10-2B from the DECC database, but this information was obtained from the well completion report.

An effective sonic transit time analysis requires laterally extensive and thick, relatively homogeneous formations (Japsen *et al.* 2002). As previously indicated, shales and mudstones are preferred for sonic transit time analyses over coarser grained lithologies such as sandstone. We found that the Upper Cretaceous to Lower Palaeocene marine shale successions of the Shetland Group generally had a consistent and less-variant log response with depth (Fig. 6) and is the only succession within the entire FSR that meets the requisite criteria for detailed interval sonic transit time analysis. Analysis of overcompacted marine shale units of the Shetland Group should permit any post-Danian or Cenozoic net exhumation magnitudes to be estimated. We also considered the use of sonic transit times from Eocene shales, but found that lithologies were too laterally variable across the entire region.

The Shetland Group is subdivided into the Danian Sullom Formation; the Campanian to Maastrichtian Jorsalfare Formation; and the Campanian (to Turonian) Kyrre Formation (Fig. 6). The Shetland Group conformably overlies Cenomanian to Turonian chalks of the Herring and Hidra formations (i.e. Chalk Group) in the North Rona Basin and Solan Basin, and the Berriasian to Albian Cromer Knoll Group in the rest of the basins in the FSR (Stoker & Ziska 2011). The Danian Sullom Formation is overlain by the Selandian Valia Formation. This boundary is conformable in the deepest parts of the FSR region, though in some areas (e.g. the Judd and Rona highs) the Sullom Formation is absent and the boundary is unconformable. Where present, the upper parts of the Sullom Formation are characterised by an increase in sandstone beds (Knox *et al.* 1997; Stoker & Varming 2011).

Lithologically, the Jorsalfare Formation and Kyrre Formation are characterised by light grey to grey-brown, soft to firm, sticky, generally calcareous mudstones and claystones with sporadic interbedded argillaceous limestones and dolomites, common pyrite and glauconite and rare sandstones and siltstones, which witness deposition in aerobic siliciclastic marine shelf to upper bathyal slope and outer sublittoral (neritic) zones (Stoker & Ziska 2011). Similarly, the Danian Sullom Formation is dominated by green to dark grey calcareous mudstone and subordinate sandstones (Stoker & Ziska 2011). The Shetland Group mudstones are relatively homogenous with depth, regionally extensive (with the exception of the Orkney Basin, West Solan Basin and Westray High) and thick (reaching ~1500 m in well 205/22-1A; Fig. 6). These properties make them highly suitable for sonic transit time analyses (cf. Japsen *et al.* 2002). In the following text we refer to these mudstones as shales because of their petrophysical properties (Rider & Kennedy 2011), and our analyses only considers the upper-most Shetland Group shales of Campanian, Maastrichtian and Danian (C-M-D) ages.

5.2 Data Acquisition & Processing

We first adjusted the depths of all wireline well log and chronostratigraphic data to seabed depths, which represents the compactional frame of reference (Corcoran & Mecklenburgh 2005). Because inclinometry data was not available for all the wells that were designed and drilled close to vertical for exploration, we assumed that the measured depths correspond approximately to true vertical depth. We then used the procedure outlined in Tassone *et al*. (2013) to remove any sonic transit time logging artefacts (e.g. cycle skipping, noise triggering) and isolate shale lithologies from non-shale lithologies (e.g. chalks, carbonates, sandstone intervals). This was completed using gamma ray logs as a proxy for shale volume (e.g. Rider 1996) in conjunction with lithological descriptions of sidewall cuttings described in well completions reports. For shaley lithological successions, the average sonic transit time response over a thickness of approximately 15 ± 2.5 m was considered as a single shale unit data point in our sonic transit time analysis.

A number of wells penetrated Paleogene sills and lavas, which are easily identified in wireline well log data as they are characterised by abrupt changes in the log response i.e. very low gamma ray responses and very low sonic transit time responses. Examples of this are highlighted below. The thicknesses of igneous sills within Cretaceous sediments vary from a few metres to over 100 m (Gibb *et al.* 1986) and are mostly composed of tholeiitic olivine dolerites (Passey & Hitchen 2011). Intruded sills have a lower sonic transit time response (~50-61 μs ft^{-1}) in comparison to extruded lavas (~67-87 μs ft^{-1}) and impact the surrounding sedimentary rocks through contact metamorphism (Passey & Hitchen 2011). Contact metamorphism reduces porosity and results in anomalously low sonic transit times. To avoid confusion with porosity reduction due to exhumation, sonic transit times that are obviously influenced by igneous bodies have been removed. Furthermore, sonic transit time data obviously influenced by logging operations were removed prior to analysis, as well as invalid data such as anomalously low sonic transit times typical of casing responses.

Of the 37 wells available for this study, only 32 intercepted the Shetland Group and contained shale units that permitted estimation of exhumation magnitudes. These wells are grouped into three sets according to their geographical location (southwest, central and northwest; Fig. 1).

5.3 Construction of a Normal Sonic Transit Time-depth Baseline Trend for Campanian-Maastrichtian-Danian Marine Shales

Estimates of exhumation magnitude depend critically on the form of the normal sonic transit time-depth baseline trend (Japsen *et al.* 2007*b*). In order to establish an empirical sonic transit time-depth baseline trend for the Shetland Group marine shales, we sought average shale unit sonic transit time data from wells presently at their maximum burial depths (i.e. B_{max}). Although a number of Rona High wells have arcuate maximum palaeotemperature profiles that indicate hotter temperatures in the past related to transient hot-fluid flow (Fig. 2), wells in which AFTA and VR data define a palaeogeothermal gradient close to, or at, the present-day geothermal gradient may be used to construct a normal baseline trend for the Shetland Group marine shales if these maximum temperatures at the present-day are the result of burial.

After reviewing both published (Duddy *et al.* 1998; Green *et al*. 1999; Parnell *et al*. 1999, 2005; Mark *et al.* 2008) and unpublished (Geotrack International reports) AFTA and VR data, we found that samples collected from wells 206/03-1 and 219/20-1 clearly show that all preserved units at these locations are now at their maximum post-depositional temperatures and thus burial depths. This is illustrated in Fig. 7 in which palaeotemperature constraints from AFTA and VR samples in the 206/3-1 well are consistent with the present-day temperature profile defined by a thermal gradient of ~36.4°C km^{-1} derived from corrected bottom hole temperature (BHT) measurements.

It should be noted that well 219/20-1 is located towards the main depocentre of the Møre Basin (Stoker & Ziska 2011) and that well 206/03-1 is located very close to the Clair Lineament (Fig. 1) within the Foula sub-Basin (Fig. 4a). Previous workers have inferred from regional gravity and magnetic datasets that the lineaments within the FSR striking northwest-southeast and sub-perpendicular to the major northeast-southwest structural features (Fig. 1) are zones of large-scale Palaeocene strike-slip to transpressional deformation (e.g. Dean *et al*. 1999). If so, then any transpressional deformation along this zone near well 206/03-1 may have important implications for the burial history in the immediate vicinity. Well-calibrated 3D seismic reflection data, however, shows little evidence of major faulting within the Palaeogene section near the Clair Lineament (Moy & Imber 2009). These authors suggest the high density of intrusive igneous sills within the underlying Upper Cretaceous section, which were dated along the Flett High to be of similar age to the earliest Ypressian Balder Tuff (~55.0 ± 0.6 Ma; Moy & Imber 2009: Fig. 3) may have caused localised uplift in the vicinity of this well, though any uplift that may have occurred does not appear to be associated with erosion of the Palaeocene sequence prior to the deposition of the Eocene Stronsay Group (see Fig. 7 of Moy & Imber (2009)). Igneous sills were not intersected within well 206/03-1 and AFTA and VR data does not support any palaeotemperature anomalies associated with advective heating by hot fluids or contact heating by igneous intrusions (Fig. 2), indicating that igneous intrusions have had little bearing on the burial and thermal history of well 206/03-1 (Fig. 7).

In order to construct a reliable baseline, shale sections need to be both hydrostatically pressured and brine-saturated (Japsen *et al.* 2007b). Overpressures occur at depths >3000 m in the FSR, with Mesozoic sections generally showing the largest formation overpressures (Iliffe *et al.* 1999). Average shale unit sonic transit times (Δt_{ave}) are plotted against the corresponding shale unit mid-point depth (Z_{MP}) in metres below seabed (m bSB) for wells 206/03-1 and 219/20-1 in Fig. 8a. While Δt_{ave} data in both wells over depths shallower than ~2500 m bSB plot on the same trend, in well 219/20-1 Δt_{ave} data from depths >2500 m bSB exhibit a number of reversal sonic transit time trends (Fig. 8a). Sonic transit time reversals can be diagnostic of overpressure in sedimentary rocks (Tingay *et al.* 2009) or changes in sediment composition and mineralogy, e.g. the dissolution of smectite and precipitation of illite (Storvoll *et al*. 2005). Unfortunately, no formation pore pressure data are available to verify whether or not overpressure occurs in this well. It can be seen in Fig. 8a that the gamma ray response increases drastically at ~2590 m bSB, which is ~90 m below the depth where Δt_{ave} values become higher. This suggests that the increase in Δt_{ave} values may not simply be related to lithology, or that there is some sort of lithological transition zone to an alternative normal sonic transit time-depth trend that reflects the change in gamma ray response. Deeper than ~2745 m bSB in well 219/20-1, Δt_{ave} values are complicated by numerous igneous sills (Fig. 8a), which are easily identifiable by their very low sonic transit time and gamma ray response. Although it is beyond the scope of this study to investigate the subsurface formation pressures in detail, if this interval was also laterally surrounded by connecting, impermeable igneous rocks, then such compartmentalisation may have the ability to cause overpressures (Rateau *et al*. 2013). Due to the uncertainty in pore pressure conditions below ~2500 m, average shale unit sonic transit times below this depth were disregarded in the baseline construction. Formation pore pressure data from wireline formation tests (WFTs) were available from well 206/03-1 indicating that the Upper Cretaceous Shetland Group section is hydrostatically pressured, whereas the deeper Lower Cretaceous section is overpressured (Fig. 8b). Hence, the normally pressured sonic transit times of shale units in wells 206/03-1 and 219/20-1 encompassing a depth range between ~1500-2500 m below seabed were ultimately chosen to constrain the baseline(s).

We constrained two empirical baselines using the approach of Heasler & Kharitonova (1996), Japsen (2000), Ware & Turner (2002) and Corcoran & Mecklenburgh (2005). This involves fitting an exponential function to the sonic transit times against shale unit mid-point depth (Z_{MP}) below seabed in order to define the exponential decay constant, *b*. It also considers simple boundary conditions related to physical rock properties such as the (constant) sonic transit time at initial deposition (Δt_0) and when depth, *Z*, approaches infinity (i.e. $Z \rightarrow \infty$), Δt approaches the (asymptotic) mineral matrix sonic transit time, *C* (Corcoran & Mecklenburgh 2005; Japsen *et al.* 2007b). In this instance, Z_{MP} is equivalent to the depth at maximum burial, B_{max} and the exponential function for the sonic transit time baseline ($\Delta t_{baseline}$) thus takes the form:

$$\Delta t_{baseline} = (\Delta t_0 - C)e^{-b \times B_{\max}} + C \qquad (3)$$

Logarithmically transforming the exponential function to:

$$\ln(\Delta t_{baseline} - C) - \ln(\Delta t_0 - C) = -b \times B_{\max} \qquad (4)$$

yields a linear expression where a least squares regression can be applied to determine the exponential decay constant *b* for an optimized *C* value (Fig. 8c). We assume the sonic transit time at initial deposition to be $\Delta t_0 \approx 206$ μs ft^{-1} for Shetland Group shale units, similar to that used by Japsen *et al.* (2007b) for Jurassic marine shales in the North Sea Basin.

Using least squares regression, we optimised the exponential decay constant *b* in order to yield the highest R^2 values. A maximum R^2 value of 0.9337 was achieved when $C \approx 48$ μs ft^{-1} and $b = 0.0004410$ m^{-1}. We hereafter refer to the baseline based on these parameters as the 'best-fit' baseline (Fig. 8d). This estimation of the mineral matrix sonic transit time is much less than that obtained by Japsen (2000) for the Jurassic marine shales in the North Sea Basin ($C \approx 56$ μs ft^{-1}) and reflects that our dataset is poorly constrained within deeper sections, whereas Japsen (2000) based his shale baseline on data between 1500 and 3500 m depth. Nevertheless, the similarity in *b* in comparison to Japsen (2000)'s *b* value (~0.0004598 m^{-1}) for the Jurassic marine shale in the North Sea Basin over our shorter constrained depth range may indicate that the normal sonic transit time-depth trend reflects physical parameters of a distinct lithological composition rather than depending on age or basin locality. Hence, we reduced another degree of freedom by considering the case when both Δt_0 and C were fixed constraints and assumed $C \approx 56$ μs ft^{-1}, similar to that obtained for Jurassic North Sea marine shales (Japsen *et al.* 2007b). The baseline based on these constraints is hereafter referred to as the 'constrained' baseline. This yielded a *b* value of 0.0004865 m^{-1} ($R^2 = 0.9313$), which only slightly differs from the best-fit baseline. For depths less than 3 km, both baselines appear to be nearly identical (Fig. 8a).

The sonic transit time-depth functions for these two constructed baselines are shown in Table 1 and the range between the two functions is represented in Fig. 8 and Fig. 9. We emphasise once more that compaction-based estimates of exhumation magnitude depend critically on the form of the baseline, which is often subject to uncertainty. Most previous compaction-based exhumation studies have defined a unique, empirically derived baseline function from which they quote an absolute estimate of exhumation, the standard deviation of the exhumation estimate, and broader error associated with the uncertainty in baseline definition (e.g. Ware & Turner, 2002). In our study, the baseline is poorly constrained at deeper intervals due to a lack of available and reliable data. To quantify this uncertainty we defined a zone of uncertainty associated with the depth interval difference between the upper and lower limits of the two constructed baselines (Figs. 8a, 9). The maximum depth interval difference within this zone of uncertainty is minor, being generally less than ~35 m. However, as sonic transit times decrease to less than ~80 μs ft^{-1} (corresponding to depths below ~3690 m bSB) the maximum depth interval difference rapidly increases, showing that Δt_{ave} are prone to larger uncertainties with increasing depth as a result of the baselines being poorly constrained below 2500 m bSB.

In Fig. 9 we compare the Shetland Group marine shale baselines with a number of published baselines for 'shales' of different age (Jurassic to Oligocene) and depositional origin (marine or terrestrial), but predominantly from North Sea and Norwegian margin basins (Hansen 1996; Japsen 2000; Storvoll *et al.* 2005; Japsen *et al.* 2007b; Tassone *et al.* 2013). As to be expected given the similarity in physical property values used (i.e. Δt_0 and C), our FSR Upper Cretaceous baselines most closely resemble the North Sea Basin Jurassic Marine Shale baseline. Nevertheless, the exponential decay constant values (i.e. b) are also similar, which likely reflects the similarity in shale mineral composition and geometry (i.e. both marine shales). For example, Jurassic marine shales of the North Sea Basin have estimated values for b = 0.0004598 m^{-1} by Japsen (2000) in comparison to b = 0.0004410-0.0004865 m^{-1} in this study. It is also worth noting the significant difference between the baseline trends of the two terrestrial shale stratigraphic units (Japsen 2000; Tassone *et al*. 2013) in comparison with the marine shale baseline trends (Hanson 1996; Japsen 2000; Storvoll *et al*. 2005). If the fluvial shale trend of Tassone *et al.* (2013) was used instead the C-M-D baseline trend, which loses porosity more rapidly at only moderate depth of ~ 1500 m below ground level due to its volcanogenic composition, then exhumation magnitudes within the FSR maybe significantly under-estimated (~980 m vertical difference at Δt = 110 μs ft^{-1}) or indicating perhaps undercompaction rather than overcompaction. This again highlights the importance of establishing a correct baseline trend.

6 RESULTS

6.1 Sonic Transit Time-depth Relationships for C-M-D Marine Shales of the Shetland Group

Average shale unit sonic transit times (Δt_{ave}) for Shetland Group marine shales in wells within the northeastern, central and southwestern areas of the FSR are plotted against shale unit midpoint depth (Z_{MP}) with respect to seabed in Fig. 10 as well as the 'best-fit' and 'constrained' baselines and the zone of baseline uncertainty.

It is clear that Δt_{ave} values in C-M-D shales in wells from within the southwest FSR in Fig. 10a plot consistently vertically above the baseline trends (e.g. wells 202/08-1 and 205/21-1A). This indicates that the C-M-D shales in these wells are overcompacted and have likely been buried more deeply in the past than they are today and thus must have been exhumed. In contrast, Δt_{ave} values from C-M-D shales in wells located within the northeast FSR plot very close to the baseline trends (e.g. wells 219/28-1 and 219/20-1; Fig. 10c), indicating that the post-Danian stratigraphic units in these wells are likely to be presently at, or very close to, their maximum burial depths. The C-M-D shales in wells within the central FSR reveal some degree of variation in compaction, with shale units exhibiting overcompaction (e.g. wells 206/07-1 and 206/05-1), albeit less than within the southwestern FSR, as well as undercompaction (e.g. wells 214/27-1 and 214/28-1; Fig. 10b).

The majority of Δt_{ave} data from across the entire FSR plot in trends similar (i.e. parallel) to the baselines with increasing depth, although the C-M-D shale units in a number of wells do vary slightly. Similar to when constructing the baselines using Δt_{ave} data from well 219/20-1, reversals in the Δt_{ave} data trends can be seen in wells 209/06-1 and 208/17-1 in the northeast FSR (Fig. 10c). Whilst this may indicate a ~500 m interval overpressured shale compartment section, it also may simply reflect changes in lithology. Additional pressure and mineralogical data were not available from these wells; therefore, we cannot conclusively determine the origin of any overpressures. An exception from within the northeast FSR is well 219/27-1 in which the C-M-D Δt_{ave} values are anomalously high for their given depth, plotting substantially below the baselines at depths shallower than ~2500 m bSB. Drilling data from this well report a pore pressure indicator (i.e. a minor connection gas) from a fractured limestone stringer at ~2270 m bSB within the Campanian sequence. This suggests that formation pore pressures are near-hydrostatic with an equivalent mud weight of ~9.4 pounds per gallon (ppg), and it is plausible that the Δt_{ave} data in this well is simply erroneous.

Another noteworthy observation is the lower gradient of Δt_{ave} data with depth in a number of wells, and the angle of their trends with respect to the constructed baselines (e.g. wells 202/03-2, 206/09-1, 206/09-2, 210/04-1 and 210/05-1). In addition to impacting the estimates of net exhumation, this suggests that the baseline trend for the C-M-D marine shale units does not simply follow an exponential trend in its entirety, but may in fact follow a step-wise trend similar to the terrestrial Triassic shales of the North Sea Basin as proposed by Japsen (2000) (Fig. 9). Japsen (2000) suggests that mechanical adjustment of flaky kaolin gains during compaction would lead to increased contact between the grains, which could explain the rapid increase in velocity (or rapid decrease in sonic transit time in our case) observed at burial depth of ~2000 m bSB. Since our constructed baselines are poorly constrained at depths shallower than ~1600 m bSB (Fig. 8a), it is difficult to conclude whether or not a similar step-wise change in normal sonic transit-depth trend occurs regionally throughout the FSR, or is perhaps instead due to local variations in mineral composition in the claystones or 'shales'.

Major reversal in the Δt_{ave} data trends also appear in the deepest C-M-D shales at well locations 214/27-1 and 214/28-1, located along the Flett High (Fig. 10b). Here, both the anomalously high Δt_{ave} data at the deepest depths and the Δt_{ave} data prior to the onset of reversal plot below the baselines (Fig. 10b). It is possible that the pre-reversal, Δt_{ave} data trend that plots parallel with the constructed baselines (Fig. 8, Table 1) may in fact represent a more constrained normal sonic transit time-depth baseline at depths deeper than ~3800 m bSB (Fig. 10b). For example, Δt_{ave} values at ~4000 m bSB in these wells are ~82 μs ft^{-1}, which does correlate reasonably well with sonic transit times of normally compacted Jurassic and Oligocene marine shales of the North Sea Basin and Norwegian margin predicted by the baseline trends of Japsen (2000) and Storvoll *et al.* (2005), respectively (Fig. 9). Despite this, the reversal in Δt_{ave} data to anomalously high values suggests undercompaction, which is a key indication of potential formation overpressure.

Similar to well 219/20-1,well 214/28-1 located on the Flett High penetrated a number of igneous sills that intrude Shetland Group shales and are differentiated by their low gamma ray and sonic transit time response (Fig. 11). Δt_{ave} values change abruptly at dolerite sill contacts suggesting sections of C-M-D stratigraphic sequences are compartmentalized. Gas influxes were recorded within two dolerite sill intervals, which consequently forced drilling mud weights to be raised to ~13.4 ppg (or ~16.5 MPa km^{-1}). At ~4153 m bSB and ~4332 m bSB, connection gases were reported within the C-M-D section within the dolerite sills whilst drilling with (static) mud weights of 13.3 ppg and 13.6 ppg, respectively. This indicates that pore pressures in this section were high, supporting the undercompacted response of the sonic transit time data with respect to the constructed baselines. Whilst comparing drilling data with pore pressure predictions from sonic transit time data and understanding overpressure mechanisms is beyond the scope of this study, it is clear that more detailed igneous sill mapping combine with fracture mapping and basin modelling is need in this area to fully understand formation pore pressures within compartmentalised intervals (e.g. Holford *et al*. 2012; Rateau *et al*. 2013).

6.2 Estimating Net Exhumation Magnitudes

We calculated net exhumation magnitudes (E_N,) for each well that contained average shale unit sonic transit time data (Δt_{ave}) using the simple relationship described in Equation 1. This states that $B_{present\text{-}day}$ is equivalent to the shale unit midpoint depth, Z_{MP}, in metres below seabed and B_{max} is the maximum burial depth in metres (Fig. 12), which is determined by rearranging the baseline functions in Table 1 and Fig. 8 and substituting $\Delta t_{baseline}$ for Δt_{ave}:

$$E_N = \frac{\ln\left[(\Delta t_{ave} - C) \big/ (\Delta t_0 - C) \right]}{-b} - Z_{MP} \tag{5}$$

This yields a series of individual E_N estimates, the mean value of which gives an estimate of the average net exhumation magnitude (E_{N_ave}) for the C-M-D shales in that well. This was done using the values of Δt_0, C and b for both the 'best-fit' and 'constrained' baseline trends (Fig. 8, Table 1) and uncertainties for both constructed baselines were quantified at one standard error (*SE*) from E_{N_ave}. It can be seen in Fig. 8 that at depths deeper and shallower than ~2600 m bSB the 'constrained' baseline describes the lower and upper limit, respectively, of the zone of exhumation magnitude uncertainty (X) and vice-versa for the 'best-fit' baseline. Therefore, the entire uncertainty of E_N magnitudes associated for the C-M-D shales for each well depicted in Fig. 12 corresponds to the zone of uncertainty (X) defined by the estimates of E_{N_ave} for both of the constructed baselines as well as half the standard error (*SE*) of E_{N_ave} for both baselines depending if they bound the lower or upper limit of *X*. Note, the quoted uncertainties include all Δt_{ave} data, irrespective of overpressure and lithology variation.

Fig. 13 shows the spatial distribution of net exhumation magnitudes within the FSR for the C-M-D Shetland Group marine shales. For the purposes of illustration, net exhumation magnitudes plotted in Fig. 13 correspond to the average value of E_{N_ave} for that well (E_{N_well}) and can be associated with the mid-point of *X* in Fig. 12. The average, range and standard error values of net exhumation calculated for each well in this study are provided in Table 2, along with the number of data points used to estimate E_{N_ave}.

It can be seen in Fig. 12 and Fig. 13 that estimates of net exhumation increase from northeast to southwest throughout the FSR. Wells located in the Møre and Magnus basins, Erlend, Flett and Foula sub-basins, and Erlend and Flett Highs give values of net exhumation generally within ±100 m, which we interpret to mean that Shetland Group shales in these areas are presently at their maximum burial depths. A number of wells including 214/27-1, 214/28-1 and 219/27-1 exhibit significant negative burial anomalies (cf. Japsen 1999; Fig. 12). As discussed above, these may be indicative of undercompaction associated with overpressures or erroneous sonic transit time data (Japsen *et al.* 2007b) in some shale sections. Nevertheless, it is reasonable, to assume that the C-M-D shales in these wells are also presently at their maximum burial depth given that Δt_{ave} data for each of these wells lie near or on the baseline over given depths. If the Δt_{ave} data above significant sonic transit time reversals in wells 214/27-1 and 214/28-1 constrains better baselines for depths deeper than ~3800 m bSB (Fig. 10b), then the higher sonic transit time baseline values would consequently cause larger estimates of net exhumation to be calculated for the C-M-D shales in well 208/17-1. This is a result of the deepest Maastrichtian Δt_{ave} data below 4000 m bSB and less than ~75 μs ft^{-1}, where the zone of uncertainty (X) between the two constructed baselines becomes large. This is why this well has the largest value of X than any other well in this study, despite the fact that Danian Δt_{ave} data indicates near maximum burial conditions. Thus, given that the shallower section indicates maximum burial, the C-M-D shales within well 208/17-1 are also likely to be at maximum burial regardless of the minor exhumation amounts calculated.

The largest magnitudes of net exhumation occur in the North Rona Basin (~1000 m in 202/08-1), the southwestern region of the Rona High (~650 m in 205/21-1A), West Shetland Basin (~430 m in 205/23-1) and Solan Bank High (~410 m in 202/09-1) (Fig. 12 and Fig. 13). C-M-D shales in wells located on the central to north-eastern region of the Rona High and West Shetland Basin show moderate magnitudes of net exhumation between ~120-350 m (Fig. 12 and Fig. 13). While the cluster of wells near the Clair Field (oil and gas) are depicted in Fig. 13 to have exhumed C-M-D shales that lie within the 100-300 m and 300-500 m bins over a relatively short distance (~10-15 km), it can be seen in Table 2 and Fig. 12 that there is only actually <50 m difference in net exhumation estimates between wells 206/07-1, 206/08-2, 206/08-5 and 206/09-1 if well 206/09-2 is excluded. Although there is some scatter in the Maastrichtian Δt_{ave} data in well 206/08-2 (Fig. 10), the Maastrichtian Δt_{ave} data in well 206/08-5 defines a clear trend that is parallel with the constructed baseline whereas Δt_{ave} data in wells 206/09-1 and 206/09-2 are sub-parallel. As discussed above, this may due to over-simplified and less constrained exponential normal sonic transit time-depth baseline trend(s) at shallower depths, perhaps due to changes or differences in local claystone or 'shale' mineral compositions. If we consider disregarding the Maastrichtian Δt_{ave} data in well 206/09-2, then net exhumation magnitudes are estimated to be ~360 m, similar to the other nearby wells around the Clair Field (Fig. 12 and Fig. 13). Alternatively, disregarding the Campanian Δt_{ave} data in this well would suggest near-maximum burial (i.e. <50 m), which is why this well carries the largest uncertainty among these closely spaced wells (Fig. 12).

While the Rona Fault separates the Faroe-Shetland Basin (i.e. Foula and Flett sub-basins) from the north-western boundary of the Rona High horst block (Fig. 1 and Fig 4), it is interesting to highlight the differences between net exhumation estimates from both sides of this fault zone along strike from the northeast to southwest (Fig. 13). The Δt_{ave} data in well 208/26-1, which is located in the immediate hangingwall of the Rona Fault within the Foula sub-Basin, indicates the C-M-D strata has exhumed by ~410 (Fig. 12 and Fig. 13), although this is based on only 3 data points. Further southwest, within the immediate hangingwall to the Rona Fault, well 206/05-1, which has >65 data points, also indicates modest amounts of exhumation (~350 m). This is despite its close proximity to well 206/03-1, from which Δt_{ave} data was used to constrain the baselines (Fig. 12 and Fig. 13). Continuing southwest along the northern boundary of the Rona High towards it centre, well 206/11-1 located in the hangingwall of the Rona Fault has been estimated to have relatively minor amounts of net exhumation (~180 m) whereas well 205/20-1 located on the nearby Rona High has net exhumation magnitudes >310 m (Fig. 12 and Fig. 13). Finally, at the southwestern end of the Rona High, relatively significant amounts of net exhumation are observed in well 205/21-1A (~650 m), whereas immediately north of this location within the Foula sub-Basin and the hangingwall of the Rona Fault, the estimated net exhumation magnitude in well 205/22-1A is <300 m (Fig. 12 and Fig. 13). Based on our limited well control and assuming the present-day overcompaction occurred at maximum burial (i.e. subsequent later affects), it appears that net exhumation magnitudes along the footwall of the Rona Fault bounding the northwestern boundary of the Rona High horst block increase towards the southwest whilst in the immediate hangingwall zone of the Rona Fault within the Flett and Foula sub-basins, net exhumation magnitudes remain fairly constant or perhaps increase slightly towards the NE (Fig. 13).

It is worth reiterating that our estimates of net exhumation provide no information regarding the deeper burial in pre-Campanian sections. Hence, in the following section, we do not discuss our results with respect to possible Palaeozoic or Mesozoic exhumation episodes. Instead, we only discuss exhumation episodes subsequent to the Danian Stage in which our results provide constraints – otherwise referred to as post-Danian net exhumation or Cenozoic net exhumation. Furthermore, since our results describe deeper palaeoburial constraints, we often refer to our results as being at maximum burial prior to a subsequent exhumation event. In order to estimate the magnitude of gross exhumation or removed section, however, the timing of the key exhumation event from maximum burial needs to be known.

7 TIMING AND GROSS EXHUMATION MAGNITUDES

There is growing recognition that the Cenozoic stratigraphic record of the FSR records a complex tectonic history related to continental breakup and passive margin development (Stoker *et al.* 2005a,b,c; 2010). Our results contribute to this notion of a dynamic Cenozoic tectonic history by demonstrating significant and spatially variable net exhumation across structural highs and depocentres, with the largest magnitudes (between ~300 to 1000 m) observed in the southwest FSR (e.g. North Rona Basin, southwestern Rona High, West Shetland Basin and Solan Bank High). Because our sonic transit time analysis is only based on data from Campanian to Danian shales, the only possible temporal constraints on the chronology of exhumation is that it occurred subsequent to the Danian (i.e. younger than the age of the shales analysed in this study). This is because when a single stratigraphic succession is used in a compaction study, it is sensitive to only the maximum post-depositional burial depth of the unit in question, and is unable to resolve multiple burial episodes or the absolute timing of maximum burial (Japsen 2000; Corcoran & Doré 2005).

To convert values of net exhumation to estimate the total amount of section that has been removed since maximum burial following the onset of exhumation (i.e. gross exhumation, E_G), it is necessary to add the amount of re-burial (B_E in Equation 2) that has occurred subsequent to the exhumation phase. This, in turn, requires identification of the unconformity representing the period within which the missing section was deposited to maximum burial and then removed. In the following section, we attempt to delineate the likely timing of exhumation in the FSR associated with our net exhumation magnitudes, firstly by integrating our results with the regional stratigraphic constraints identified from seismic reflection mapping and secondly, by comparing our calculated gross exhumation magnitudes with constraints from thermal history (i.e. AFTA and VR) and seismic reflection data.

7.1 Integrating Regional Stratigraphic Constraints to Delineate the Timing of Maximum Burial

Recent studies of the Cenozoic tectonic development of the FSR and adjacent areas have identified four key syn- to post-rift tectonic phases (e.g. Maclennan & Jones 2006; Shaw Champion *et al.* 2008; Hartley *et al*. 2011; Davies *et al*. 2004; Stoker &Varming 2011; Andersen *et al*. 2000; Stoker 2002; Johnson *et al*. 2005; Stoker *et al.* 2005a,b,c; Ritchie *et al*. 2011; Praeg *et al.* 2005) (Fig. 3). In this section, we acknowledge the likelihood that one or more of these tectonic phases and associated unconformities could feasibly account for the distribution and magnitude of post-Danian net exhumation recorded by sonic transit time data. The four key tectonic phases and associated unconformities (Fig. 3) identified from well data and seismic-stratigraphic mapping that could have caused the observed exhumation are as follows:

1. Mid-/Late Paleocene to earliest Eocene tectonism in the FSR was a precursor to continental breakup. Over this interval (Selandian to early Ypresian), differential movements were linked to several phases of enhanced magmatic activity, including surface volcanism, the emplacement of numerous volcanic centres (with associated intrusions) and shallow sills (e.g. Fig. 8a and Fig. 11: Naylor *et al*. 1999; Passey & Hitchen 2011; Stoker & Varming 2011). It has been proposed that during a phase of late Thanetian uplift, the southern margin of the Faroe-Shetland Basin adjacent to the West Shetland High was raised up to 1000 m above sea-level, which then subsided rapidly below sea-level within 1-2 Myr (Hartley *et al.* 2011). During this time, sub-aerial exposure resulted in erosion of the unconformity at the top of the Lamba Formation (Fig. 3) of no more than 60 metres, or possibly up to 200 m in incised valleys (Smallwood & Gill 2002; Maclennan & Jones 2006; Hartley *et al.* 2011). The effects of this uplift phase were probably experienced over a wide area of the FSR (Naylor *et al*. 1999), including erosion of the previously erupted late Selandian to mid-Thanetian volcanic rocks of the Faroe Platform (the Beinisvørd and Lopra formations of Passey & Jolley 2009). However, despite the potentially large area affected by this uplift, its transient nature coupled with the minimal denudation associated with the resultant unconformity lead us to consider it unlikely that our estimates of Cenozoic net exhumation reflect this event.

2. Post-rift (i.e. Chron 21) Eocene tectonism affected large parts of the FSR (Fig. 3). Significant, albeit episodic, input of clastic material into the Faroe-Shetland Basin occurred during the Mid-/Late Eocene in response to differential uplift and erosion of the flank of the Faroe-Shetland Basin leading to the development of deltaic and shelf-margin clastic wedges. This tectonism affected different parts of the FSR at different times. For

example, the Faroe Platform, Munkagrunnur Ridge and West Shetland High were locally uplifted above sea level in the mid-Lutetian as the Judd inversion instigated, leading to the contemporary Eocene shelf being eroded with sediments reworked and transported further north in the Faroe-Shetland Basin where they were deposited as the Mid-Eocene basin floor fans (Robinson *et al*. 2004; Ölavsdöttir *et al*. 2010, 2013; Stoker & Varming 2011; Stoker *et al*. in press). Seismic reflection data shows that the deltaic and shelf-margin clastic wedges are the largest build-out of Cenozoic sediments from the West Shetland Platform prior to Plio-Pleistocene and have been variably deformed subsequently in other areas of the Faroe-Shetland Basin by early growth on compressional domes, such as the Judd and Westray anticlines since the Lutetian (Fig. 3: Ritchie *et al*. 2003, 2008; Davies *et al*. 2004; Smallwood 2004; Johnson *et al*. 2005; Stoker *et al*. 2005c, in press). It is difficult to infer a regional unconformity during this Mid to Late Eocene interval, though clastic wedge development in response to uplift and erosion of the Faroe Platform and West Shetland High is possibly associated with an intra-Lutetian Unconformity (ILU) around Chrons 20 and 21 (Fig. 3). This is similar to stratigraphic hiatuses seen elsewhere within the Rockall and Norway basins (Stoker *et al*. 2012; Gernigon *et al*. 2012), before compression and rapid deepening during the latest Eocene to earliest Oligocene developed the UEU in response to strongly differential subsidence (Praeg *et al*. 2005).

3. Oligocene to Mid-Miocene differential uplift and subsidence across the entire FSR (Fig. 3). This tectonic phase probably represents the most significant interval of change in the shape of the continental margin since breakup (Andersen *et al*. 2000; Ritchie *et al*. 2011; Stoker & Varming 2011). The most visible consequences of change are manifest by the present bathymetric highs of the Fugloy, Wyville Thomson and Munkagrunnur ridges (Fig. 1b: Johnson *et al*. 2005; Stoker *et al*. 2005a,b; Ritchie *et al*. 2011), whose development was coeval with basinal subsidence (e.g. Faroe-Shetland Basin) and the instigation of the

deep-water Faroe-Shetland and Faroe Bank channels and Faroe conduit (Fig.3: Stoker *et al*. 2005c; Stoker & Varming 2011). This development is expressed by the observation that the Eocene succession is folded about the axes of these structural highs, which were subsequently onlapped at increasingly higher angles by Oligocene and Lower to Middle Miocene deposits as the inversion of the ridges progressed (Johnson *et al*. 2005). This is illustrated particularly well at the Wyville Thomson Ridge–Faroe Bank Channel area, where seismic-stratigraphic evidence suggests that maximum enhancement of these inversion structures probably occurred in the Early to Mid-Miocene (Johnson *et al*. 2005, Stoker *et al*. 2005c). Differential uplift/subsidence of several kilometres resulted from this Oligocene to Mid-Miocene tectonic phase and the BNU and IMU unconformities developed in response to compressional tectonism in the latest Oligocene to early mid-Miocene (Fig. 3: Boldreel & Andersen 1993; Stoker *et al*. 2005c; Praeg *et al*. 2005). This interval also witnessed renewed growth of the Judd and Westray anticlines that resulted in broad-wavelength, low-amplitude inversion of the basin-fill (Ritchie *et al*. 2008).

4. Early Pliocene tilting of the West Shetland margin. Uplift and erosion of the margin and hinterland (i.e. West Shetland High) resulted in the initiation of northwesterly prograding sediment wedges and fans into the adjacent deep-water basin (e.g. Foula and Rona wedges: Stoker 2002; Stoker *et al.* 2005a,b). Pliocene-Pleistocene sediments attain thicknesses >700 m (i.e. >1200 ms TWT) in the north-eastern FSR towards the Møre Basin, where the majority of wells appear to be presently at their maximum burial depths based on our sonic transit time analysis (Fig. 12 and Fig. 13). For example at well 219/28-1 in the Møre Basin (Fig. 1), if the preserved Cenozoic succession represents continuous, cumulative burial throughout this interval, then without any additional palaeoburial constraints, the Cenozoic burial history would be similar to that illustrated in Fig. 14, which we have termed its 'default' burial history. If erosion in this part of the study area occurred in response to an

exhumation event prior to the Pliocene (e.g. Mid-/Late Eocene or Oligocene to Mid-Miocene), any evidence of this former deeper burial from sonic transit time data would have been overprinted during subsequent burial (Fig. 14). Hence, any evidence of erosion (i.e. gross exhumation) from seismic profile data in the northeastern part of the FSR, perhaps associated with the IPU (Fig. 3) or otherwise, therefore, must be less than the amount of rapid Pliocene-Pleistocene burial. Given that Pliocene-Pleistocene sediments appear to be largely preserved and relatively thick in southwestern and central parts of the FSR in the vicinity of the Rona and Foula wedges, we consider it unlikely that exhumation associated with this event could account for the anomalously low sonic transit times observed within the Shetland Group marine shales.

Based on the preceding considerations, we consider it most likely that the net exhumation magnitudes recorded by sonic transit time data occurred in response to either the Mid-/Late Eocene or Oligocene to Mid-Miocene tectonic phases described above, although a Mid-/Late Paleocene to earliest Eocene or Early Pliocene timing cannot be discounted based on our results. Thus, assigning the determined palaeoburial constraints to either one of these exhumation phases is not straightforward, especially in parts of the FSR where there is evidence for differential vertical movements (Ebdon *et al*. 1995; Dean *et al*. 1999; Lamers & Carmichael 1999) or where distinct unconformities merge to become composite unconformities (e.g. BNU and IMU; Stoker et al. 2005a).

7.2 Limitations to Quantifying Gross Exhumation Magnitudes within the Faroe-Shetland Region

Delineating the timing of exhumation and estimating gross exhumation magnitudes using a compaction-based approach requires a good understanding of the preserved Cenozoic stratigraphic succession and of unconformities within the Middle Eocene to Upper Miocene section that may correspond to the Mid-/Late Eocene or Oligocene to Mid-Miocene tectonic phases (Fig. 3). With this in mind, a couple of observations with respect to the available DECC chronostratigraphic database and published sequence seismic-stratigraphic maps that are used in this study are worth highlighting: 1) In many wells the upper Cenozoic section has not been sampled, and so Paleogene and Neogene sequences are often undifferentiated (e.g. wells 206/03-1 (Fig. 7), 206/10-1 (Fig. 2a), 206/09-2 (Fig. 2b)); 2) The assigned ages of the preserved strata are very variable in their precision. For example, the Eocene interval in well 219/28-1 located within the Møre Basin depocentre is differentiated into Lower, and Middle Eocene sequences, whereas in well 206/09-2 located along the central Rona High region the Eocene is undifferentiated (Fig. 2b).

While the preserved Eocene sequence in parts of the central and northeastern FSR depocentres is moderately thick (Fig. 4), most of our data comes from the margin of the Faroe-Shetland Basin (e.g. Rona High) and adjacent 'marginal' basins where the preserved Oligocene–Miocene succession, in particular, is generally thin or absent (Iliffe *et al.* 1999). Few wells test the entire post-rift succession, but the deeper-water Cenozoic basins (e.g. Faroe-Shetland Basin) provide clear evidence of significant sediment accumulation and onlap onto tilted stratigraphic sequences (e.g. Eocene deltaic and clastic wedges; Stoker *et al.* in press). These deep-water basins, where eroded clastic sediments have accumulated episodically throughout the Paleogene and Neogene, contain stratigraphic sequences with multiple unconformities (Stoker *et al.* in press). The age of the stratigraphic sequences and hiatuses within these deepwater basins have been precisely determined in the past due to the hydrocarbon potential of the clastic sediments (Davies *et al*. 2004). In contrast, the Cenozoic successions in the marginal basins have typically been regarded as overburden during past conventional hydrocarbon exploration and thus not examined in detail, but more importantly these basins did not accumulate as much sediment as the adjacent deepwater basins (Fig. 4).

Not only does this highlight the potential shortcomings of failing to recognise stratigraphic 'gaps' and potentially relevant unconformities that can be used to delineate the timing of exhumation, but this also means that it can be difficult to link net exhumation magnitudes identified in peripheral wells to specific unconformities that are better developed and observed in the adjacent basin. In the previous section, we discussed the complex Cenozoic tectonic history within the FSR in detail and highlighted that exhumation of the marginal basins has been clearly balanced by subsidence in the adjacent deep-water basins (i.e. during the Eocene and Miocene). There is also strong evidence for differential vertical movements on specific structures, as opposed to epeirogenic exhumation that affected the entire region (Ebdon *et al*. 1995; Dean *et al*. 1999; Lamers & Carmichael 1999). For these reasons, attempting to resolve the timing of maximum burial prior to exhumation based solely on our sonic transit analysis is very problematic. Furthermore, estimating gross exhumation magnitudes at all well locations where C-M-D shales are exhumed in response to either a Mid-/Late Eocene or Oligocene to Mid-Miocene tectonic phase is fraught with major uncertainty in wells where the Cenozoic stratigraphic sequences are poorly constrained.

7.3 Estimates of Gross Exhumation Magnitudes (Removed Section) at Key Locations

We found that estimating gross exhumation magnitudes at all well locations where C-M-D shales are exhumed, assuming either Mid-/Late Eocene or Oligocene to Mid-Miocene tectonic phases was too ambiguous given the general imprecision of the defined Cenozoic stratigraphy within our study area. Preliminary analyses using the available chronostratigraphic database (DECC) at the time of this study indicated that gross exhumation estimates could not be presented with confidence and results were potentially misleading both in terms of magnitude and distribution. Future sequence and bio-stratigraphic studies may be able to shed more light on this topic if integrated with our results.

In general, the application of compaction data to quantify gross exhumation magnitude dictates that greater magnitudes of gross exhumation are required to honour net exhumation constraints if maximum burial occurred earlier in the tectonic history. We now consider two well locations that provide some insights into the spatial variability of burial and exhumation within our study area: well 206/08-2 in the central Rona High region adjacent to the Foula sub-Basin and well 205/21-1A in the southwestern Rona High region adjacent to the Flett sub-Basin as well as the East Solan Basin (Fig. 1).

7.3.1 Central Rona High region

Gross exhumation magnitudes assuming a timing of exhumation during the Mid-/Late Eocene or Oligocene to Mid-Miocene tectonic phases are determined at well 206/08-2 in an attempt to reconcile the net exhumation magnitudes we observe in the vicinity of the Clair oil and gas field, within the central region of the Rona High marginal basin (Fig. 13). Here, the C-M-D shales have been exhumed by ~295 m and both well and seismic data indicate the presence of much thicker Paleocene to Oligocene section in comparison to the southwestern Rona High region (Fig. 4; Lamers & Carmichael 1999). Cenozoic sequences have often been undifferentiated in past studies of this region, including in this well where the preserved Eocene stratigraphic sequence is ~320 m thick and is overlain by ~310 m and ~295 m of preserved Oligocene and Pliocene to Holocene rocks, respectively (Fig. 15a). A simplified, 'default' burial history for well 206/08-1 that assumes no exhumation prior to the deposition of the ~925 m thick Cenozoic section is shown in (Fig. 15b). If we assume that the undifferentiated Eocene and Oligocene overburden sections are actually separated by an unconformity that has removed Upper Eocene rocks (Fig. 15a) that developed in response to a Mid-/Late Eocene tectonic phase, then erosion of ~900 m (i.e. gross exhumation) at this location is required to account for ~295 m of addition burial and ~605 m of post-exhumation re-burial (Fig. 15c). Such erosion and gross exhumation from maximum burial during this time is irrespective of any subsequent minor exhumation and burial events. Alternatively, if the timing of exhumation from maximum burial depths occurred in response to an Oligocene to Mid-Miocene tectonic phase then an additional ~590 m of Oligocene to Miocene section must have deposited and subsequently eroded prior to Pliocene–Holocene re-burial in order to honour the palaeoburial constraints placed by sonic transit time data (Fig. 15d). We note that without more precise differentiation of the overlying Eocene and Oligocene sections in this area, gross exhumation estimates in response to a Mid-/Late Eocene tectonic phase at this stage can only be speculated on.

7.3.2 Southwestern Rona High region

Mid-/Late Eocene and Oligocene to Mid-Miocene gross exhumation magnitudes are determined at well 205/21-1A to reconcile the net exhumation magnitudes observed within the southwestern Rona High marginal basin area. The C-M-D shales at this location indicate larger magnitudes of net exhumation (~650 m) in comparison to the central Rona High area (~300 m), and seismic reflection data reveals that Paleocene to Oligocene rocks are very thin to absent in comparison to further northeast along the Rona High (Fig. 4; Lamers & Carmichael 1999). The preserved post-Maastrichtian succession within well 205/21-1A comprises ~25 m of undifferentiated Miocene rocks overlain by ~150 m thick Pliocene to Pleistocene section (Fig. 16a). According to the DECC chronostratigraphic database, no Paleocene, Eocene or Oligocene rocks are preserved at this location (Fig. 16a). If the Campanian and Maastrichtian marine shales were presently at maximum post-depositional burial depths and the sonic transit time data did not offer any additional palaeoburial constraints, then the 'default' Cenozoic burial history plot would be similar to that shown in Fig. 16b. However, net exhumation of ~650 m recorded by the sonic transit time data suggests that the Campanian and Maastrichtian shales have been more deeply buried in the Cenozoic. At this location, assigning the timing of exhumation from maximum burial to either a Mid-/Late Eocene or Oligocene to Mid-Miocene tectonic phase makes little difference to the corresponding estimates of gross exhumation magnitude. This is due to the lack of Eocene and Oligocene stratigraphic units at this location (Fig. 16a), with estimates of gross exhumation magnitude calculated for a Mid-/Late Eocene or Oligocene to Mid-Miocene tectonic phase to be ~810 m (Fig. 16c) and ~835 m (Fig. 16d), respectively. In fact, exhumation from maximum burial depths occurring any time after the Maastrichtian and prior to the Miocene would yield similar values of gross exhumation similar during a Mid-/Late Eocene gross exhumation or potentially Paleocene gross exhumation event. The absence of Paleocene to Oligocene rocks at this location emphasises once more that the only possible temporal constraint achievable based solely on our sonic transit time analysis is that exhumation from maximum burial occurred subsequent to the Danian, or in this case, the Maastrichtian since Danian rocks are not preserved in well 205/21-1A.

Mid-/Late Eocene and Oligocene to Mid-Miocene gross exhumation magnitudes were calculated for wells 206/08-2 and 205/21-1A to provide representative palaeoburial constraints around the central and southwestern Rona High, respectively. Comparisons between gross exhumation magnitudes for either a Mid-/Late Eocene or Oligocene to Mid-Miocene tectonic phase can be seen in Fig. 17a, where the range of uncertainty is the same as for the corresponding estimate of net exhumation magnitude (Table 2). Maastrichtian shales occur close to seabed around the southwestern Rona High area at well 205/21-1A and there is little preserved Cenozoic burial, consequently causing estimates of gross exhumation magnitude to be similar (i.e. ~810-835 m) regardless of the assumption of the precise timing of maximum burial and subsequent exhumation (Fig. 17a). The central Rona High area near well 206/08-2, has better differentiation between potential Mid-/Late Eocene and Oligocene to Mid-Miocene gross exhumation magnitudes with estimates of ~900 m and ~590 m, respectively (Fig. 17a).

If the timing of gross exhumation following maximum burial occurred in response to a Mid-/Late Eocene tectonic phase, then the amount of section removed at both the central and southwestern Rona High areas would be broadly similar (Fig. 17b). This may suggest that uplift and erosion of the southwestern and central Rona High marginal basins from maximum burial depths occurred simultaneously and to the same extent before greater amounts subsidence and reburial occurred in the central Rona High area (Fig. 4). If the timing of gross exhumation following maximum burial occurred in response to an Oligocene to Mid-Miocene tectonic phase, however, then a greater magnitude of gross exhumation would have occurred at southwestern Rona High area in comparison the central Rona High marginal basin (Fig. 17c). This alternative scenario suggests that the southwestern Rona High area was differentially uplifted and more severely eroded following maximum burial depths in comparison to the central Rona High area, with the differential uplift possibly controlled by the underlying pre- and syn-rift structure. An alternative scenario is that the two regions were differentially exhumed following maximum burial at different times in response to different tectonic phases e.g. maximum burial and subsequent exhumation in the central Rona High area in response to an Oligocene to Mid-Miocene tectonic phase and maximum burial and subsequent exhumation in the southwestern Rona High area in response to a Mid-/Late Eocene tectonic phase, coincidently yielding broadly similar gross exhumation magnitudes (Fig. 17b,c).

7.4 Comparisons of Gross Exhumation Magnitudes with Thermal History and Seismic Reflection Data at Key Locations

Based on 2D seismic reflection data, Booth *et al.* (1993) suggested that where erosion was most severe, up to 1250 m of Eocene to Mid-Miocene strata has been eroded from the crest of the southwestern Rona High in the vicinity of well 205/21-1A. Whilst these authors concluded that erosion likely occurred during the Mid-Miocene, contemporaneous with minor reverse reactivation along Late Cretaceous to Paleocene-age fault systems, the lack of Eocene section at this location suggests that exhumation in response to a Mid-/Late Eocene tectonic phase is also possible. In comparison to our estimate of either Mid-/Late Eocene or Oligocene to Mid-Miocene gross exhumation at well 205/21-1A (~810 and ~835 m, respectively, from Fig. 16), the estimate of Eocene to Mid-Miocene erosion by Booth *et al*. (1993) based on seismic reflection data appears to overestimate the magnitude of removed section (Fig. 17a). However, Booth *et al*. (1993) suggested that up to 1250 m was removed from the crest of the southwestern Rona High, so their upper limit estimation may not be directly comparable at the 205/21-1A well location. Estimating new magnitudes of removed section from seismic reflection data (cf. Corcoran & Doré 2005; Corcoran & Mecklenburgh 2005) was beyond the scope of this study, and unfortunately, no published estimates of removed section based on have seismic reflection data are available for the central Rona High area for direct comparison with our results at well 206/08-2.

In principle, application of thermal history data (e.g. AFTA and VR data) in the wells showing appreciable amounts of exhumation should allow determination of the time at which exhumation began, as illustrated for example by Green & Duddy (2013). However, quantifying the timing and magnitude of Cenozoic exhumation in the FSR using thermal history data is not straightforward. This is because Cenozoic palaeothermal effects at many well locations are dominated by heating processes that are unrelated to deeper burial, such as advective heating by hot fluids and contact heating by igneous intrusions, most likely associated with late Cretaceous and Paleocene magmatism (Duddy *et al.* 1998; Parnell *et al.* 1999; Green *et al.* 1999; Baron *et al*. 2008). Heating due solely to deeper burial should produce a more or less linear palaeotemperature profile in AFTA and VR data, with a gradient similar to that of the present-day geotherm (i.e. as calculated from corrected bottom hole temperatures). Heating caused by elevated basal heat flow (possibly with some degree of deeper burial) will produce a broadly linear palaeotemperature profile, characterised by a higher gradient in comparison to the present-day gradient. Assuming that heterogeneities in lithology through the preserved and missing section are sufficient to smooth out any potential large-scale variations in thermal conductivity (Bray *et al.* 1992; Green *et al.* 2002), then extrapolation of linear palaeotemperature profiles fitted to the AFTA and VR data to an appropriate palaeosurface temperature can provide an estimate of the amount of missing section removed during exhumation (see Fig. 22 of Green & Duddy 2013).

Cenozoic palaeotemperatures estimated using AFTA and VR data from wells located along the central Rona High area (e.g. 206/08-7, 206/08-8, 206/10-1 (Fig. 2a), 206/09-2 (Fig. 2b)), mostly define distinctive non-linear to arcuate palaeotemperature profiles, that are diagnostic of transient lateral heating caused by hot flowing fluids (Duddy *et al.*1998; Parnell *et al.* 1999; Mark *et al.* 2008). This is also true for well 205/21-1A in the southwestern Rona High area in which VR data alone shows a more arcuate palaeotemperature profile in comparison to AFTA data (Fig. 18). If the Cenozoic palaeotemperatures around 100°C defined by VR values in well 205/21-1A (Parnell *et al.* 1999) were due to burial alone, more than 2000 m of additional Cenozoic burial and gross exhumation between 80 and 0 Ma would be required. This amount of gross exhumation is significantly greater than both our Mid-/Late Eocene or Oligocene to Mid-Miocene gross exhumation estimate of ~810-835 m (Fig. 16) and that of Booth *et al*. (1993) based on seismic reflection data (<1250 m) using a stratigraphical-type approach, showing that these palaeotemperatures cannot be explained by deeper burial.

Independent evidence for Cenozoic transient heating effects from hot fluids in wells along the Rona High and Faroe-Shetland Basin is provided by fluid inclusion data (Wycherley *et al.* 2003; Parnell *et al.* 2005; Baron *et al.* 2008). Cenozoic palaeotemperatures defined from AFTA, VR and fluid inclusion data in many wells are much higher than can be accommodated by the amounts of additional burial defined from the sonic transit time data (Parnell *et al.* 1999). This again highlights how transient hot fluids have masked any palaeothermal evidence of Cenozoic deeper burial. Thermal history data from such wells along the southwestern and central Rona High areas cannot therefore be used to provide any meaningful constraints on the timing of exhumation or magnitudes of removed section. Parnell *et al*. (2005) speculated that the release of hot flowing fluids may have been triggered by the Oligocene–Miocene inversion event, which may indirectly constrain the timing of exhumation if maximum burial and subsequent exhumation is indeed related to this inversion event.

Only in one well in the FSR (i.e. 204/19-1, located on the Westray High) have palaeotemperature data been attributed with confidence to the effects of deeper burial associated with the Eocene-Miocene unconformity (Fig. 19a; Parnell *et al.* 2005). Unfortunately, no C-M-D section is preserved in this well (Stoker & Ziska, 2011) so a direct comparison with sonic transit time data is not possible. The initial analysis of AFTA and VR data from this well by Green *et al.* (1999) concluded that all stratigraphic units are at maximum temperatures at the present day. However, revised and improved stratigraphic information provided by Iliffe *et al.* (1999) that defined an unconformity spanning the Mid-Eocene to Mid-Miocene, together with new AFTA and VR data from Paleocene core samples allowed Parnell *et al.* (2005) to estimate 630-950 m of additional burial and subsequent (gross) exhumation or removed section on this potentially composite unconformity (Fig. 19b). This range of gross exhumation magnitude (i.e. ~630-950 m) seems to accord with values determined from sonic transit times in this study, in particular from offset wells to the southeast such as well 205/21-1A around the southwestern Rona High area (Fig. 17a).

Fluid inclusion data indicating homogenization temperatures up to 200 °C in Paleocene–Eocene reservoir sandstones provide evidence for the passage of hot fluids through this section, but no evidence of this is recorded in AFTA and VR data, implying that fluid flow must have been extremely rapid and short-lived (< 100 yr: Parnell *et al.* 2005). Although Parnell *et al.* (2005) were able to estimate the magnitude of Cenozoic exhumation in this well they were unable to constrain the absolute timing of the onset of cooling recorded by AFTA, beyond determining that the Palaeocene samples must have cooled subsequent to the deposition of Mid-Eocene rocks underlying the unconformity in the well.

8 TECTONIC CONTROLS ON EXHUMATION

A key implication of our results is that a large thickness (>500 m) of mid-Cenozoic age rocks must have been deposited across parts of the West Shetland Basin, North Rona Basin and Rona High prior to their removal during exhumation, though determining the precise timing of maximum burial and subsequent exhumation is challenging at present due to the poorly resolved Cenozoic stratigraphic record in the FSR.

Booth *et al*. (1993) concluded that minor reverse motion (i.e. inversion) on Late Cretaceous to Paleocene fault systems (i.e. Rona Fault) during the Mid-Miocene was contemporaneous with uplift and erosion of the southwestern Rona High area, but acknowledged that the cause of the associated major unconformity was probably tectonic in origin. Boldreel & Andersen (1993) also reported a Miocene compressional deformation phase (in addition to late Paleocene-early Eocene and Oligocene compressional phases) within the Wyville-Thomson Ridge area; however, they suggested that this compression was driven by seafloor spreading in the North Atlantic through a combination of ridge push and rigid plate movements (Boldreel & Andersen 1993). Subsequent workers have also highlighted early to mid-Miocene compressional/transpressional deformation in the NE Faroe–Shetland Basin (e.g. Richie *et al*. 2003, 2008; Johnson *et al*. 2005) and Doré *et al.* (2008) suggested that the arcuate compressional deformation pattern along the NW European margin maybe associated with enhanced body forces due to the development of the Iceland Insular Margin.

Several recent regional tectonic studies have highlighted a major, complex reorganisation of the North Atlantic seafloor spreading system during mid-Cenozoic times, possibly instigated at chron 21/18 (Mid-Eocene), and intensified between chron 13 to about chron 6 (i.e. Oligocene to Mid-

Miocene), and the effect of this reorganisation on post-rift compressional deformation along the margin (Gaina *et al*. 2009; Gernigon *et al*. 2012). Significant components of this plate boundary reorganisation include the cessation of spreading in the Labrador Sea and along the Ægir Ridge in the Norway Basin; the shift from an orthogonal to an oblique spreading direction in the NE Atlantic; the separation of the Jan Mayen Microcontinent from Greenland; and the eventual linkage of the Reykjanes and Kolbeinsey ridges resulting in a single spreading system linking the Arctic and Atlantic Oceans (Gernigon *et al*. 2012). Based on palinspastic reconstructions of the North Atlantic seafloor, Le Breton *et al*. (2012), suggested that left-lateral reactivation of northwest trending transfer zones sub-parallel to the Faroe Fracture Zone probably initiated the compression deformation of the Fugløy Ridge during the Eocene and Oligocene. This more likely occurred during the Oligocene than the Eocene since significant erosion and growth on the Fugløy Ridge is interpreted to have occurred during this time from seismic reflection data (Ritchie *et al*. 2003). This also coincides with the dominant timing of major strike/slip reactivation of the Great Glen Fault bisecting onshore Scotland (Le Breton *et al*. 2103) and exhumation of NW Scotland (Holford *et al*. 2010; Fig. 3). Widespread erosion of Eocene and Oligocene stratigraphic sequences on the Faroes Platform during uplift and sea-level fall in the Late Oligocene also supports an Oligocene to Miocene timing (Sørensen 2003).

If maximum burial and subsequent localised exhumation in the southwestern FSR occurred during the broad interval spanning the Oligocene to Mid-Miocene, then it would represent another manifestation (combined with the growth of the Fugloy, Wyville-Thomson and Munkagrunnur ridges) of post-breakup restructuring along this section of the NE Atlantic margin. We interpret the exhumation and restructuring along the FSR segment of the NE Atlantic margin as a key example of post-breakup deformation of a passive margin driven by a change in dynamics of the adjacent ocean spreading system; this probably relates to the effects of compression on the margin driven by plate boundary forces responding to the plate readjustments described above, and which might have been further enhanced by the coeval development of the Iceland Insular Margin between the Reykjanes and Kolbeinsey Ridges (Boldreel & Andersen 1993; Doré *et al.* 2008 Gernigon *et al*. 2012; Stoker *et al*. 2012). We suggest that the spatial and temporal variations in Cenozoic differential movements within the FSR witness the variable responses of a complexly structured continental margin to fluctuating intraplate stress magnitudes and orientations primarily governed by the dynamics of the adjacent oceanic spreading system.

9 CONCLUSIONS

The basins in the Faroe-Shetland region along the NE Atlantic passive margin have witnessed a complex history of spatially and temporally variable post-breakup vertical motions (i.e. burial and exhumation) throughout the Cenozoic. Results of previous thermal history studies have been dominated by non-burial related heating processes, principally reflecting localised heating due to hot fluids (Fig. 2), and in most cases determining magnitudes of exhumation has not been possible. The compaction-based approach undertaken in this study is less susceptible to distortions from the effects of transient heating, and has provided new constraints on Cenozoic burial and exhumation magnitudes in the UK sector of the Faroe-Shetland region, using sonic transit time data from Upper Cretaceous marine shales of the Shetland Group.

The key outcomes of this study are as follows:

- New baseline trends constructed for the Campanian-Maastrichtian-Danian (C-M-D) marine shales in the Faroe Shetland region (Fig. 8) are consistent with published baseline trends for Jurassic marine shales from the nearby North Sea Basin (Fig. 9). This indicates that the baseline sonic transit time-depth trend is likely to reflect physical parameters of a distinct lithological composition rather than depending on age or basin locality. It can therefore be used with confidence to determine exhumation magnitudes in wells that are not currently at maximum burial depths in the FSR, in addition to estimating magnitudes of pore pressure using wireline log data (cf. Eaton 1972).

- In wells located in the Møre and Magnus basins, Erlend, Flett and Foula sub-basins, and Erlend and Flett highs, in the northeast FSR, the late Cretaceous to Cenozoic section is predominately at or near maximum burial depths at the present day (Fig. 12 and Fig. 13).
- The largest amounts of Cenozoic net exhumation (E_{N_well}) occur in the North Rona Basin, southwestern Rona High, southwestern West Shetland Basin and Solan Bank High in the southwestern FSR. Wells in these areas define net exhumation magnitudes between ~300-1000 m (Fig. 12 and Fig. 13), implying that large thicknesses of Cenozoic sediments were deposited and subsequently completely removed by exhumation in parts of this region following maximum burial.
- Determining the precise timing of maximum burial and exhumation from net exhumation results is problematic because of differential vertical movements as well as the complex and variable Cenozoic post-rift stratigraphy over the entire FSR. Calculated gross exhumation magnitudes are consistent with maximum burial and exhumation occurring during either the Mid-/Late Eocene or Oligocene to mid-Miocene (Fig. 17), with the latter representing our preferred timing on the basis of regional geological evidence. Gross exhumation magnitudes are also broadly consistent with estimates of removed section from thermal (Parnell *et al*. 2005) and seismic-stratigraphic approaches (Booth *et al*. 1993) nearby to the southwestern Rona High area. An early Palaeogene and late Neogene timing of maximum burial and exhumation, however, cannot be ruled out on our data alone and

future sequence and bio-stratigraphic studies is needed to shed more light on this topic if integrated with our results.

- If our net exhumation results in the southwestern FSR occurred during the broad interval spanning the Oligocene to Mid-Miocene, then it would represent another manifestation of perhaps the most important period of post-breakup restructuring along this section of the NE Atlantic margin. This exhumation and restructuring is also probably linked to a coeval and significant reorganisation of the northern North Atlantic spreading system (e.g. change in direction and speed), implying a causative relationship between post-breakup passive margin deformation and a change in dynamics of an adjacent ocean spreading system.

10 ACKNOWLEDGEMENTS

This work forms part of ARC Discovery Project DP0879612, ASEG Research Foundation Project RF09P04 and represents TRaX contribution 259. We thank Sandy Henderson for his assistance with data loading, and gratefully acknowledge the British Geological Survey for access to well-log data and hospitality. The contribution of Stoker and Johnson are made with the permission of the Director of the British Geological Survey (Natural Environmental Research Council).

11 REFERENCES

ANDERSEN, M.S., NIELSEN, T., SØRENSEN, A.B., BOLDREEL, L.O. & KUIJPERS, A. (2000) Cenozoic sediment distribution and tectonic movements in the Faroe region. *Global and Planetary Change*, **24**, 239–259.

BARON, M., PARNELL, J., MARK, D., CARR, A., PRZYJALGOWSKI, M. & FEELY, M. (2008) Evolution of hydrocarbon migration style in a fractured reservoir deduced from fluid inclusion data, Clair Field, West of Shetland, UK. *Marine and Petroleum Geology*, **25**, 153–172.

BOOTH, J., SWIECICKI, T. & WILCOCKSON, P. (1993) Tectono-stratigraphy of the Solan Basin, west of Shetland. In: *Petroleum Geology of Northwest Europe: Proceedings of the 4th Conference* (Ed. by J.R. Parker), 987–998. *The Geological Society, London*.

BOLDREEL, L.O. & ANDERSEN, M.S. (1993) Late Paleocene to Miocene compresseion in the Faereo-Rockall area. In: *Petroleum Geology of Northwest Europe: Proceedings of the 4th Conference* (Ed. by J.R. Parker), 1025–1034. *The Geological Society, London*.

BRAY, R.J., GREEN, P.F. & DUDDY, I.R. (1992) Thermal History Reconstruction using apatite fission track analysis and vitrinite reflectance: a case study from the UK East Midlands and the Southern North Sea. In: *Exploration Britain: Into the next decade* (Ed. by R.F.P Hardman), *Geol. Soc. London, Spec. Publ.*, **67**, 3–25.

CERAMICOLA, S. STOKER, M.S., PRAEG, D., SHANNON, P.M., DE SANTIS, L., HOULT, R., HJELSTUEN, B.O., LABERG, S. & MATHIESEN, A. (2005) Anomalous Cenozoic subsidence along the ‘passive’ continental margin from Ireland to mid-Norway. *Marine and Petroleum Geology*, **22**, 1045–1067.

CLIFT, P.D. & TURNER, J. (1998) Paleogene igneous underplating and subsidence anomalies in the Rockall-Faeroe-Shetland area. *Marine and Petroleum Geology*, **15**, 223–243.

CORCORAN, D.V. & DORÉ, A.G. (2005) A review of techniques for the estimation of magnitude and timing of exhumation in offshore basins. *Earth-Science Reviews*, **72**, 129–168.

CORCORAN, D.V. & R. MECKLENBURGH (2005) Exhumation of the Corrib Gas Field, Slyne Basin, offshore Ireland. *Petroleum Geoscience*, **11**, 239–256.

DAVIES, R., CLOKE, I., CARTWRIGHT, J., ROBINSON, A. & FERRERO, C. (2004) Post-breakup compression of a passive margin and its impact on hydrocarbon prospectivity: an example from the Tertiary of the Faore-Shetland Basin, United Kingdom. *AAPG Bulletin*, **88**, 1–20.

DEAN, K., MCLACHLAN, K. & CHAMBERS, A. (1999) Rifting and the development of the Faeroe-Shetland Basin. In: *Petroleum Geology of Northwest Europe: Proceedings of the 5th Conference* (Ed. by A.J. Fleet, & S.A.R. Boldy), 533–544. *The Geological Society, London*.

DORÉ, A.G. & JESNEN, L.N. (1996) The impact of late Cenozoic uplift and erosion on hydrocarbon exploration: offshore Norway and some other uplifted basins. *Global and Planetary Change*, **12**, 415–436.

DORÉ, A.G., LUNDIN, E.R., JENSEN, L.N., BIRKELAND, O., ELIASSEN, P.E. & FICHLER, C. (1999) Principal tectonic events in the evolution of the northwest European Atlantic margin. In: *Petroleum Geology of Northwest Europe: Proceedings of the 5th Conference* (Ed. by A.J. Fleet, & S.A.R. Boldy), 41–61. *The Geological Society, London*.

DORÉ, A.G., CORCORAN, D.V. & SCOTCHMAN, I.C. (2002) Prediction of the hydrocarbon system in exhumed basins, and application to the NW European margin. In: *Exhumation of the North Atlantic Margin: Timing, Mechanisms and Implications for Petroleum*

Exploration (Ed. by Doré, A.G., Cartwright, J.A., Stoker, M.S., Turner, J.P. & N.J. White), *Geol. Soc. London, Spec. Publ.,* **196**, 401–429.

DORÉ, A.G., LUNDIN, E.R., KUSZNIR, N.J. & PASCAL, C. (2008) Potential mechanisms for the genesis of Cenozoic domal structures on the NE Atlantic margin: pros, cons, and some new ideas. In: *The nature and origin of compression in passive margins* (Ed. Johnson, H., Doré, A.G., Gatliff, R.W., Holdsworth, R., Lundin, E.R. & Ritchie, J.D.), *Geol. Soc. London, Spec. Publ.,* **306**, 1–26.

DUDDY, I.R., GREEN, P.F., HEGARTY, K.A, BRAY, R.J. & O'BRIEN, G.W. (1998) Dating and duration of hot fluid flow events determined using AFTA® and vitrinite reflectance-based thermal history reconstruction: In: *Dating and Duration of Hot Fluid Flow and Fluid-Rock Interaction.* (Ed. by Parnell, J.), *Geol. Soc. London, Spec. Publ.,* **144**, 41–51.

EATON, B.A., (1972) Graphical method predicts geopressures worldwide. *World Oil*, **183**, 51–56.

EBDON, C.C., GRANGRE, P.J., JOHNSON, H.D. & EVANS, A.M. (1995) Early Tertiary evolution and sequence stratigraphy of the Faroe-Shetland Basin: implications for hydrocarbon prospectivity: In: *Tectonic, sedimentation and palaeoceanography of the North Atlantic region* (Ed. Scrutton, R.A., Stoker, M.S., Shimmield, G.B. & Tudhope, A.W.), *Geol. Soc. London, Spec. Publ.,* **90**, 51–69.

ELLIS, D. & STOKER, M.S. (in press) The Faroe-Shetland Basin: A regional perspective from the Palaeocene to the Present day and its relationship to the opening of the North Atlantic Ocean: In: *Hydrocarbon Exploration and Exploitation West of Shetlands* (Ed. Cannon, S.J.C. & Ellis, D.) *Geol. Soc. London, Spec. Publ.*

EVANS, D.J. (1997) Estimates of the eroded overburden and the Permian-Quaternary subsidence history of the area west of Orkney. *Scottish Journal of Geology*, **33**, 2, 169–182.

FOULGER, G.R. (2002) Plumes, or plate tectonic processes? *Astronomy & Geophysics*, **43** (6), 19–23.

GAINA, C., GERNIGON, L. & BALL, P. (2009) Palaeocene-Recent plate boundaries in the NE Atlantic and the formation of the Jan Mayen microcontinent. *Journal of the Geological Society, London*, **166**, 601–616.

GERNIGON, L., GAINA, C., OLESEN, O., BALL, P.J., PÉRON-PINVIDIC, G. & YAMASAKI, T. (2012) The Norway Basin revisited: From continental breakup to spreading ridge extinction. *Marine & Petroleum Geology*, **35**, 1–19.

GIBB, F.G.F., KANARIS-SOTIRIOU, R. & NEVES, R. (1986) A new Tertiary sill complex of mid ocean ridge basalt type NNE of the Shetland Islands: a preliminary report. *Transactions of the Royal Society of Edinburgh: Earth Sciences*, **77**, 223–230.

GILES, M.R., S.L. INDRELID, & JAMES, D.M.D. (1998) Compaction - the great unknown in basin modelling, In: *Basin Modelling: Practice and Progress* (Ed. by Duppenbecker, S.J. & J.E. Iliffe), *Geol. Soc. London, Spec. Publ.*, **141**, 15–43.

GRADSTEIN, F.M., OGG, J.G., SCHMITZ, M. & OGG, G. (2012) A Geologic Time Scale 2012. Cambridge University Press, Cambridge.

GREEN, P.F. & DUDDY, I.R. (2013) Thermal history reconstructions in sedimentary basins using apatite fission-track analysis and related techniques. *SEPM Special Publication*, **103**, 65–104.

GREEN, P.F., DUDDY, I.R., HEGARRTY, K.A. & BRAY, R.J. (1999) Early Tertiary heat flow along the UK Atlantic margin and adjacent areas. In: *Petroleum Geology of Northwest Europe: Proceedings of the 5th Conference* (Ed. by A.J. Fleet, & S.A.R. Boldy), 349–357. *The Geological Society, London*.

GREEN, P.F., DUDDY, I.R. & HEGARRTY, K.A. 2002 Quantifying exhumation from apatite fission-track analysis and vitrinite reflectance data: precision, accuracy and latest results from the Atlantic margin of NW Europe. In: *Exhumation of the North Atlantic Margin: Timing, mechanisms and Implications for Petroleum Exploration* (Ed. by Doré, A.G., Cartwright, J., Stoker, M.S., Turner, J.P. & N. White), *Geol. Soc. London, Spec. Publ.*, **196**, 331–354.

HANSEN, S. (1996) A compaction trend for Cretaceous and Tertiary shales on the Norwegian Shelf based on sonic transit times. *Petroleum Geoscience*, **2**, 159–166.

HARTLEY, R.A., ROBERTS, G.A., WHITE, N. & RICHARDSON, C. (2011) Transient convective uplift of an ancient buried landscape. *Nature Geoscience*, **4**, 562–565.

HEASLER, H.P. & KAHARITONOVA, N.A. (1996) Analysis of sonic well logs applied to erosion estimates in the Bighorn Basin, Wyoming. *AAPG Bulletin*, **80**, 630–646.

HILLIS, R.R. (1995a) Regional Tertiary Exhumation in and around the United Kingdom. In: *Basin Inversion* (Ed. Buchanan, J.G. & Buchanan, P.G.), *Geol. Soc. London, Spec. Publ.*, **88**, 167–190.

HILLIS, R.R. (1995b) Quantification of Tertiary exhumation in the United Kingdom southern North Sea using sonic velocity data. *AAPG Bulletin*, **79**, 1, 130–152.

HILLIS, R.R., K. THOMSON, & UNDERHILL, J.R. (1994) Quantification of Tertiary erosion in the Inner Moray Firth using sonic velocity data from the Chalk and Kimmeridge Clay. *Marine and Petroleum Geology*, **11**, 283–293.

HOLFORD, S.P., GREEN, P.F., TURNER, J.P., WILLIAMS, G.A., HILLIS, R.R., TAPPIN, D.R. & DUDDY, I.R. (2008) Evidence for kilometre-scale Neogene exhumation driven by compressional deformation in the Irish Sea basin system. In: *The nature and origin of* *compression in passive margins* (Ed. Johnson, H., Doré, A.G., Gatliff, R.W., Holdsworth, R., Lundin, E.R. & Ritchie, J.D.), *Geol. Soc. London, Spec. Publ.*, **306**, 91–119.

HOLFORD, S.P., TURNER, J.P., GREEN, P.F. & HILLIS, R.R. (2009) Signature of cryptic sedimentary basin inversion revealed by shale compaction data in the Irish Sea, western British Isles. *Tectonics*, **28**, TC4011, doi:10.1029/2008TC002359.

HOLFORD, S.P., GREEN, P.F., HILLIS, R.R., UNDERHILL, J.R., STOKER, M.S. & DUDDY, I.R. (2010) Multiple post-Caledonian exhumation episodes across NW Scotland revealed by apatite fission-track analysis. *Journal of the Geological Society, London*, **167**, 675–694, doi:10.1144/0016-76492009-167.

HOLFORD, S.P., SCHOFIELD, N., MACDONALD, J.D., DUDDY, I.R. & GREEN, P.F. (2012) Seismic analysis of igneous systems in sedimentary basins and their impacts on hydrocarbon prospectivity: examples from the southern Australian margin. *APPEA Journal*, **52**, 229–252.

ILIFFE, J.E., ROBERTSON, A.G., WARD, G.H.F., WTNN, C., PEAD, S.D.M. & CAMERON, N. (1999) The importance of fluid pressure and migration to the hydrocarbon prospectivity of the Faroe-Shetland White Zone. In: *Petroleum Geology of Northwest Europe: Proceedings of the 5th Conference* (Ed. by A.J. Fleet, & S.A.R. Boldy), 601–611. *The Geological Society, London*.

JAPSEN, P. (1998) Regional velocity-depth anomalies, North Sea Chalk: a record of overpressure and Neogene uplift and erosion. *AAPG Bulletin*, **82**, 2031–2074.

JAPSEN, P. (1999) Overpressured Cenozoic shale mapped from velocity anomalies relative to a baseline for marine shale, North Sea. *Petroleum Geoscience*, **5**, 321–336.

JAPSEN, P. (2000) Investigation of multi-phase erosion using reconstructed shale trends based on sonic data. Sole Pit axis, North Sea. *Global and Planetary Change*, **24**, 189-210.

JAPSEN, P. & CHALMERS, J.A. (2000) Neogene uplift and tectonics around the North Atlantic: overview. *Global and Planetary Change*, **24**, 165–173.

JAPSEN, P., BIDSTRUP, T. & LIDMAR-BERGSTRM, K. (2002) Neogene uplift and erosion of southern Scandinavia induced by the rise of the South Swedish Dome. In: *Exhumation of the North Atlantic Margin: Timing, Mechanisms and Implications for Petroleum Exploration* (Ed. by Doré, A.G., J.A. Cartwright, M.S. Stoker, J.P. Turner, & N.J. White), *Geol. Soc. London, Spec. Publ.,* **196**, 183–207.

JAPSEN, P., GREEN, P.F., NIELSEN, L.H., RASMUSSEN, E.S. & BIDSTRUP, T. (2007a) Mesozoic-Cenozoic exhumation events in the eastern North Sea Basin: a multi-disciplinary study based on palaeothermal, palaeoburial, stratigraphic and seismic data. *Basin Research*, **19**, 451–490.

JAPSEN, P., MUCKERJI, T. & MAVKO, G. (2007b) Constraints on velocity-depth trends from physics models. *Geophysical Prospecting*, **55**, 135–154.

JAPSEN, P., BONOW, J.M., GREEN, P.F., COBBOLD, P.R., CHIOSSI, D., LILLETVEIT, R., MAGNAVITA, L.P. & PEDREIRA, A. (2012) Episodic burial and exhumation in NE Brazil after opening of the South Atlantic. *Geological Society of America Bulletin*, doi:10.1130/B30515.1

JOHNSON, H. RITCHIE, J.D., HITCHEN, K., MCINROY, D.B. & KIBELL, G.S. (2005) Aspects of the Cenozoic deformation history of the Northeast Faroe-Shetland Basin, Wyville-Thomsen Ridge and Hatton Bank areas. In: *Petroleum Geology: North-west Europe and Global Perspectives – Proceedings of the 6th Conference* (Ed. by A.J. Døre & B.A. Vining), 993–1007. *The Geological Society, London*.

JONES, S.M., WHITE, N. & LOVELL, B. (2001) Cenozoic and Cretaceous transient uplift in the Porcupine Basin and its relationship to a mantle plume. In: *The Petroleum Exploration of*

Ireland's Offshore Basins (Ed. by Shannon, P.M., Haughton, P.D.W. & D.V. Corcoran), *Geol. Soc. London, Spec. Publ.*, **188**, 345–360.

JONES, S.M., WHITE, N., CLARKE, B.J., ROWLEY, E. & GALLAGHER, K. (2002) Present and past influence of the Iceland Plume on sedimentation. In: *Exhumation of the North Atlantic Margin: Timing, Mechanisms and Implications for Petroleum Exploration* (Ed. by Doré, A.G., Cartwright, J.A., Stoker, M.S., Turner, J.P., & N. White), *Geol. Soc. London, Spec. Publ.*, **196**, 13–25.

KNOX, R.W.O'B., HOLLOWAY, S., KIRBY, G.A. & BAILEY, H.E. (1997) Stratigraphic nomenclature of the UK North West Margin. 2. Early Palaeogene lithostratigraphy and sequence stratigraphy. (Keyworth, Nottingham: British Geological Survey).

LAMERS, E. & CARMICHAEL, S.M.M. (1999) The Paleocene deepwater sandstone play West of Shetland. In: *Petroleum Geology of Northwest Europe: Proceedings of the 5th Conference* (Ed. by A.J. Fleet, & S.A.R. Boldy), 645–659. *The Geological Society, London*.

LARSEN, M., RASMUSSEN, T. & HJELM, L. (2010) Cretaceous revisited: exploring the syn-rift play of the Faroe–Shetland Basin. In: *Petroleum Geology – From Mature Basins to New Frontiers: Proceedings of the 7th Conference* (Ed. by B.A. Vining & S.C. Pickering), 953–962. *The Geological Society, London*.

LE BRETON, E., COBBOLD, P.R., DAUTEUIL, O. & LEWIS, G. (2012) Variations in amount and direction of sea-floor spreading along the North East Atlantic Ocean and resulting deformation of the continental margin of North West Europe. *Tectonics*, **31**, TC5006, doi:10.1029/2011TC003087.

LE BRETON, E., COBBOLD, P.R. & ZANELLA, A. (2013) Cenozoic reactivation of the Great Glen Fault, Scotland: additional evidence and possible causes. *Journal of the Geological Society*, **170** (3), 403–415.

LOVELL, B. (2010) *A pulse in the planet: regional control of high-frequency changes in relative sea level by mantle convection. Journal of the Geological Society, London*, **167** (4), 637–648.

LUNDIN, E. & DORÉ, A.G. (2002) Mid-Cenozoic post-breakup deformation in the ‘passive’ margins bordering the Norwegian-Greenland Sea. *Marine and Petroleum Geology*, **19**, 79–93.

LUNDIN, E. & DORÉ, A.G. (2005) NE Atlantic break-up: a re-examination of the Iceland mantle plume model and the Atlantic–Arctic linkage. In: *Petroleum Geology: North-west Europe and Global Perspectives – Proceedings of the 6th Conference* (Ed. by A.J. Døre & B.A. Vining), 739–754. *The Geological Society, London*.

MACKAY, L.M. & WHITE, N.J. (2006) Accurate estimates of the spatial pattern of denudation by inversion of stacking velocity data: an example from the British Isles. *Geochemistry Geophysics, Geosystems,* **7** (10). Art. No. Q10007.

MACLENNAN, J. & JONES, S.M. (2006) Regional uplift, gas hydrate dissociation and the origins of the Paleocene–Eocene Thermal Maximum. *Earth and Planetary Science Letters*, **245**, 65–80.

MAGARA, K., (1978) Compaction and Fluid Migration. *Practical Petroleum Geology*. Elsevier, Amsterdam.

MARK, D., GREEN, P.F., PARNELL, J., KELLY, S.P., LEE, M.R. & SHERLOCK, S.C. (2008) Late Palaeozoic hydrocarbon migration through the Clair field, West of Shetland, UK Atlantic margin. *Geochimica et Cosmochimica Acta*, **72**, 2510–2533.

MOSAR, J., LEWIS, G. & TORSVIK, T.H. (2002) North Atlantic sea-floor spreading rates: implications for the Tertiary development of inversion structures of the Norwegian-Greenland Sea. *Journal of the Geological Society, London*, **159**, 503–515.

MOY, D.J. & IMBER, J. (2009) A critical analysis of the structure and tectonic significance of rift-oblique lineaments (‘transfer zones’) in the Mesozoic–Cenozoic succession of the Faroe–Shetland Basin, NE Atlantic margin. *Journal of the Geological Society*, *London*, **166**, 831–844.

NAYLOR, P.H., BELL, B.R., JOLLEY, D.W., DURNALL, P. & FREDSTED, R. (1999) Palaeogene magmatism in the Faeroe–Shetland Basin: influences on uplift history and sedimentation. In: *Petroleum Geology of Northwest Europe: Proceedings of the 5th Conference* (Ed. by A.J. Fleet, & S.A.R. Boldy), 545–558. *The Geological Society, London*.

ÓLAVSDÓTTIR, J., BOLDREEL, L.O. & ANDERSEN, M.S. (2010) Development of a shelf margin delta due to uplift of the Munkagrunnur Ridge at the margin of Faroe-Shetland Basin: a seismic sequence stratigraphic study. *Petroleum Geoscience*, **16**, 91–103.

ÓLAVSDÓTTIR, J., ANDERSEN, M.S. & BOLDREEL, L.O. (2013) Seismic stratigraphic analysis of the Cenozoic sediments in the NW Faroe Shetland Basin – Implications for the inherited structural control of sediment distribution. *Marine & Petroleum Geology*, **46**, 19–35.

OSBORNE, M.J. & SWARBRICK, R.E. (1997) Mechanisms for generating overpressure in sedimentary basins: a re-evaluation. *AAPG Bulletin*, **81** (6), 1023–1041.

PARNELL, J., CAREY, P. F., GREEN, P.F. & DUNCAN, W. (1999) Hydrocarbon migration history, West of Shetland: integrated fluid inclusion and fission track studies. In: *Petroleum Geology of Northwest Europe: Proceedings of the 5th Conference* (Ed. by A.J. Fleet, & S.A.R. Boldy), 613–625. *The Geological Society, London*.

PARNELL, J., GREEN, P.F., WATT, G. & MIDDLETON, D. (2005) Thermal history and oil charge on the UK Atlantic Margin. *Petroleum Geoscience*, **11**, 99–112.

PASSEY, S. & HITCHEN, K. (2011) Cenozoic (igneous). In: *Geology of the Faroe-Shetland Basin and adjacent areas* (Ed. by Ritchie, J.D., Ziska, H., Johnson, H. & D. Evans), *British*

Geological Report Survey Research Report, RR/11/01; Jarofeingi Research Report RR/11/01. 209–228.

PASSEY, S.R & JOLLEY, D.W. (2009) A revised lithostratigraphic nomenclature for the Palaeogene Faroe Islands basalt Group, NE Atlantic Ocean. *Earth and Environmental Science Transaction of the Royal Society of Edinburgh*, **99**, 127–158.

PRAEG, D., STOKER, M.S., SHANNON, P.M., CERAMICOLA, S., HJELSTUEN, B., LABERG, J.S. & MATHIESEN, A. (2005) Episodic Cenozoic tectonism and the development of the NW European 'passive' continental margin. *Marine and Petroleum Geology*, **22**, 1007–1030.

QUINN, M., VARMING, T. & ÖLAVSDÖTTIR, J. (2011) Petroleum Geology. In: *Geology of the Faroe-Shetland Basin and adjacent areas* (Ed. by Ritchie, J.D., Ziska, H., Johnson, H. & D. Evans), *British Geological Report Survey Research Report, RR/11/01; Jarofeingi Research Report RR/11/01*. 254–280.

RATEAU, R., SCHOFIELD, N. & SMITH, M. (2013) The potential role of igneous intrusions on hydrocarbon migration, West of Shetland, *Petroleum Geoscience*, **19**, 259–272.

RIDER, M.H. (1996) *The Geological Interpretation of Well Logs*. Whittles Publishing, Caithness.

RIDER, M.H. & KENNEDY, M. (2011) *The Geological Interpretation of Well Logs*. Whittles Publishing, Caithness.

RITCHIE, J.D., GATLIFF, R.W. & RICHARDS, P.C. (1999) Early Tertiary magmatism in the offshore NW UK margin and surrounds. In: *Petroleum Geology of Northwest Europe: Proceedings of the 5th Conference* (Ed. by A.J. Fleet & S.A.R. Boldy), 573–584. *The Geological Society, London*.

RITCHIE, J.D., JOHNSON, H. & KIMBELL, G.S. (2003) The nature and age of Cenozoic contractional dating within the NE Faroe-Shetland Basin, *Marine Geology*, **20**, 399–409.

RITCHIE, J.D., JOHNSON, H., QUINN, M.F. & GATLIFF, R.W. (2008) The effects of Cenozoic compression within the Faroe-Shetland Basin and adjacent areas. In: *The nature and origin of compression in passive margins* (Ed. Johnson, H., Doré, A.G., Gatliff, R.W., Holdsworth, R., Lundin, E.R. & J.D. Ritchie), *Geol. Soc. London, Spec. Publ.,* **306**, 121–136.

RITCHIE, J.D. ZISKA, H., KIMBELL, G., QUINN, M. & CHADWICK, A. (2011) Structure. In: *Geology of the Faroe-Shetland Basin and adjacent areas* (Ed. by Ritchie, J.D., Ziska, H., Johnson, H. & D. Evans), *British Geological Report Survey Research Report, RR/11/01; Jarofeingi Research Report RR/11/01*. 9–70.

ROBERTS, D.G., THOMPSON, M., MITCHENER, B., HOSSACK, J., CARMICHAEL, S. & BJØRNSETH, H.M. (1999) Palaeozoic to Tertiary rift and basin dynamics: mid-Norway to the Bay of Biscay – a new context for hydrocarbon prospectivity in the deep water frontier. In: *Petroleum Geology of Northwest Europe: Proceedings of the 5th Conference* (Ed. by A.J. Fleet & S.A.R. Boldy), 7–40. *The Geological Society, London*.

ROBINSON, A.M., CARTWRIGHT, J., BURGESS, P.M. & DAVIES, R.J. (2004) Interactions between Topography and Channel Development from 3D Seismic Analysis: an Example from the Tertiary of the Flett Ridge, Faroe-Shetland Basin, UK. In: *3D Seismic Technology: Application to the Exploration of Sedimentary Basins* (Ed. by Davies, R.J., Cartwright, J.A., Stewart, S.A., Lappin, M. & J.R. Underhill) *The Geological Society, London, Memoirs*, **29**, 73–82.

SAUNDERS, A.D., JONES, S.M., MORGAN, L.A., PIERCE, K.L., WIDDOWSON, M. & XU, Y.G. (2007) Regional uplift associated with continental large igneous provinces: The roles of mantle plumes and the lithosphere. *Chemical Geology*, **241**, 282–318.

SHAW CHAMPION, M.E., WHITE, N.J., JONES, S.M. & LOVELL, J.P.B. (2008) Quantifying transient mantle convective uplift: An example from the Faroe-Shetland basin. Tectonics, **27**, TC1002, doi:10.1029/2007TC002106.

SMALLWOOD, J.R. (2004) Tertiary inversion in the Faroe-Shetland Channel and the development of major erosional scarps. In: *3D Seismic Technology: Application to the Exploration of Sedimentary Basins* (Ed. by Davies, R.J., Cartwright, J.A., Stewart, S.A., Lappin, M. & J.R. Underhill) *The Geological Society, London, Memoirs*, **29**, 187–198.

SMALLWOOD, J.R. & GILL, C.E. (2002) The rise and fall of the Faroes–Shetland Basin: evidence from seismic mapping of the Balder Formation. *Journal of the Geological Society, London*, **159**, 627–630.

SMITH, K. (2012) The Fascadale Fault: A tectonic link between the Cenozoic volcanic centres of Rum and Ardnamurchan, Scotland, revealed by multibeam survey. *Scottish Journal of Geology*, **48**, 91–102.

SØRENSEN, A.B. (2003) Cenozoic basin development and stratigraphy of the Faroes area. *Petroleum Geoscience*, **9**, 189–207.

STOKER, M.S. (2002) Late Neogene development of the UK Atlantic margin. In: *Exhumation of the North Atlantic Margin: Timing, Mechanisms and Implications for Petroleum Exploration* (Ed.by Doré, A.G., Cartwright, J.A., Stoker, M.S., Turner, J.P., & N. White), *The Geological Society, London, Special Publication*, **196**, 313–329.

STOKER, M.S. & ZISKA, H. (2011) Cretaceous. In: *Geology of the Faroe-Shetland Basin and adjacent areas* (Ed. by Ritchie, J.D., Ziska, H., Johnson, H. & D. Evans), *British Geological Report Survey Research Report, RR/11/01; Jarofeingi Research Report RR/11/01*. 123–150.

STOKER, M.S. & VARMING, T. (2011) Cenozoic (sedimentary). In: *Geology of the Faroe-Shetland Basin and adjacent areas* (Ed. by Ritchie, J.D., Ziska, H., Johnson, H. & D.

Evans), *British Geological Report Survey Research Report, RR/11/01; Jarofeingi Research Report RR/11/01*. 151–208.

STOKER, M.S., NIELSEN, T., VAN WEERING, T.C.E. & KUIJPERS, A. (2002) Towards an understanding of the Neogene tectonostratigraphic framework of the NE Atlantic margin between Ireland and the Faroe Islands. *Marine Geology*, **188**, 233–248.

STOKER, M.S., PRAEG, D., SHANNON, P.M., HJLESTUEN, B.O., LABERG, J.S., NIELSEN, T., VAN WEERING, T.C.E., SEJRUP, H.P. & EVANS, D. (2005a) Neogene evolution of the Atlantic continental margin of NW Europe (Lofoten Islands to SW Ireland): anything but passive. In: *Petroleum Geology: North-west Europe and Global Perspectives – Proceedings of the 6th Conference* (Ed. by A.J. Døre & B.A. Vining), 1057–1076. *The Geological Society, London*.

STOKER, M.S., PRAEG, D., HJLESTUEN, B.O., LABERG, J.S., NIELSEN, T. & SHANNON, P.M. (2005b) Neogene stratigraphy and the sedimentary and oceanographic development of the NW European Atlantic margin. *Marine & Petroleum Geology*, **22**, 977–1005.

STOKER, M.S., HOULT, R.J., NIELSEN, T., HJLESTUEN, B.O., LABERG, J.S., SHANNON, P.M., PRAEG, D., MATHIESEN, A., VAN WEERING, T.C.E. & MCDONNELL, A. (2005c) Sedimentary and oceanographic responses to early Neogene compression on the NW European margin. *Marine & Petroleum Geology*, **22**, 1031–1044.

STOKER, M.S., HOLFORD, S.P., HILLIS, R.R., GREEN, P.F. & DUDDY, I.R. (2010) Cenozoic post-rift sedimentation off northwest Britain: recording the detritus of episodic uplift on a passive continental margin. *Geology*, **38**, 7, 595–598, doi: 10.1130/G30881.1

STOKER, M.S., KIMBELL, G.S., MCINROY, D.B. & MORTON, A.C. (2012) Eocene post-rift tectonostratigraphy of the Rockall Plateau, Atlantic margin of NW Britain: Linking early spreading tectonics and passive margin response. *Marine & Petroleum Geology*, **30**, 98–125.

STOKER, M.S., LESLIE, A.B. & SMITH, K. (in press) A record of Eocene (Stronsay Group) sedimentation in BGS borehole 99/3, offshore NW Britain: implications for the early post-breakup development of the Faroe-Shetland Basin. *Scottish Journal of Geology*.

STORVOLL, V., BJØRLYKKE, K. & N.H. MONDOL, N.H. (2005) Velocity-depth trends in Mesozoic and Cenozoic sediments from the Norwegian Shelf. *AAPG Bulletin*, **89**, 3, 359–381.

TASSONE, D.R., HOLFORD, S.P., DUDDY, I.R., GREEN, P.F. & HILLIS, R.R (2013) Quantifying Cretaceous-Cenozoic exhumation in the Otway Basin using sonic velocity data: implications for conventional and unconventional hydrocarbon prospectivity. *AAPG Bulletin*.

TINGAY, M.R.P., HILLIS, R.R., SWARBRICK, R.E., MORELEY, C.K. & DAMIT, A.R. (2009) Origin of overpressures and pore-pressure prediction in the Baram province, Brunei. *AAPG Bulletin*, **93**, 1, 51–74.

TURNER, J.D. & SCRUTTON, R.A. (1993) Subsidence patterns in western margin basins: evidence from the Faeroe-Shetland basin. In: *Petroleum Geology of Northwest Europe: Proceedings of the 4th Conference* (Ed. by J.R. Parker), 975–983. *The Geological Society, London*.

WARE, P.D. & TURNER, J.P. (2002) Sonic velocity of the Tertiary denudation of the Irish Sea basin. In: *Exhumation of the North Atlantic Margin: Timing, Mechanisms and Implications for Petroleum Exploration* (Ed.by Doré, A.G., Cartwright, J.A., Stoker, M.S., Turner, J.P., & N. White), *Geol. Soc. London, Spec. Publ.*, **196**, 355–370.

WHITE, R. & MACKENZIE, D. (1989) Magmatism at Rift Zones: The Generation of Volcanic Continental Margins and Flood Basalts. *Journal of Geophysical Research*, **94** (B6), 7685–7729.

WYCHERLEY, H.L., PARNELL, J., WATT, G.R., CHEN, H. & BOYCE, A.J. (2003) Indicators of hot fluid migration in sedimentary basins: evidence from the UK Atlantic Margin. *Petroleum Geoscience*, **9**, 357–374.

12 Figure Captions

Fig. 1: (a) The distribution of wells in which interval sonic transit time, gamma ray and chrono-stratigraphic top data are investigated in this study, superimposed on a structural elements map of the FSR, illustrating the major structural highs and depocentres across the FSR (modified after Stoker & Ziska 2011). (b) Bathymetric map of the FSR, indicating the division of wells into geographical regions (southwest, central and northeast) for displaying results in Fig. 10.

Fig. 2: Palaeotemperature constraints from AFTA and VR data plotted against depth in (a) wells 206/10-1 (Green *et al*. 1999; Mark *et al.* 2008) and (b) well 206/09-2 (Green *et al*. 1999; Mark *et al.* 2008). In comparison to the present-day geothermal gradients calculated from bottom hole temperatures, the AFTA and VR data indicate higher Cenozoic palaeotemperatures. The non-linear to arcuate palaeo-geothermal profiles defined by these palaeotemperatures are characteristic of heating caused by transient or steady-state lateral hot fluid flow (Duddy *et al.* 1998). These palaeotemperatures mask any heating effects which may have been produced by deeper burial. Determining the magnitude of exhumation in wells across the FSR using thermal history data is therefore problematic.

Fig. 3: Cenozoic tectono-stratigraphy for the Faroe-Shetland region (FSR; see text for details). Information derived from the following sources: Chrono/litho stratigraphy and unconformable surfaces – Knox *et al*. (1997); Stoker *et al*. (2005a,b,c); Praeg *et al*. (2005); Gernigon *et al*. (2012). FSR Sedimentary Architecture – Stoker *et al*. (2010). FSR Tectonics – Boldreel & Andersen (1993), Andersen *et al*. (2000), Stoker (2002), Robinson (2004), Robinson *et al*. (2004), Smallwood (2004), Johnson *et al*. (2005), Parnell *et al*. (2005), Ritchie *et al*. (2008), Shaw Champion *et al*. (2008), Passey & Jolley (2009), Ölavsdöttir *et al*. (2010), Stoker *et al*. (2010), Hartley *et al*. (2011), and Stoker & Varming (2011) and Stoker *et al*. (in press). Note, numbers 1–4 in 'FSR Tectonics' column relate to Discussion section 7.1. European Plate Tectonics: NW

Scotland Exhumation – Holford *et al*. (2010); Alpine orogeny - Doré *et al*. (2008); Reactivation of Great Glen Fault – Le Brenton *et al*. (2013). North-East Atlantic plate tectonics – Doré *et al*. (2008), Gernigon *et al*. (2012); Spreading half-rate (NE Atlantic) – Mosar *et al*. (2002);. Timescale is from Gradstein *et al*. (2012).

Fig. 4: Interpretation of regional dip seismic profiles modified after Lamers & Carmichael (1999) showing the structural style and preserved stratigraphy within the FSR. In particular, the sections highlight the following: 1) the wedge-shaped geometry of the Eocene succession; 2) the Middle Eocene basin-floor fans; 3) the differential uplift/subsidence along the eastern margin of the Faroe-Shetland Basin; 4) the build-out of the Plio-Pleistocene wedge; and, 5) the difference in preserved (compacted) thickness of Eocene stratigraphy in the central FSR in comparison to the south-western FSR, especially over the Rona High (see text for further details). Locations of seismic profiles are shown in Fig. 1.

Fig. 5: Evolution of interval transit time (proxy for porosity) vs. depth in exhumed sedimentary basins where porosity reduction is assumed to be controlled solely by burial (modified after Corcoran & Doré 2005 and Japsen 1998); (a) 'normal' sonic transit time-depth trend (i.e. baseline) as a function of burial depth under hydrostatic conditions in a subsiding basin (i.e. the reference curve); (b) exhumation leads to an anomalously slow interval transit time-depth trend (i.e. overcompacted) with vertical displacement from the baseline yielding an estimate of gross exhumation, E_G; (c) post-exhumation re-burial, B_E, reduces the vertical displacement between the anomalously slow interval transit time-depth trend and the baseline to yield an estimate of net exhumation, E_N, at a given well location; (d) rapid burial of low permeability stratigraphy (e.g. mudstones) can lead to an anomalously fast interval transit time-depth trend (i.e. undercompacted) with vertical displacement from the baseline indicating possible abnormal pore pressures (i.e. overpressure) caused by a disequilibrium compaction mechanism.

Fig. 6: Preserved chonostratigraphies as well as gamma ray (*GR*) and sonic transit time (Δt_p) responses for wells 206/03-1 and 205/22-1A in the FSR. The lithostratigaphy of the Danian-Cretaceous strata is also highlighted for these wells (Stoker & Ziska 2011). Note the less-variant and consistent sonic transit time response in the Upper Cretaceous strata as well as thickness and the dominantly mudstone lithology (despite relatively low gamma ray responses), especially in the Danian Sullom Formation and Maastrichtian to Campanian Jorsalfare and Kyrre formations, which are ideal for sonic transit time analysis.

Fig. 7: Palaeotemperature constraints from AFTA and VR data (unpublished) in well 206/03-1 are consistent with present-day temperatures calculated using the present-day thermal gradient of 36.4°C/km determined from corrected bottom hole temperatures. This suggests that units throughout the section are currently at their maximum post-depositional temperatures, which we interpret as indicating that all units are also at their maximum burial depths.

Fig. 8: (a) Average shale unit sonic transit times (Δt_{ave}) vs. shale unit mid-point depth below seabed (Z_{MP}) for the Campanian-Maastrichtian-Danian (C-M-D) stratigraphic sections of the Shetland Group marine shale in wells 206/03-1 and 219/20-1. AFTA and VR data (unpublished) from these well locations indicates that maximum (palaeo) temperatures are at the present-day, suggesting the C-M-D strata are likely to be at maximum burial at the present-day and, therefore, can be used to construct a C-M-D normal sonic transit time-depth baseline trends. Also shown is the gamma ray response over the C-M-D section in both wells, in particularly highlighting the low gamma ray response characteristic of igneous rocks within well 219/20-1. Apparently overcompacted and reversal trends within the interval transit times within unchanged lithology (i.e. from gamma ray log) were neglected due to the uncertainty in pore pressure state and normal compaction, respectively (represented by the unfilled symbols). (b) Pressure-depth below ground level plotted to show reservoir pressure in well 206/03-1. (c) Logarithmically transforming the exponential baseline function with respect to depth (assuming considered average shale unit sonic

transit times are at maximum burial (B_{max}) – Equation 4) in order to determine the exponential decay constant, b (i.e. the linear slope of plot). The best-fit case occurs when the mineral matrix sonic transit time (C) is ~40 µs ft^{-1} ('best-fit C'), yielding a least squares regression (R^2) of ~0.8719 (d). Given this value is lower than previously published estimates and reflects the lack of constraints in deeper sections, we also further constrain the baseline function using C = ~56 µs ft^{-1} ('constrained C'; Japsen 2000) to determine b (c), although yielding a lesser R^2 value (d). Both these determine baseline functions are plotted (in their original form – Equation 3) in (a) and the vertical distance between the baselines define a zone of uncertainty, represented by the grey shade.

Fig. 9: Comparison of published baselines for shales and sandstones of different ages and origin in near-by basins with respect to the C-M-D marine shale baseline zone of uncertainty constructed in this study. Note the similarity between the lower limit on our baseline and Japsen's (2000) marine shale baseline trend. On the right-hand depth axis, the thick grey curve shows the maximum depth interval difference within the baseline zone of uncertainty highlighting the great amounts of uncertainty in the potential net exhumation estimate when Δt_{ave} fall below ~80 µs ft^{-1}.

Fig. 10: Average shale unit interval transit time vs. shale unit mid-point depth plot of the C-M-D (Shetland Group) marine shales for wells located in (a) the southwest (b) central and (c) northeast regions (see Fig. 1). Also shown are the constructed baseline trends (see Table 1 and Fig. 8a) as well as the baseline zone of uncertainty (grey shaded area) Note in (a) how the sonic transit times are lower (i.e. overcompacted) with respect to the baselines whereas in (c) the sonic transit times are similar to the baselines. Also note the reversal in sonic transit time trend in (b) within the deeper section such that sonic transit times are higher (i.e. undercompacted) with respect to the baselines.

Fig. 11: Gamma ray and sonic transit time response with depth within well 214/28-1, also showing the corresponding formation pore pressure inferred from wireline formation tests (WFT) and drilling data, in which (static) mud weight data and connection gases were used as a proxy for

formation pore pressure magnitude. Note the low gamma ray and sonic transit time responses characteristic of dolerite sills, which all have intruded shale lithologies and some even flowed gas through fracture porosity and permeability (Rateau *et al*. 2013), necessitating raising drilling mud weights and wellbore pressures. Towards the wellbore's terminal depth the relatively high sonic transit time response with respect to the baseline trends indicates undercompaction, while the abrupt changes at dolerite sill boundaries potentially indicate (vertically) compartmentalised overpressures given the connection gases observed at high drilling mud weights.

Fig. 12: Comparison of net exhumation estimates calculated using the two C-M-D marine shale baselines constructed in this study. Grey shade represents the baseline zone of uncertainty. While wells in the northeast are presently close to or at maximum burial depths, the majority of wells along the Rona High and Foula sub-Basin have moderate magnitudes of exhumation (~200-400 m), and the wells in the southwest have large magnitudes of net exhumation (~400-1000 m). Wells with large negative net exhumation magnitudes likely represents overpressured sections, however, this requires a more comprehensive pore pressure analysis that is beyond the scope of this study.

Fig. 13: Distribution of Cenozoic net exhumation magnitudes determined in this study (Table 2) superimposed on a structural element map of the FSR modified after Stoker & Ziska (2011). Magnitudes illustrated are the average net exhumation amounts from the 'best-fit *C*' and 'constrained *C*' baselines (Fig. 8). Results show that Cenozoic net exhumation magnitudes increase from the northeast, where wells are at or near to maximum burial depths, to the southwest where wells have ~300-1000 m of Cenozoic net exhumation magnitudes.

Fig. 14: Burial history and preserved sediment thickness plots for well 219/28-1 in the Møre Basin showing the post-Danian burial histories based entirely on the thickness of preserved (compacted) stratigraphy ("default" burial history). Although post-Danian gross exhumation may have occurred at this well location sometime during the Cenozoic, thick Pliocene-Recent sedimentation has overprinted any evidence of deeper burial, such that units intersected in this well are presently

at maximum burial depth. Thus, net exhumation (E_N) is zero. mP = Mid-Palaeocene, lP = Late Palaeocene, eE = Early Eocene, mE = Mid-Eocene, lE = Late Eocene, eO = Early Oligocene, lO = Late Oligocene, eM = Early Miocene, mM = Mid-Miocene, lM = Late Miocene, P-R = Pliocene to Recent.

Fig. 15: Burial history plots over the last 60 Myr (or post-Danian) for well 206/08-2 to represent the central Rona High area. (a) thicknesses of preserved chronostratigraphic sequences (m) from the Mid Paleocene to present, (b) default post-Danian burial history based entirely on the thickness of preserved (compacted) stratigraphy, (c) burial and uplift history incorporating exhumation in the Mid-/Late Eocene, and (d) burial and uplift history incorporating exhumation in the Oligocene to Mid-Miocene. In b and c, amounts of gross exhumation are those required in order to honour the maximum palaeo-burial estimated from sonic transit time data. Here, Eocene and Oligocene stratigraphy is undifferentiated and is therefore impossible to assign a precise timing of maximum burial and subsequent exhumation as well as the unconformity that relates to our net exhumation estimates. mP = Mid-Palaeocene, lP = Late Palaeocene, eE = Early Eocene, mE = Mid-Eocene, lE = Late Eocene, eO = Early Oligocene, lO = Late Oligocene, eM = Early Miocene, mM = Mid-Miocene, lM = Late Miocene, P-R = Pliocene to Recent.

Fig. 16: Burial history plots over the last 60 Myr (or post-Danian) for well 205/21-1A to represent the southwestern Rona High area. (a) thicknesses of preserved chronostratigraphic sequences (m) from the Mid Paleocene to present, (b) default post-Danian burial history based entirely on the thickness of preserved (compacted) stratigraphy, (c) burial and uplift history incorporating exhumation in the Mid-/Late Eocene, and (d) burial and uplift history incorporating exhumation in the Oligocene to Mid-Miocene. In b and c, amounts of gross exhumation are those required in order to honour the maximum palaeo-burial estimated from sonic transit time data. Due to the lack of Paleocene to Miocene rocks at this location, gross exhumation estimates for both possible tectonic phases are approximately the same. mP = Mid-Palaeocene, lP = Late Palaeocene, eE =

Early Eocene, mE = Mid-Eocene, lE = Late Eocene, eO = Early Oligocene, lO = Late Oligocene, eM = Early Miocene, mM = Mid-Miocene, lM = Late Miocene, P-R = Pliocene to Recent.

Fig. 17: (a) Comparison of Mid-/Late Eocene and Oligocene to Mid-Miocene gross exhumation magnitudes calculated at wells 206/08-2 (Fig. 16) and 205/21-1A (Fig. 17) to represent the central and southwestern Rona High areas, respectively. Higher amounts of gross exhumation are required to honour the palaeo-burial constraints if maximum burial and subsequent exhumation occurred in the Mid-/Late Eocene in comparison to later on in the Oligocene to Mid-Miocene. Also shown are estimates gross exhumation magnitude (i.e. removed section) from thermal history data at well 204/19-1 (see Fig. 20; Parnell *et al*. 2005) and seismic reflection data (Booth *et al*. 1993). Distribution of both Mid-/Late Eocene (b) and Oligocene to Mid-Miocene (c) gross exhumation magnitude estimates superimposed on a structural element map of the FSR.

Fig. 18: Palaeotemperature constraints determined from AFTA and VR data in well 205/21-1A (Parnell *et al.* 1999). VR values define a distinctive non-linear to arcuate palaeotemperature profile diagnostic of transient lateral heating caused by hot flowing fluids , which are higher than values in the underlying Jurassic section. AFTA data indicate somewhat lower maximum limits to the allowed degree of heating. If the palaeotemperatures derived from the VR data were related to deeper burial rather than hot flowing fluids, then more than 2000 m of additional Cenozoic burial (i.e. gross exhumation) between 80 and 0 Ma would be required, which is ~1200 m greater than our sonic transit time gross exhumation estimates for either considered tectonic phase. The sonic data therefore confirm that these palaeotemperatures are not due to deeper burial.

Fig. 19: (a) Palaeotemperature constraints derived from AFTA and VR data in well 204/19-1 (from Parnell *et al*. 2005), plotted against depth below sea level, defining a linear palaeotemperature profile which is parallel to the present-day temperature profile but offset to higher values, indicating that heating was due to deeper burial. Parnell *et al*. (2005) interpreted these results as indicating deeper burial and subsequent exhumation during the interval

represented by the Mid-Eocene to Mid-Miocene unconformity (based on Iliffe *et al*. (1999). (b) Removed section vs. palaeogeothermal gradient plot, showing the range of values allowed by the palaeotemperatures within 95% confidence limits. Removed section in this context is equivalent to the magnitude of gross exhumation. If the palaeo-gradient was equal to the present-day value of ~34.1 °C km^{-1}, results from this well suggest between 630 m and 950 m of additional section were deposited and subsequently removed on the Eocene–Miocene unconformity in this well assuming a palaeo-surface temperature of 10 °C (after Parnell *et al.* 2005).

13 Tables

Table 1: The two baseline functions constructed in this study to describe the normal sonic transit time-depth trend of hydrostatically pressured and brine saturated Campanian to Danian marine shales of the Shetland Group. Sonic transit times (Δt) are in µs ft^{-1} and depth (Z) is in metres below seabed.

Curve	NCT Function	R^2	Symbol in Fig. 8
1. Best-fit	$\Delta t_{baseline} = 158 \times e^{-0.0004410 \times Z} + 48$	0.9337	---
2. Constrained	$\Delta t_{baseline} = 150 \times e^{-0.0004865 \times Z} + 56$	0.9313	---

Table 2: Estimates of Cenozoic exhumation magnitudes in the FSR along with the number of shale unit data (*N*) and the standard deviation (*SD*) of net exhumation, E_N, for each well. Wells that have a negative burial anomaly are assumed to be at maximum burial depth.

Well	Reference number in Fig. 13	Location	N	E_{N_ave} range (X) C – BF# (m)	$SE/2$ -LL & +UL† (m)	E_{N_well} (m)	Interpreted to be:
202/03-1A	3	North Rona Basin	7	351 – 386	27 – 27	369	Exhumed
202/03-2	4	North Rona Basin	18	235 – 268	79 – 80	252	Exhumed
202/08-1	1	North Rona Basin	14	981 – 1012	82 – 80	997	Exhumed
202/09-1	2	Solan Bank High	3	392 – 423	12 – 13	407	Exhumed
204/28-1	5	Judd High	1	176 – 209	-	193	Exhumed
204/29-1	6	Judd sub-Basin	-	-	-	-	-
205/10-2B	12	Flett High	36	284 – 251	62 – 58	268	Exhumed
205/20-1	10	Rona High	40	293 – 326	53 – 51	310	Exhumed
205/21-1A	7	Rona High	48	626 – 659	41 – 41	642	Exhumed
205/22-1A	8	Flett sub-Basin	67	271 – 298	38 – 37	284	Exhumed
205/23-1	9	West Shetland Basin	24	419 – 450	45 – 46	434	Exhumed
206/05-1	19	Foula sub-Basin	68	344 – 361	81 – 73	353	Exhumed
206/07-1	13	Rona High	27	279 – 313	38 – 37	296	Exhumed
206/08-2	14	Rona High	10	268 – 303	77 – 77	285	Exhumed
206/08-5	15	Rona High	32	302 – 336	32 – 32	319	Exhumed
206/09-1	16	West Shetland Basin	18	259 – 283	85 – 81	271	Exhumed
206/09-2	17	Rona High	29	104 – 137	99 – 97	121	Exhumed?
206/11-1	11	Foula sub-Basin	5	167 – 200	15 – 15	183	Exhumed
208/17-1	24	Flett sub-Basin	39	124 – -22	119 – 172	51 / 0	Max. Burial
208/19-1	25	Flett sub-Basin	27	62 – 41	50 – 50	52 / 0	Max. Burial
208/26-1	23	Foula sub-Basin	3	421 – 400	2 – 2	411	Exhumed
209/06-1	26	Erlend High	64	-135 – -176	94 – 95	-156 / 0	Max. Burial
209/12-1	27	Erlend High	57	142 – 165	52 – 47	153	Max. Burial?
210/04-1	28	Magnus Basin	10	-90 – -56	39 – 40	-73 / 0	Max. Burial
210/05-1	29	Magnus Basin	45	56 – 85	71 – 68	71 / 0	Max. Burial
214/27-1	20	Flett sub-Basin	24	-736 – -822	257 – 281	-779 / 0	Max. Burial
214/28-1	21	Flett High	16	-910 – -1005	274 – 307	-958 / 0	Max. Burial
214/29-1	22	Foula sub-Basin	18	215 – 214	43 – 45	214	Exhumed?
219/27-1	31	Erlend sub-Basin	5	-834 – -799	27 – 27	-817 / 0	Max. Burial
219/28-1	30	Erlend sub-Basin	42	30 – 37	51 – 55	27 / 0	Max. Burial
219/28-2Z	32	Møre Basin	26	92 – 96	35 – 40	94 / 0	Max. Burial

CC denotes 'Constrained *C*' and BCF denotes 'Best-fit *C*'; † LL denotes lower-limit and UP denotes upper-limit.

Figure 1

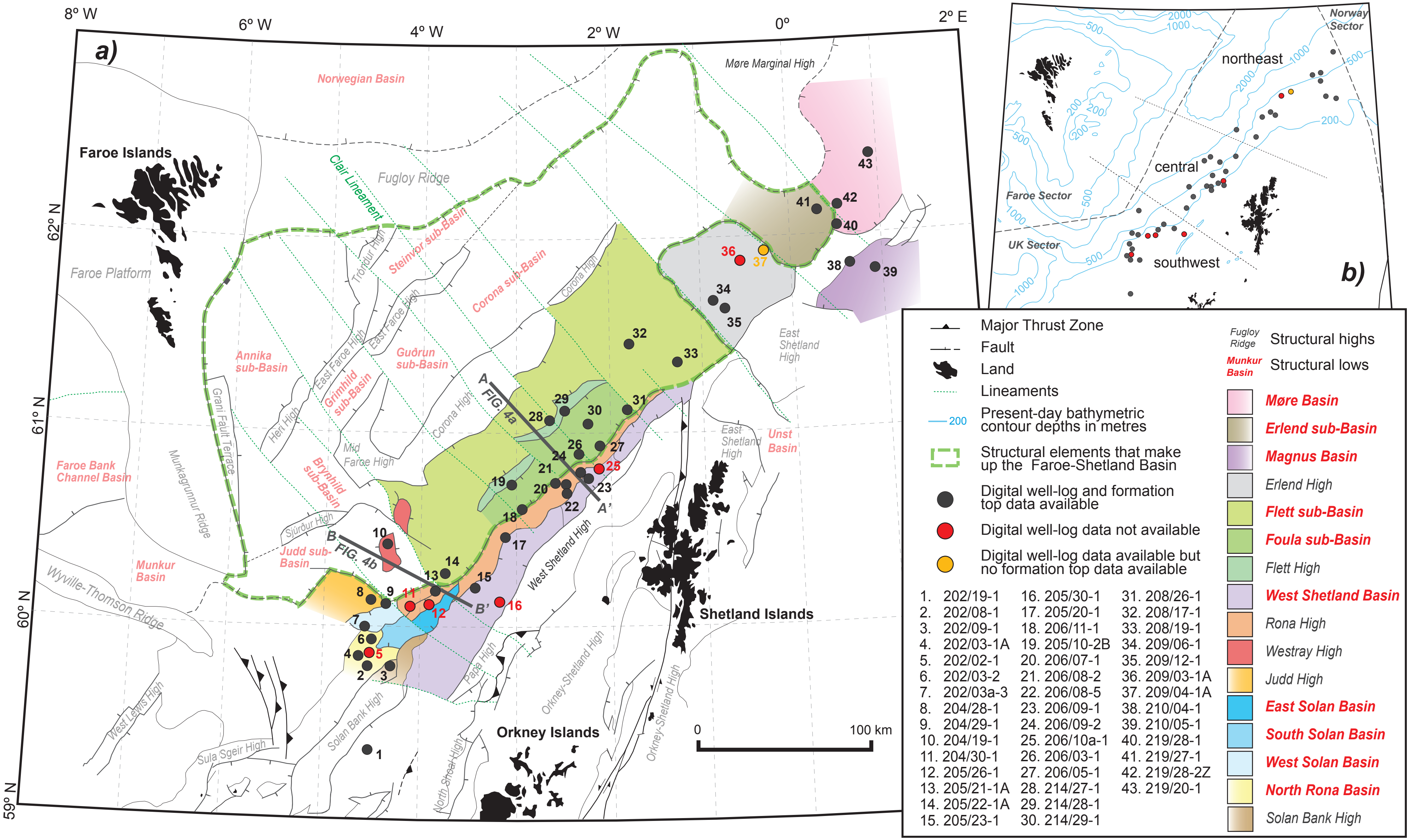
a)
8° W
6° W
4° W
2° W
0°
2° E
62° N
61° N
60° N
59° N
Faroe Islands
Faroe Platform
Norwegian Basin
Møre Marginal High
Fugloy Ridge
Clair Lineament
Steinvor sub-Basin
Corona sub-Basin
Corona High
Annika sub-Basin
Guðrun sub-Basin
East Faroe High
Grimhild sub-Basin
Heri High
Mid Faroe High
Brynhild sub-Basin
Faroe Bank Channel Basin
Munkagrunnur Ridge
Grani Fault Terrace
Sjúrður High
Judd sub-Basin
Munkur Basin
Wyville-Thomson Ridge
West Lewis High
Sula Sgeir High
Solan Bank High
North Shoal High
Papa High
West Shetland High
Orkney-Shetland High
Orkney Islands
Shetland Islands
East Shetland High
Unst Basin
FIG. 4a
FIG. 4b
A
A'
B
B'
0
100 km
b)
northeast
central
southwest
Faroe Sector
UK Sector
Norway Sector
Major Thrust Zone
Fault
Land
Lineaments
Present-day bathymetric contour depths in metres
Structural elements that make up the Faroe-Shetland Basin
Digital well-log and formation top data available
Digital well-log data not available
Digital well-log data available but no formation top data available
Structural highs
Structural lows
Møre Basin
Erlend sub-Basin
Magnus Basin
Erlend High
Flett sub-Basin
Foula sub-Basin
Flett High
West Shetland Basin
Rona High
Westray High
Judd High
East Solan Basin
South Solan Basin
West Solan Basin
North Rona Basin
Solan Bank High
1. 202/19-1
2. 202/08-1
3. 202/09-1
4. 202/03-1A
5. 202/02-1
6. 202/03-2
7. 202/03a-3
8. 204/28-1
9. 204/29-1
10. 204/19-1
11. 204/30-1
12. 205/26-1
13. 205/21-1A
14. 205/22-1A
15. 205/23-1
16. 205/30-1
17. 205/20-1
18. 206/11-1
19. 205/10-2B
20. 206/07-1
21. 206/08-2
22. 206/08-5
23. 206/09-1
24. 206/09-2
25. 206/10a-1
26. 206/03-1
27. 206/05-1
28. 214/27-1
29. 214/28-1
30. 214/29-1
31. 208/26-1
32. 208/17-1
33. 208/19-1
34. 209/06-1
35. 209/12-1
36. 209/03-1A
37. 209/04-1A
38. 210/04-1
39. 210/05-1
40. 219/28-1
41. 219/27-1
42. 219/28-2Z
43. 219/20-1

Figure 2

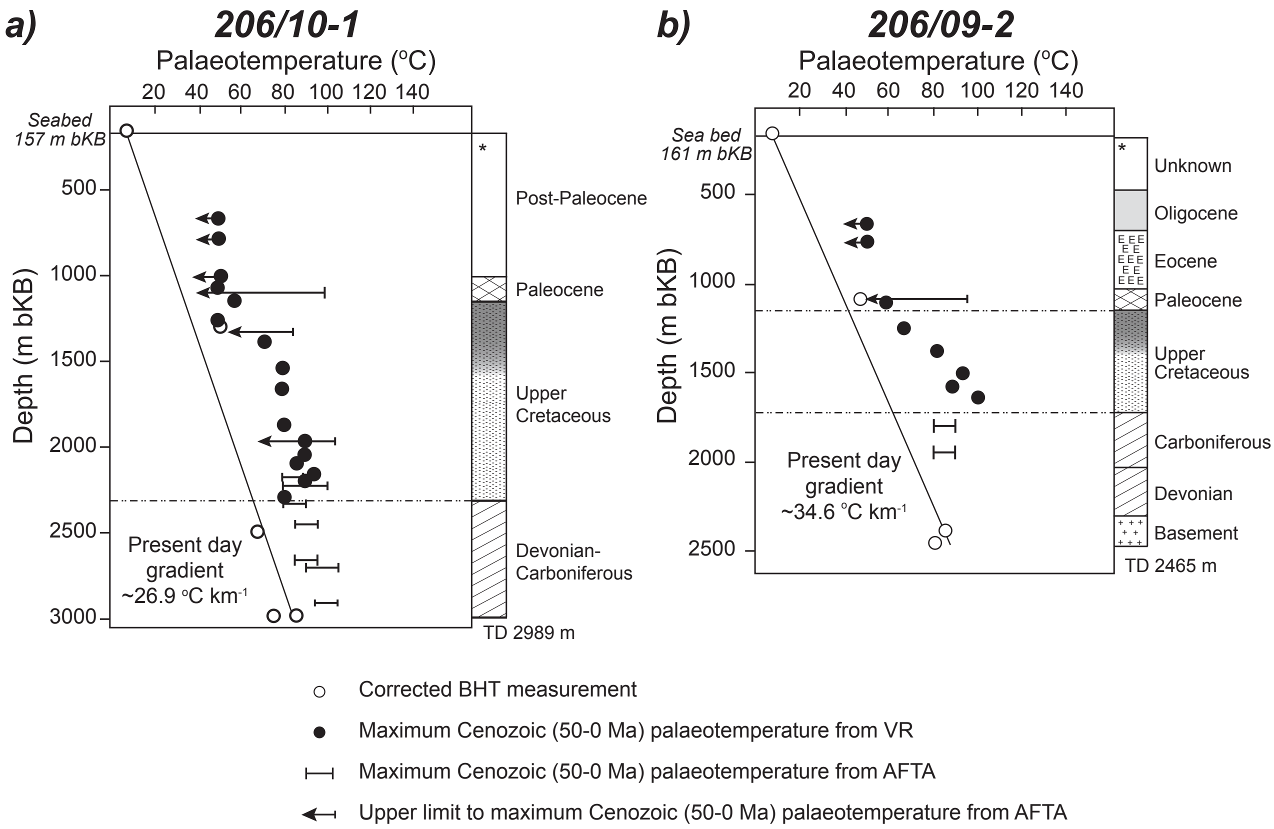

a)
206/10-1
Palaeotemperature (°C)
20 40 60 80 100 120 140
Seabed
157 m bKB
Depth (m bKB)
500
1000
1500
2000
2500
3000
*
Post-Paleocene
Paleocene
Upper
Cretaceous
Devonian-
Carboniferous
Present day
gradient
~26.9 °C km-1
TD 2989 m
b)
206/09-2
Palaeotemperature (°C)
20 40 60 80 100 120 140
Sea bed
161 m bKB
Depth (m bKB)
500
1000
1500
2000
2500
*
Unknown
Oligocene
Eocene
Paleocene
Upper
Cretaceous
Carboniferous
Devonian
Basement
Present day
gradient
~34.6 °C km-1
TD 2465 m
Corrected BHT measurement
Maximum Cenozoic (50-0 Ma) palaeotemperature from VR
Maximum Cenozoic (50-0 Ma) palaeotemperature from AFTA
Upper limit to maximum Cenozoic (50-0 Ma) palaeotemperature from AFTA

Figure 3

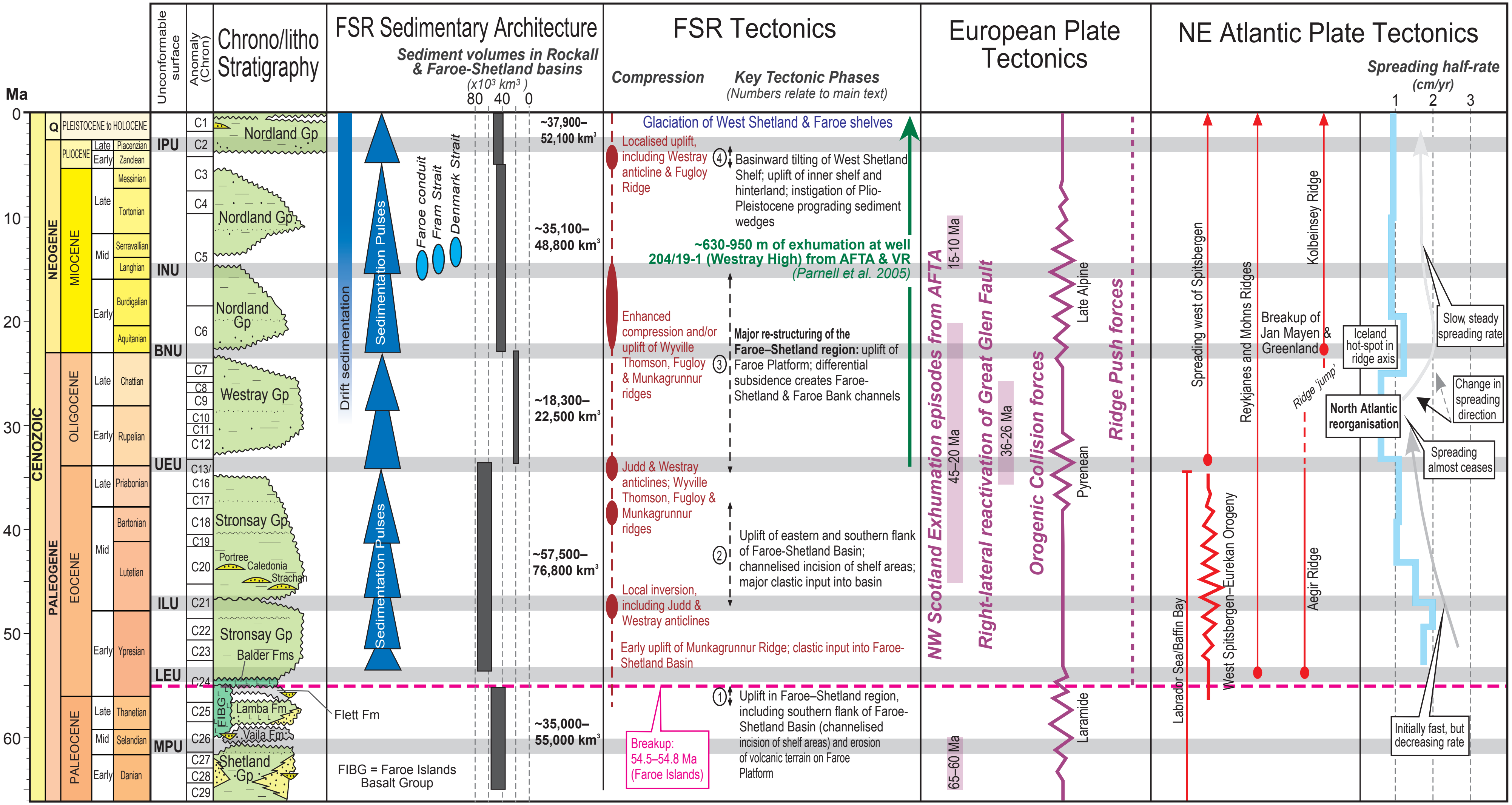

Ma
Unconformable surface
Anomaly (Chron)
Chrono/litho Stratigraphy
FSR Sedimentary Architecture
Sediment volumes in Rockall & Faroe-Shetland basins
FSR Tectonics
Compression
Key Tectonic Phases
(Numbers relate to main text)
European Plate Tectonics
NE Atlantic Plate Tectonics
Spreading half-rate (cm/yr)
CENOZOIC
NEOGENE
PALEOGENE
MIOCENE
OLIGOCENE
EOCENE
PALEOCENE
PLEISTOCENE to HOLOCENE
PLIOCENE
IPU
INU
BNU
UEU
ILU
LEU
MPU
Nordland Gp
Westray Gp
Stronsay Gp
Balder Fms
Lamba Fm
Vaila Fm
Shetland Gp
Flett Fm
FIBG = Faroe Islands Basalt Group
Drift sedimentation
Sedimentation Pulses
Faroe conduit
Fram Strait
Denmark Strait
~37,900–52,100 km³
~35,100–48,800 km³
~18,300–22,500 km³
~57,500–76,800 km³
~35,000–55,000 km³
Glaciation of West Shetland & Faroe shelves
Localised uplift, including Westray anticline & Fugloy Ridge
Basinward tilting of West Shetland Shelf; uplift of inner shelf and hinterland; instigation of Plio-Pleistocene prograding sediment wedges
~630-950 m of exhumation at well 204/19-1 (Westray High) from AFTA & VR (Parnell et al. 2005)
Enhanced compression and/or uplift of Wyville Thomson, Fugloy & Munkagrunnur ridges
Major re-structuring of the Faroe–Shetland region: uplift of Faroe Platform; differential subsidence creates Faroe-Shetland & Faroe Bank channels
Judd & Westray anticlines; Wyville Thomson, Fugloy & Munkagrunnur ridges
Uplift of eastern and southern flank of Faroe-Shetland Basin; channelised incision of shelf areas; major clastic input into basin
Local inversion, including Judd & Westray anticlines
Early uplift of Munkagrunnur Ridge; clastic input into Faroe-Shetland Basin
Uplift in Faroe–Shetland region, including southern flank of Faroe-Shetland Basin (channelised incision of shelf areas) and erosion of volcanic terrain on Faroe Platform
Breakup: 54.5–54.8 Ma (Faroe Islands)
NW Scotland Exhumation episodes from AFTA
15-10 Ma
45–20 Ma
36-26 Ma
65–60 Ma
Right-lateral reactivation of Great Glen Fault
Orogenic Collision forces
Ridge Push forces
Late Alpine
Pyrenean
Laramide
Spreading west of Spitsbergen
Reykjanes and Mohns Ridges
Kolbeinsey Ridge
Breakup of Jan Mayen & Greenland
Ridge 'jump'
Aegir Ridge
West Spitsbergen–Eurekan Orogeny
Labrador Sea/Baffin Bay
Iceland hot-spot in ridge axis
North Atlantic reorganisation
Slow, steady spreading rate
Change in spreading direction
Spreading almost ceases
Initially fast, but decreasing rate

Figure 4

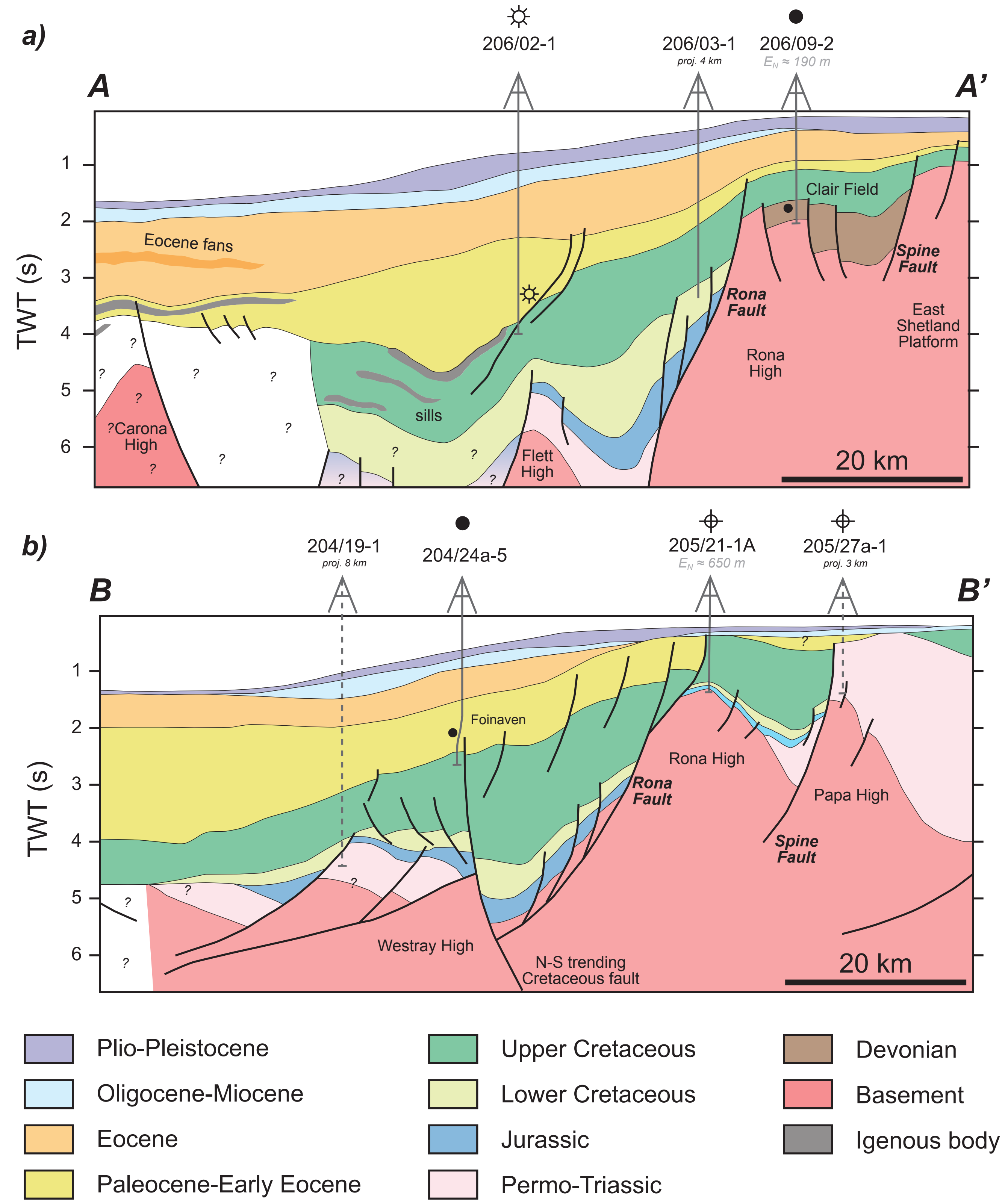
a)
206/02-1
206/03-1
proj. 4 km
206/09-2
$E_N \approx 190$ m
A
A'
TWT (s)
1
2
3
4
5
6
Eocene fans
Clair Field
Spine Fault
Rona Fault
East Shetland Platform
Rona High
sills
?Carona High
Flett High
20 km
b)
204/19-1
proj. 8 km
204/24a-5
205/21-1A
$E_N \approx 650$ m
205/27a-1
proj. 3 km
B
B'
Foinaven
Rona High
Rona Fault
Papa High
Spine Fault
Westray High
N-S trending Cretaceous fault
20 km
Plio-Pleistocene
Oligocene-Miocene
Eocene
Paleocene-Early Eocene
Upper Cretaceous
Lower Cretaceous
Jurassic
Permo-Triassic
Devonian
Basement
Igenous body

Figure 5

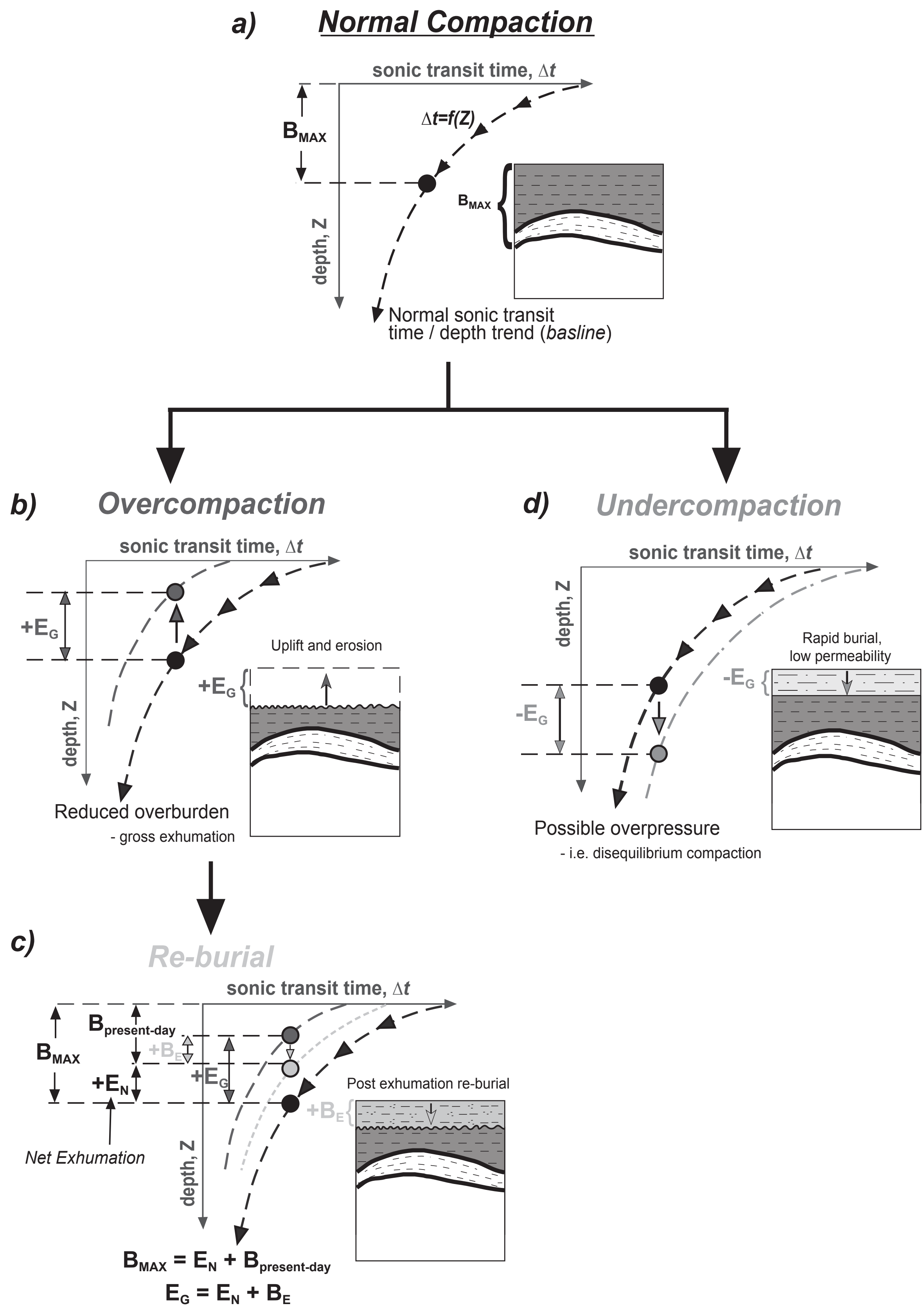
a)
Normal Compaction
sonic transit time, Δt
Δt=f(Z)
B_MAX
depth, Z
Normal sonic transit time / depth trend (basline)
b)
Overcompaction
sonic transit time, Δt
+E_G
Uplift and erosion
depth, Z
Reduced overburden
- gross exhumation
d)
Undercompaction
sonic transit time, Δt
depth, Z
Rapid burial, low permeability
-E_G
Possible overpressure
- i.e. disequilibrium compaction
c)
Re-burial
sonic transit time, Δt
B_present-day
+B_E
+E_G
+E_N
Net Exhumation
Post exhumation re-burial
depth, Z
B_MAX = E_N + B_present-day
E_G = E_N + B_E

Figure 6

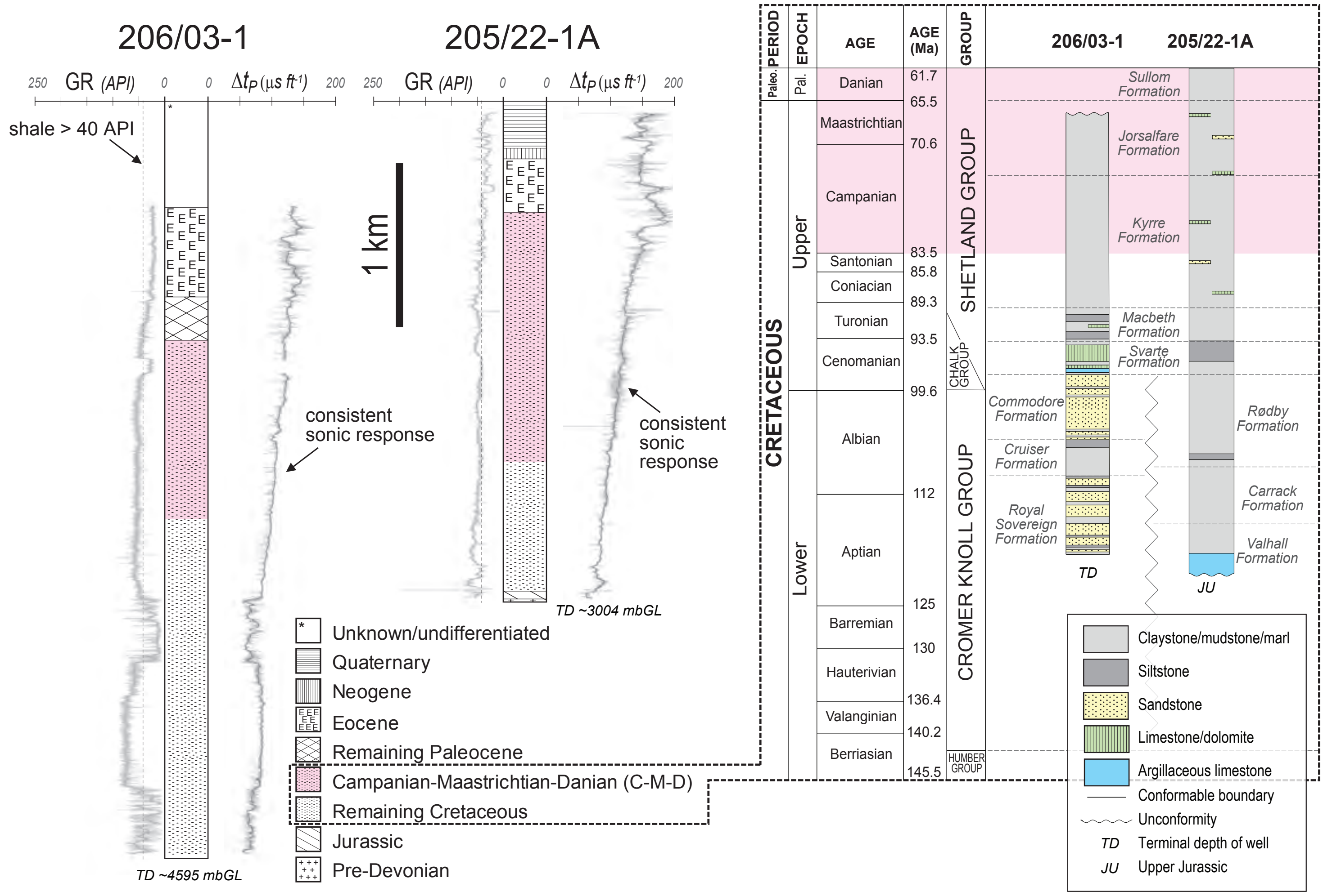

206/03-1
205/22-1A
250 GR (API) 0
0 Δtp (μs ft-1) 200
shale > 40 API
1 km
consistent sonic response
consistent sonic response
TD ~4595 mbGL
TD ~3004 mbGL
Unknown/undifferentiated
Quaternary
Neogene
Eocene
Remaining Paleocene
Campanian-Maastrichtian-Danian (C-M-D)
Remaining Cretaceous
Jurassic
Pre-Devonian
PERIOD
EPOCH
AGE
AGE (Ma)
GROUP
Paleo.
Pal.
CRETACEOUS
Upper
Lower
Danian
Maastrichtian
Campanian
Santonian
Coniacian
Turonian
Cenomanian
Albian
Aptian
Barremian
Hauterivian
Valanginian
Berriasian
61.7
65.5
70.6
83.5
85.8
89.3
93.5
99.6
112
125
130
136.4
140.2
145.5
SHETLAND GROUP
CHALK GROUP
CROMER KNOLL GROUP
HUMBER GROUP
Sullom Formation
Jorsalfare Formation
Kyrre Formation
Macbeth Formation
Svarte Formation
Commodore Formation
Cruiser Formation
Royal Sovereign Formation
Rødby Formation
Carrack Formation
Valhall Formation
TD
JU
Claystone/mudstone/marl
Siltstone
Sandstone
Limestone/dolomite
Argillaceous limestone
Conformable boundary
Unconformity
TD Terminal depth of well
JU Upper Jurassic

Figure 7

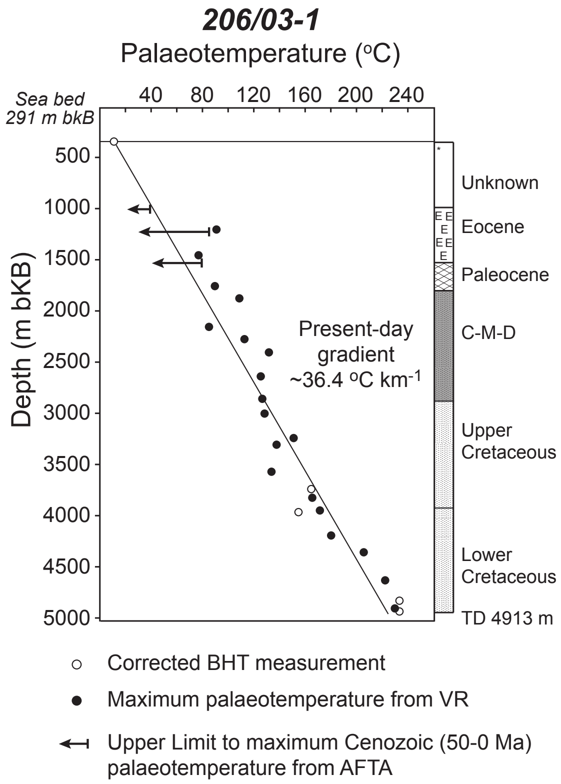

206/03-1
Palaeotemperature (°C)
Sea bed
291 m bkB
40
80
120
160
200
240
500
1000
1500
2000
2500
3000
3500
4000
4500
5000
Depth (m bKB)
Present-day
gradient
~36.4 °C km-1
Unknown
Eocene
Paleocene
C-M-D
Upper
Cretaceous
Lower
Cretaceous
TD 4913 m
Corrected BHT measurement
Maximum palaeotemperature from VR
Upper Limit to maximum Cenozoic (50-0 Ma)
palaeotemperature from AFTA

Figure 8

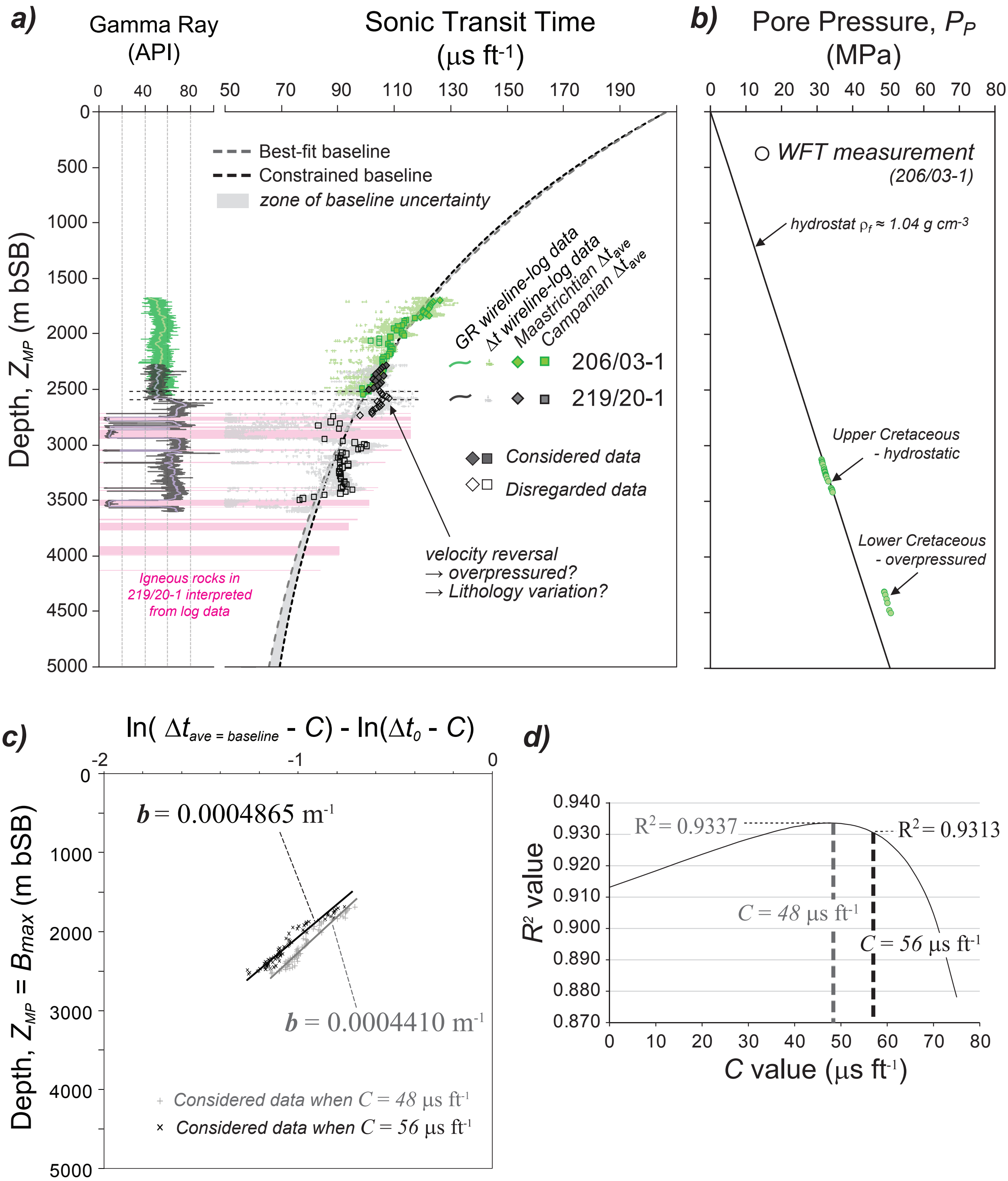

a)
Gamma Ray (API)
Sonic Transit Time (μs ft-1)
0 40 80
50 70 90 110 130 150 170 190
Depth, ZMP (m bSB)
0 500 1000 1500 2000 2500 3000 3500 4000 4500 5000
Best-fit baseline
Constrained baseline
zone of baseline uncertainty
GR wireline-log data
Δt wireline-log data
Maastrichtian Δtave
Campanian Δtave
206/03-1
219/20-1
Considered data
Disregarded data
velocity reversal
→ overpressured?
→ Lithology variation?
Igneous rocks in 219/20-1 interpreted from log data
b)
Pore Pressure, PP (MPa)
0 10 20 30 40 50 60 70 80
WFT measurement (206/03-1)
hydrostat ρf ≈ 1.04 g cm-3
Upper Cretaceous - hydrostatic
Lower Cretaceous - overpressured
c)
ln(Δtave = baseline - C) - ln(Δto - C)
-2 -1 0
Depth, ZMP = Bmax (m bSB)
0 1000 2000 3000 4000 5000
b = 0.0004865 m-1
b = 0.0004410 m-1
Considered data when C = 48 μs ft-1
Considered data when C = 56 μs ft-1
d)
R2 value
0.940 0.930 0.920 0.910 0.900 0.890 0.880 0.870
R2 = 0.9337
R2 = 0.9313
C = 48 μs ft-1
C = 56 μs ft-1
0 10 20 30 40 50 60 70 80
C value (μs ft-1)

Figure 9

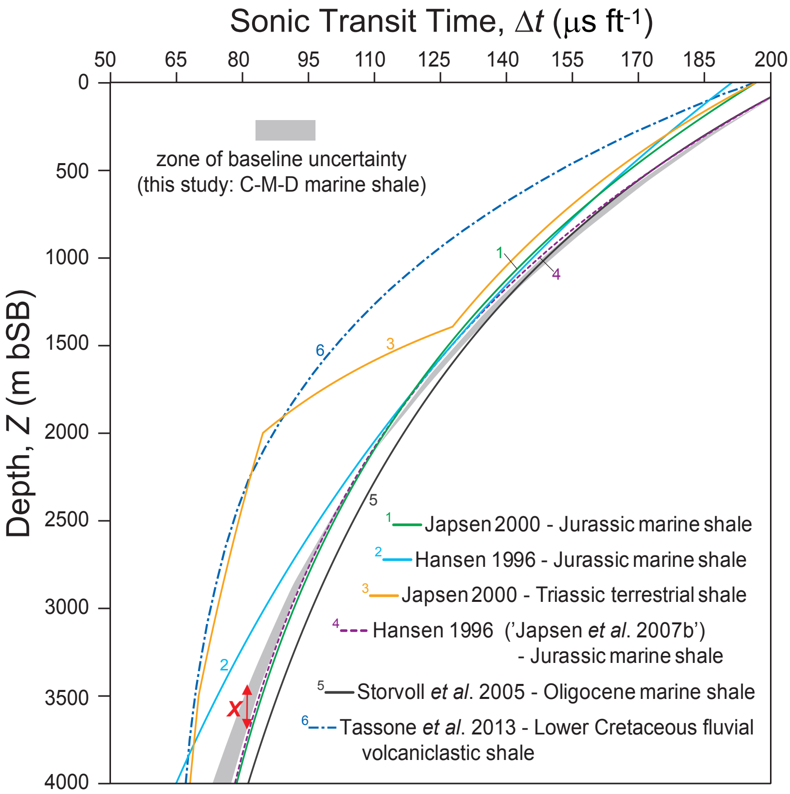

Sonic Transit Time, Δt (μs ft-1)
50
65
80
95
110
125
140
155
170
185
200
Depth, Z (m bSB)
0
500
1000
1500
2000
2500
3000
3500
4000
zone of baseline uncertainty
(this study: C-M-D marine shale)
1
2
3
4
5
6
X
1 Japsen 2000 - Jurassic marine shale
2 Hansen 1996 - Jurassic marine shale
3 Japsen 2000 - Triassic terrestrial shale
4 Hansen 1996 ('Japsen et al. 2007b') - Jurassic marine shale
5 Storvoll et al. 2005 - Oligocene marine shale
6 Tassone et al. 2013 - Lower Cretaceous fluvial volcaniclastic shale

Figure 10

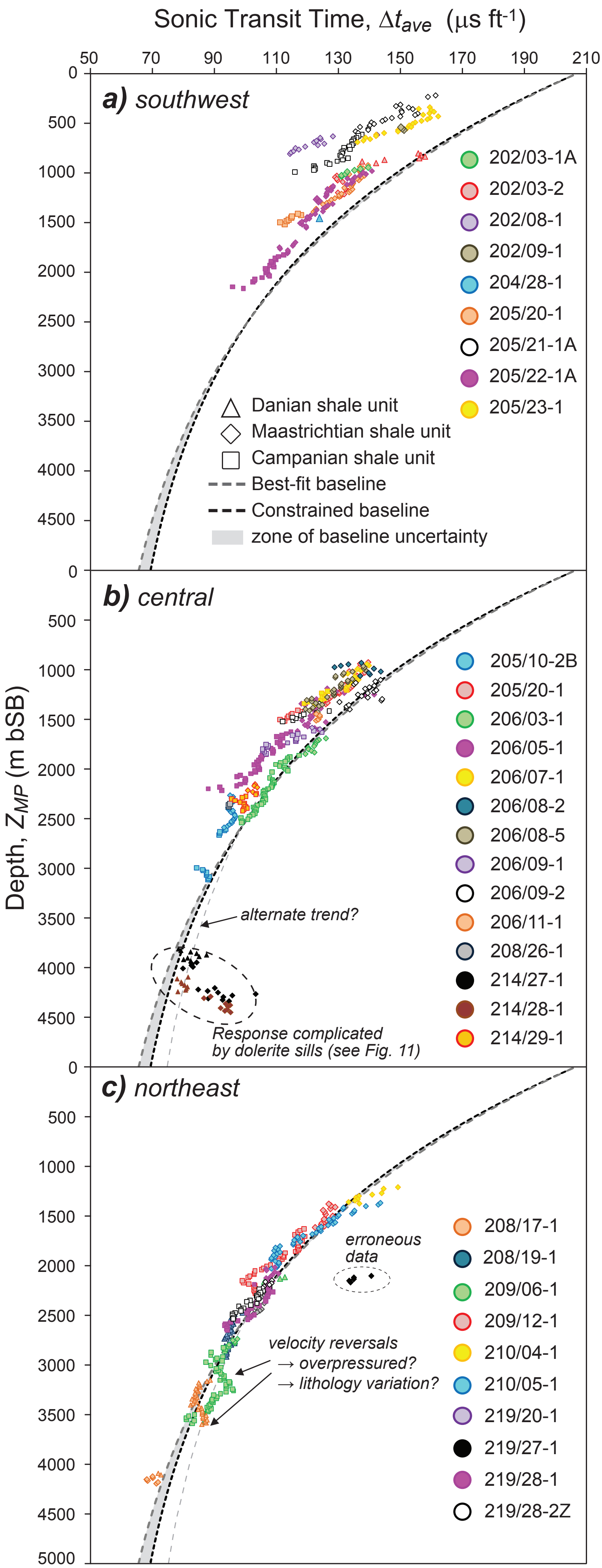

Sonic Transit Time, Δt_{ave} (μs ft^{-1})
50
70
90
110
130
150
170
190
210
Depth, Z_{MP} (m bSB)
a) southwest
202/03-1A
202/03-2
202/08-1
202/09-1
204/28-1
205/20-1
205/21-1A
205/22-1A
205/23-1
Danian shale unit
Maastrichtian shale unit
Campanian shale unit
Best-fit baseline
Constrained baseline
zone of baseline uncertainty
b) central
205/10-2B
205/20-1
206/03-1
206/05-1
206/07-1
206/08-2
206/08-5
206/09-1
206/09-2
206/11-1
208/26-1
214/27-1
214/28-1
214/29-1
alternate trend?
Response complicated
by dolerite sills (see Fig. 11)
c) northeast
208/17-1
208/19-1
209/06-1
209/12-1
210/04-1
210/05-1
219/20-1
219/27-1
219/28-1
219/28-2Z
erroneous
data
velocity reversals
→ overpressured?
→ lithology variation?
0
500
1000
1500
2000
2500
3000
3500
4000
4500
5000

Figure 11

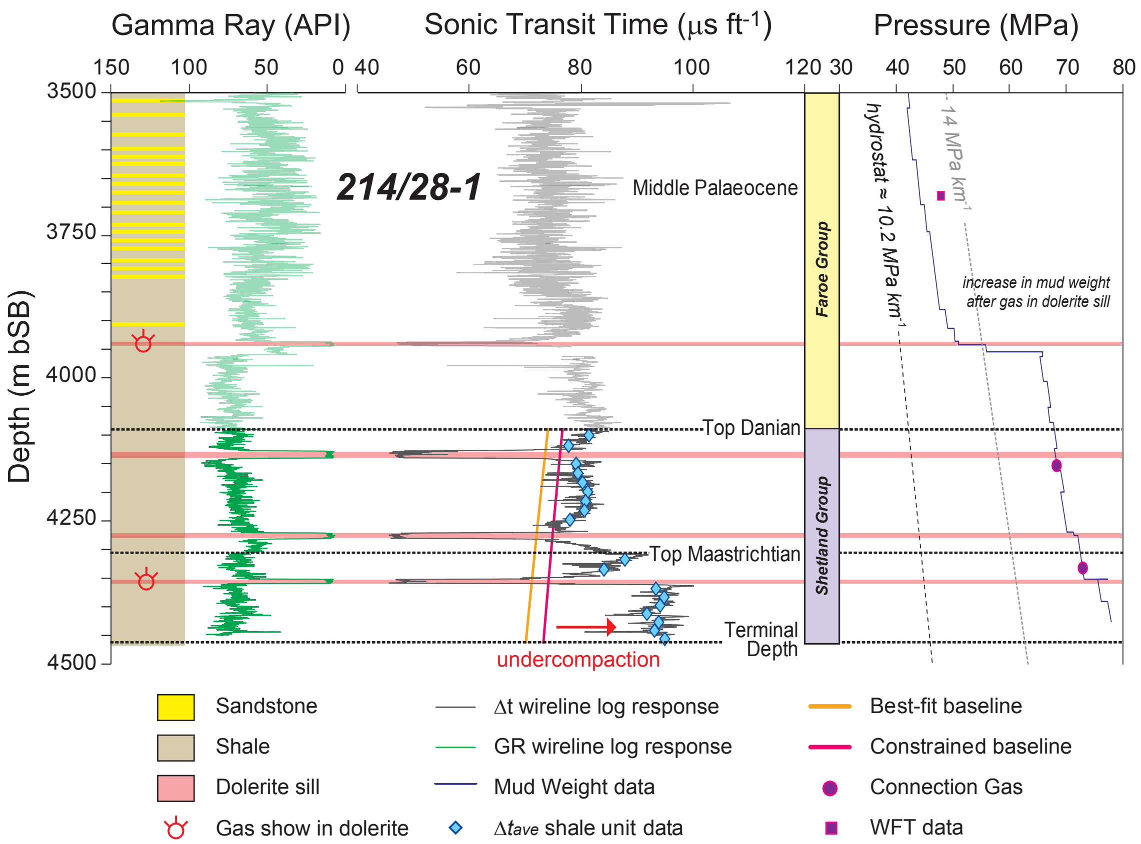

Gamma Ray (API)
150
100
50
0
Sonic Transit Time (μs ft-1)
40
60
80
100
120
Pressure (MPa)
30
40
50
60
70
80
3500
3750
4000
4250
4500
Depth (m bSB)
214/28-1
Middle Palaeocene
Top Danian
Top Maastrichtian
Terminal Depth
undercompaction
Faroe Group
Shetland Group
hydrostat ≈ 10.2 MPa km-1
14 MPa km-1
increase in mud weight after gas in dolerite sill
Sandstone
Shale
Dolerite sill
Gas show in dolerite
Δt wireline log response
GR wireline log response
Mud Weight data
Δtave shale unit data
Best-fit baseline
Constrained wireline baseline
Connection Gas
WFT data

Figure 12

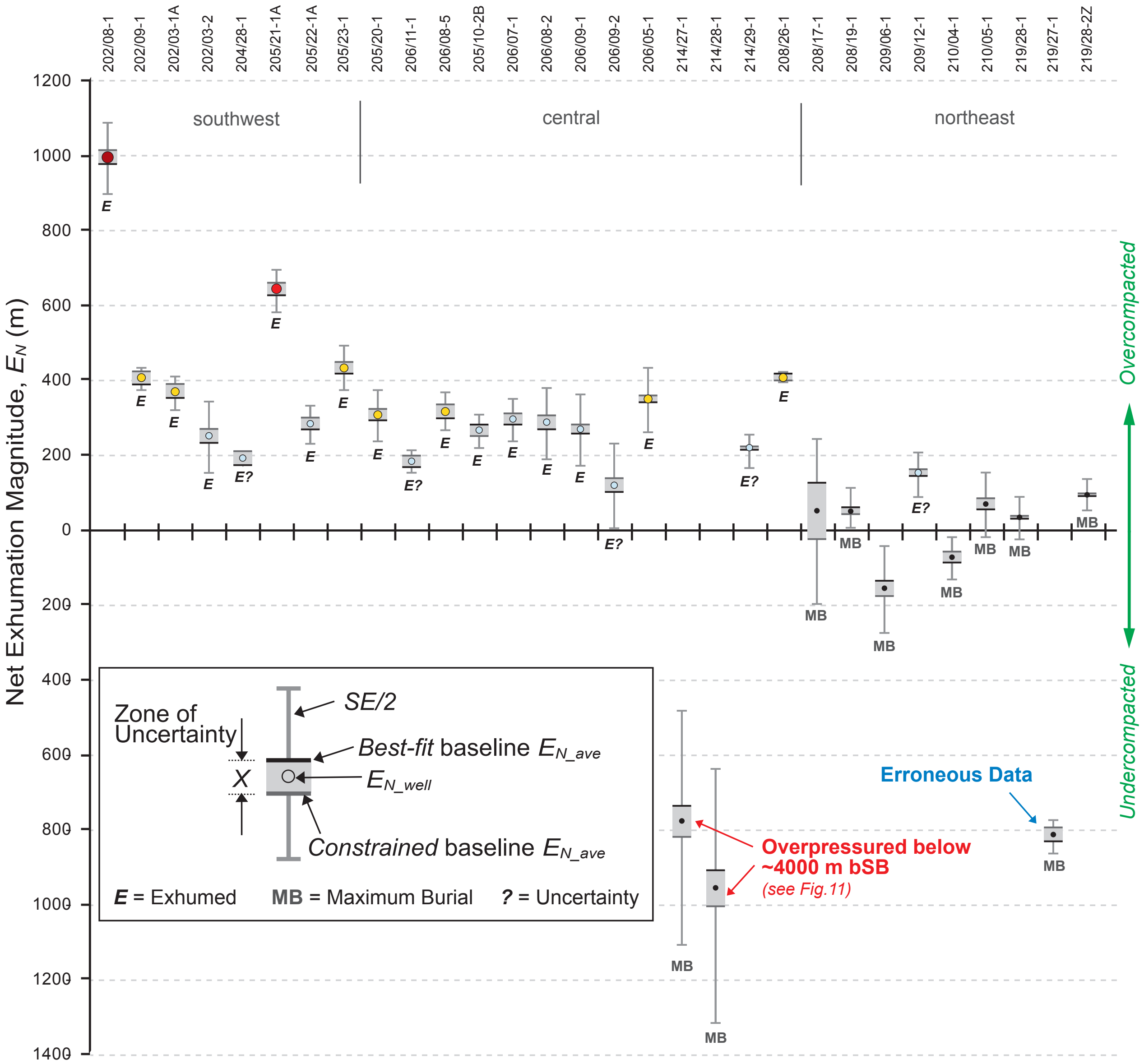

202/08-1
202/09-1
202/03-1A
202/03-2
204/28-1
205/21-1A
205/22-1A
205/23-1
205/20-1
206/11-1
206/08-5
205/10-2B
206/07-1
206/08-2
206/09-1
206/09-2
206/05-1
214/27-1
214/28-1
214/29-1
208/26-1
208/17-1
208/19-1
209/06-1
209/12-1
210/04-1
210/05-1
219/28-1
219/27-1
219/28-2Z
southwest
central
northeast
Net Exhumation Magnitude, E_N (m)
1200
1000
800
600
400
200
0
200
400
600
800
1000
1200
1400
Overcompacted
Undercompacted
E
E?
MB
Zone of Uncertainty
X
SE/2
Best-fit baseline E_{N_ave}
E_{N_well}
Constrained baseline E_{N_ave}
E = Exhumed **MB** = Maximum Burial **?** = Uncertainty
Erroneous Data
Overpressured below ~4000 m bSB
(see Fig.11)

Figure 13

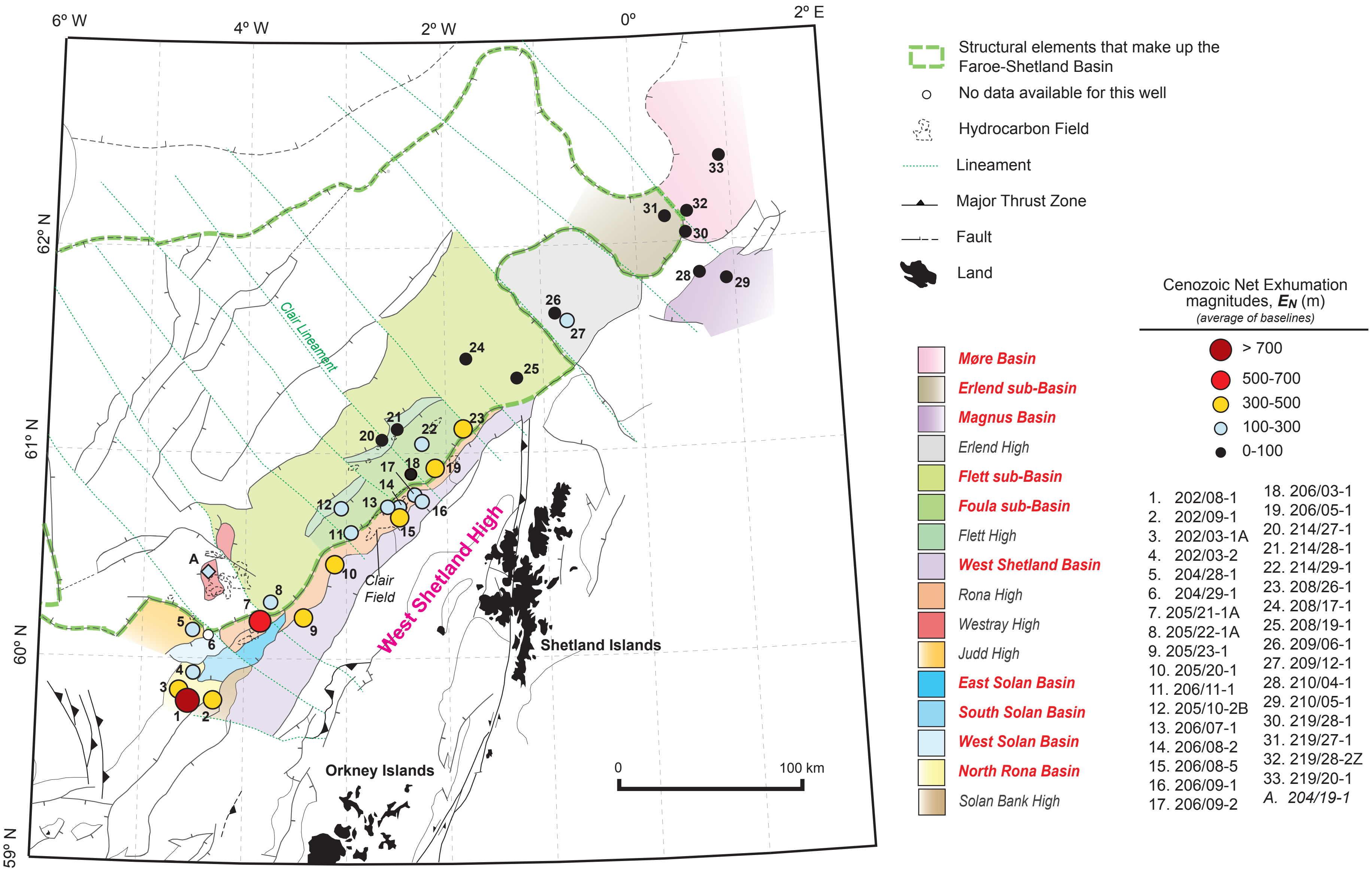
6° W
4° W
2° W
0°
2° E
62° N
61° N
60° N
59° N
Clair Lineament
Clair Field
West Shetland High
Shetland Islands
Orkney Islands
0
100 km
Structural elements that make up the Faroe-Shetland Basin
No data available for this well
Hydrocarbon Field
Lineament
Major Thrust Zone
Fault
Land
Møre Basin
Erlend sub-Basin
Magnus Basin
Erlend High
Flett sub-Basin
Foula sub-Basin
Flett High
West Shetland Basin
Rona High
Westray High
Judd High
East Solan Basin
South Solan Basin
West Solan Basin
North Rona Basin
Solan Bank High
Cenozoic Net Exhumation magnitudes, E_N (m)
(average of baselines)
> 700
500-700
300-500
100-300
0-100
1. 202/08-1
2. 202/09-1
3. 202/03-1A
4. 202/03-2
5. 204/28-1
6. 204/29-1
7. 205/21-1A
8. 205/22-1A
9. 205/23-1
10. 205/20-1
11. 206/11-1
12. 205/10-2B
13. 206/07-1
14. 206/08-2
15. 206/08-5
16. 206/09-1
17. 206/09-2
18. 206/03-1
19. 206/05-1
20. 214/27-1
21. 214/28-1
22. 214/29-1
23. 208/26-1
24. 208/17-1
25. 208/19-1
26. 209/06-1
27. 209/12-1
28. 210/04-1
29. 210/05-1
30. 219/28-1
31. 219/27-1
32. 219/28-2Z
33. 219/20-1
A. 204/19-1

Figure 14

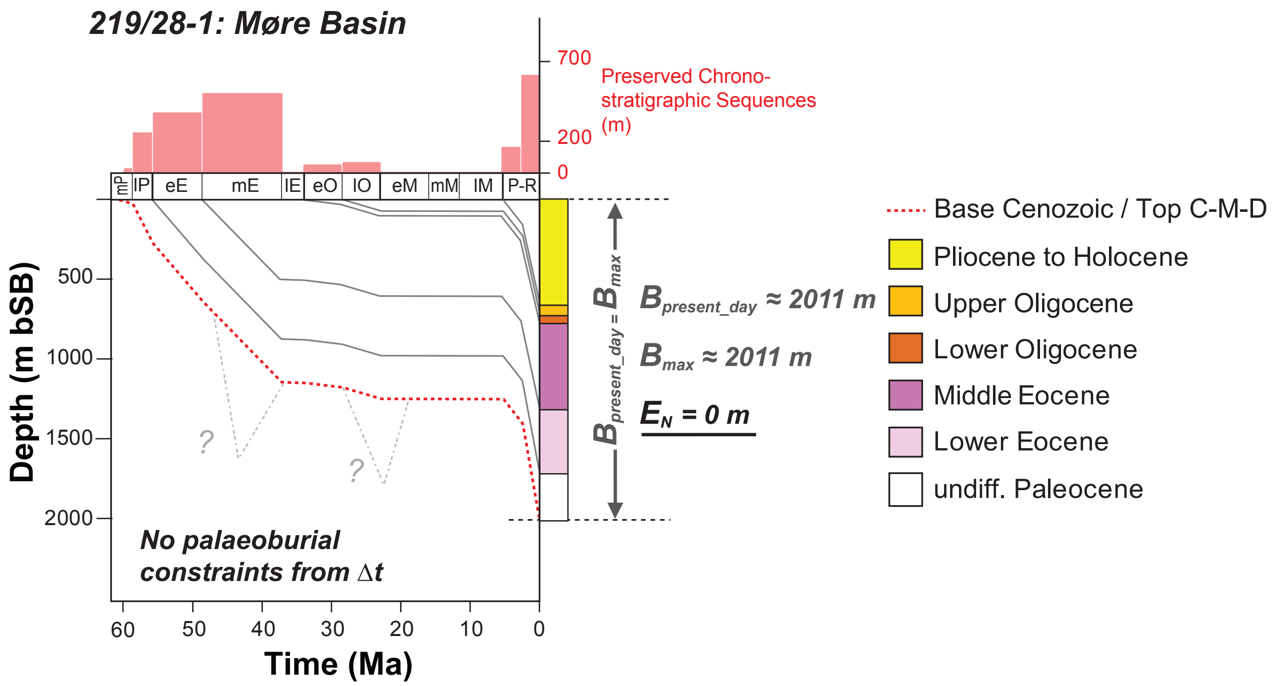

219/28-1: Møre Basin
700
200
0
Preserved Chrono-stratigraphic Sequences (m)
mP
lP
eE
mE
lE
eO
lO
eM
mM
lM
P-R
Depth (m bSB)
500
1000
1500
2000
?
?
No palaeoburial constraints from Δt
60
50
40
30
20
10
0
Time (Ma)
B_present_day = B_max
B_present_day ≈ 2011 m
B_max ≈ 2011 m
E_N = 0 m
Base Cenozoic / Top C-M-D
Pliocene to Holocene
Upper Oligocene
Lower Oligocene
Middle Eocene
Lower Eocene
undiff. Paleocene

Figure 15

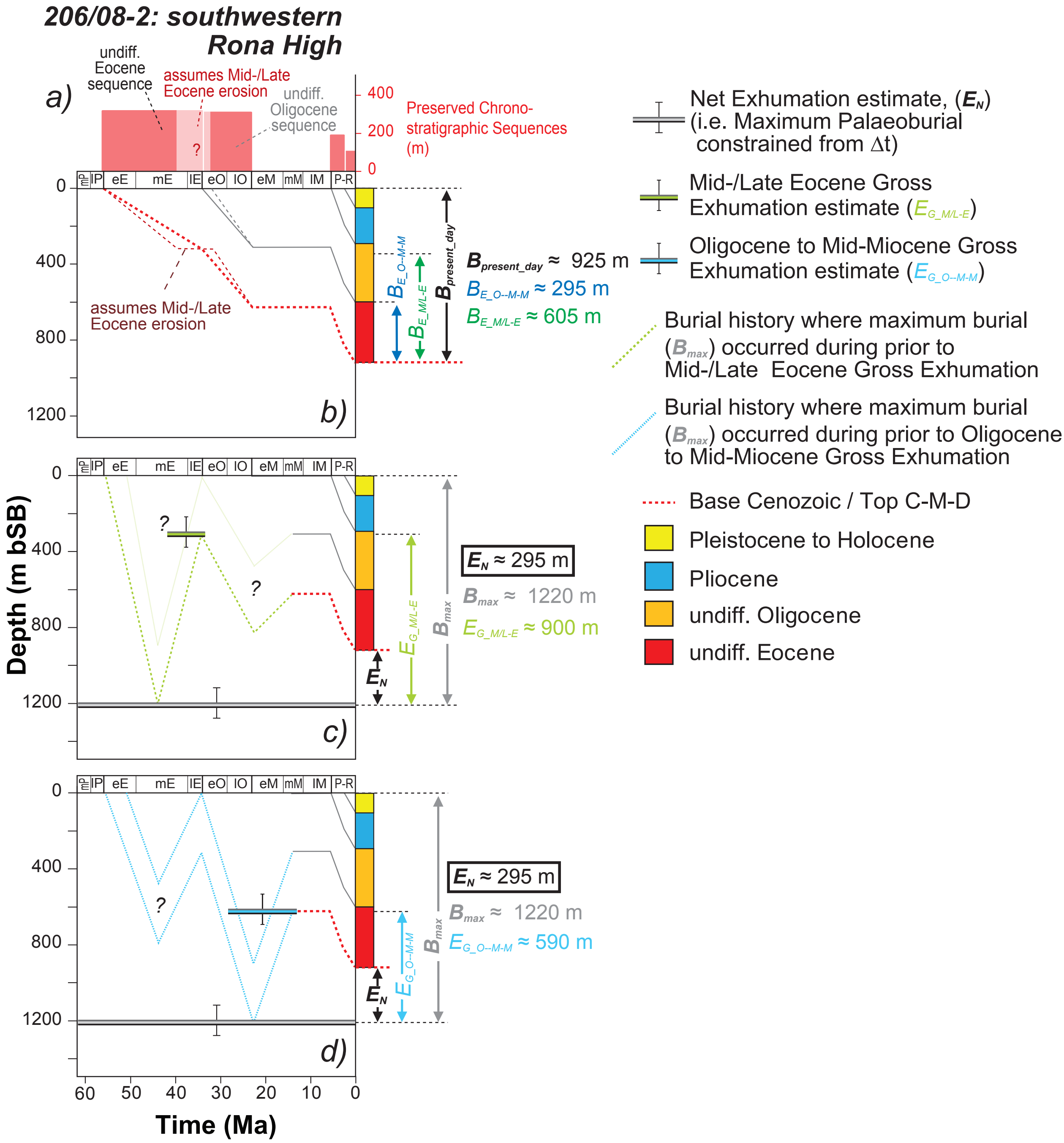

206/08-2: southwestern Rona High
a)
undiff. Eocene sequence
assumes Mid-/Late Eocene erosion
undiff. Oligocene sequence
Preserved Chrono-stratigraphic Sequences (m)
b)
assumes Mid-/Late Eocene erosion
B present_day ≈ 925 m
B E_O-M-M ≈ 295 m
B E_M/L-E ≈ 605 m
c)
E N ≈ 295 m
B max ≈ 1220 m
E G_M/L-E ≈ 900 m
d)
E N ≈ 295 m
B max ≈ 1220 m
E G_O-M-M ≈ 590 m
Depth (m bSB)
Time (Ma)
Net Exhumation estimate, (E N) (i.e. Maximum Palaeoburial constrained from Δt)
Mid-/Late Eocene Gross Exhumation estimate (E G_M/L-E)
Oligocene to Mid-Miocene Gross Exhumation estimate (E G_O-M-M)
Burial history where maximum burial (B max) occurred during prior to Mid-/Late Eocene Gross Exhumation
Burial history where maximum burial (B max) occurred during prior to Oligocene to Mid-Miocene Gross Exhumation
Base Cenozoic / Top C-M-D
Pleistocene to Holocene
Pliocene
undiff. Oligocene
undiff. Eocene

Figure 16

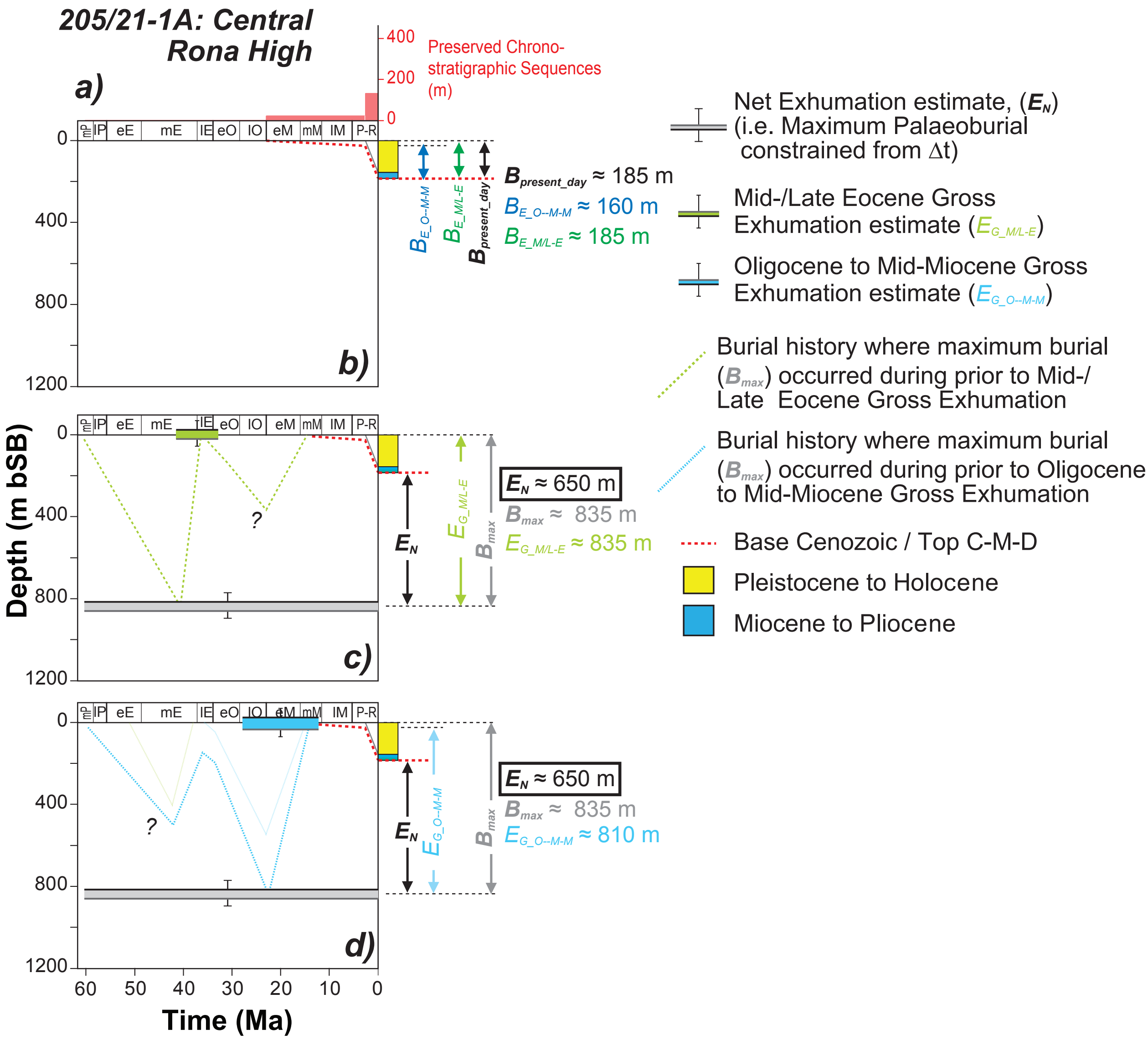
205/21-1A: Central Rona High
a)
Preserved Chrono-stratigraphic Sequences (m)
400
200
0
b)
c)
d)
Depth (m bSB)
Time (Ma)
$B_{present\_day}$ ≈ 185 m
$B_{E\_O\text{-}M\text{-}M}$ ≈ 160 m
$B_{E\_M/L\text{-}E}$ ≈ 185 m
E_N ≈ 650 m
B_{max} ≈ 835 m
$E_{G\_M/L\text{-}E}$ ≈ 835 m
E_N ≈ 650 m
B_{max} ≈ 835 m
$E_{G\_O\text{-}M\text{-}M}$ ≈ 810 m
Net Exhumation estimate, (E_N) (i.e. Maximum Palaeoburial constrained from Δt)
Mid-/Late Eocene Gross Exhumation estimate ($E_{G\_M/L\text{-}E}$)
Oligocene to Mid-Miocene Gross Exhumation estimate ($E_{G\_O\text{-}M\text{-}M}$)
Burial history where maximum burial (B_{max}) occurred during prior to Mid-/Late Eocene Gross Exhumation
Burial history where maximum burial (B_{max}) occurred during prior to Oligocene to Mid-Miocene Gross Exhumation
Base Cenozoic / Top C-M-D
Pleistocene to Holocene
Miocene to Pliocene

Figure 17

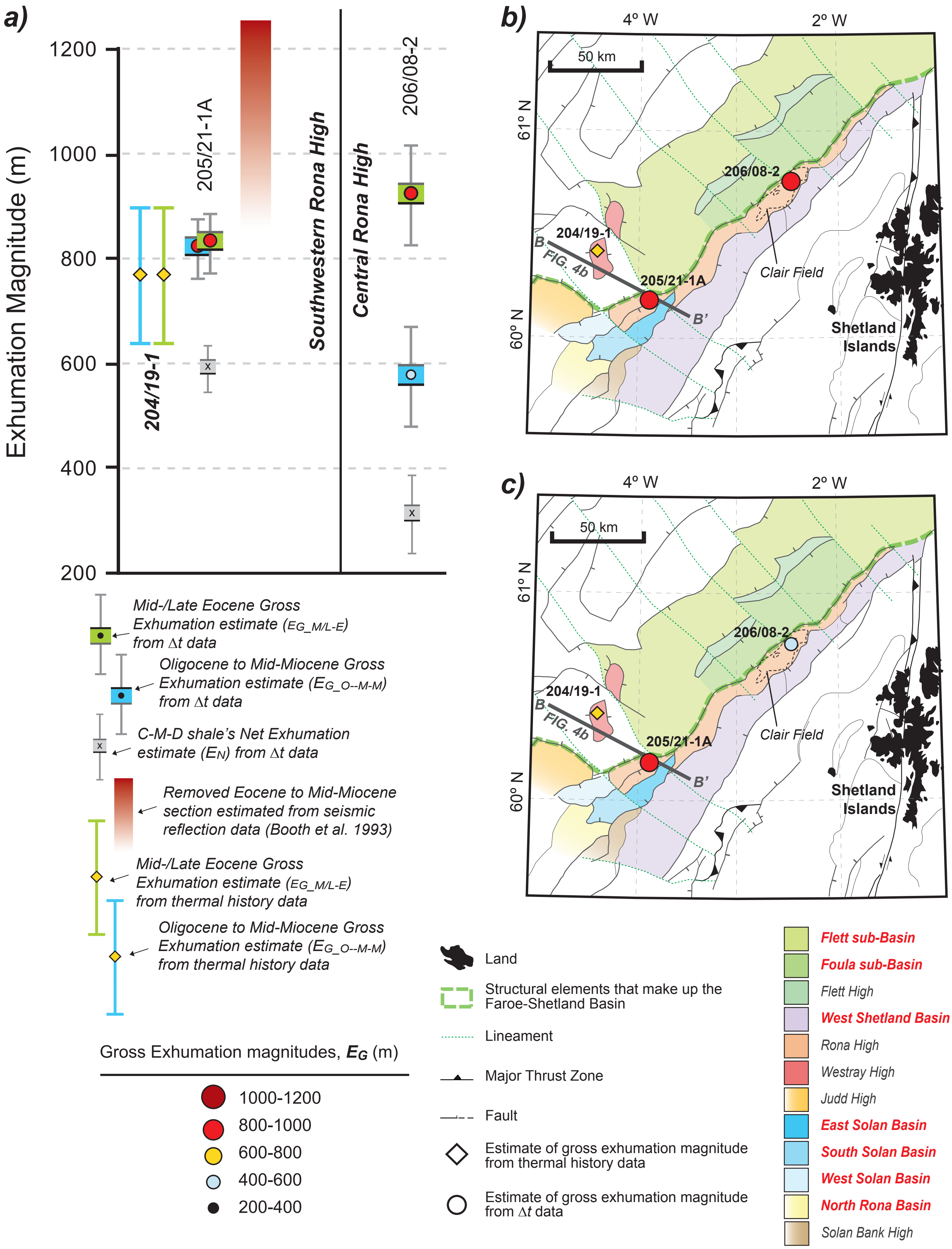
a)
Exhumation Magnitude (m)
1200
1000
800
600
400
200
204/19-1
205/21-1A
Southwestern Rona High
Central Rona High
206/08-2
Mid-/Late Eocene Gross Exhumation estimate ($E_{G\_M/L-E}$) from Δt data
Oligocene to Mid-Miocene Gross Exhumation estimate (E_{G_O-M-M}) from Δt data
C-M-D shale's Net Exhumation estimate (E_N) from Δt data
Removed Eocene to Mid-Miocene section estimated from seismic reflection data (Booth et al. 1993)
Mid-/Late Eocene Gross Exhumation estimate ($E_{G\_M/L-E}$) from thermal history data
Oligocene to Mid-Miocene Gross Exhumation estimate (E_{G_O-M-M}) from thermal history data
b)
4° W
2° W
50 km
61° N
60° N
206/08-2
204/19-1
205/21-1A
FIG. 4b
B
B'
Clair Field
Shetland Islands
c)
4° W
2° W
50 km
61° N
60° N
206/08-2
204/19-1
205/21-1A
FIG. 4b
B
B'
Clair Field
Shetland Islands
Gross Exhumation magnitudes, E_G (m)
1000-1200
800-1000
600-800
400-600
200-400
Land
Structural elements that make up the Faroe-Shetland Basin
Lineament
Major Thrust Zone
Fault
Estimate of gross exhumation magnitude from thermal history data
Estimate of gross exhumation magnitude from Δt data
Flett sub-Basin
Foula sub-Basin
Flett High
West Shetland Basin
Rona High
Westray High
Judd High
East Solan Basin
South Solan Basin
West Solan Basin
North Rona Basin
Solan Bank High

Figure 18

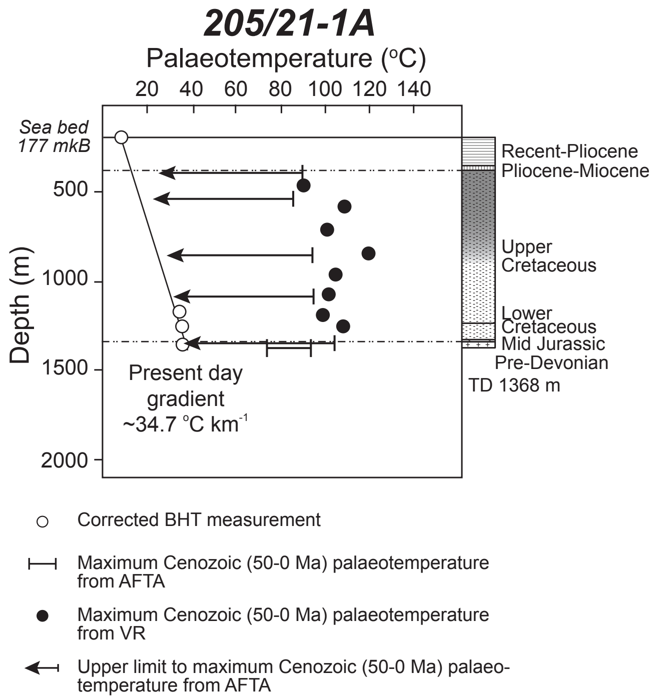

205/21-1A
Palaeotemperature (°C)
20 40 60 80 100 120 140
Sea bed
177 mkB
500
1000
1500
2000
Depth (m)
Recent-Pliocene
Pliocene-Miocene
Upper
Cretaceous
Lower
Cretaceous
Mid Jurassic
Pre-Devonian
TD 1368 m
Present day
gradient
~34.7 °C km-1
Corrected BHT measurement
Maximum Cenozoic (50-0 Ma) palaeotemperature from AFTA
Maximum Cenozoic (50-0 Ma) palaeotemperature from VR
Upper limit to maximum Cenozoic (50-0 Ma) palaeo-temperature from AFTA

Figure 19

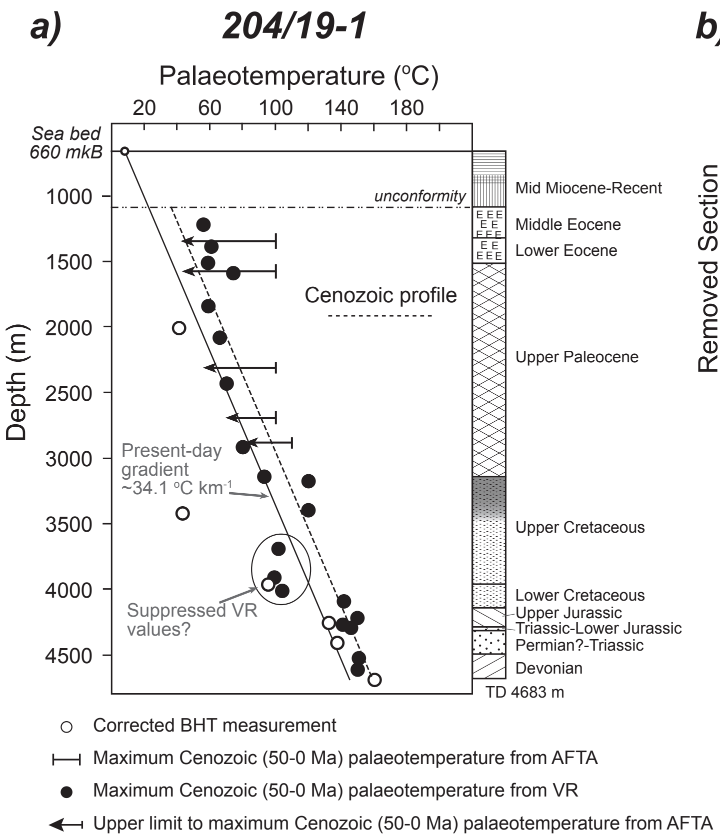

a)
204/19-1
Palaeotemperature (°C)
20
60
100
140
180
Sea bed
660 mkB
1000
1500
2000
2500
3000
3500
4000
4500
Depth (m)
unconformity
Cenozoic profile
Present-day gradient ~34.1 °C km-1
Suppressed VR values?
Mid Miocene-Recent
Middle Eocene
Lower Eocene
Upper Paleocene
Upper Cretaceous
Lower Cretaceous
Upper Jurassic
Triassic-Lower Jurassic
Permian?-Triassic
Devonian
TD 4683 m
Corrected BHT measurement
Maximum Cenozoic (50-0 Ma) palaeotemperature from AFTA
Maximum Cenozoic (50-0 Ma) palaeotemperature from VR
Upper limit to maximum Cenozoic (50-0 Ma) palaeotemperature from AFTA
b)
Eocene-Miocene
Cooling
2000
1500
1000
500
0
Removed Section
E_G (m)
Present-day
thermal gradient
34.1 °C km-1
950 m
630 m
Palaeosurface
temperature = 20°C
20
25
30
35
40
45
Palaeogeothermal
gradient (°C km-1)